Nonconvex Optimization Problems in H_∞ Optimization and Their Applications

by

Soichi Ibaraki

B.S. (Kyoto University, Japan) 1994
M.S. (Kyoto University, Japan) 1996

A dissertation submitted in partial satisfaction of the
requirements for the degree of
Doctor of Philosophy in Engineering

in

Mechanical Engineering

in the

GRADUATE DIVISION
of the
UNIVERSITY of CALIFORNIA at BERKELEY

Committee in charge:

Professor Masayoshi Tomizuka, Chair
Professor Andrew Packard
Professor Laurent El Ghaoui
Professor Seth Sanders

Fall 2000

The dissertation of Soichi Ibaraki is approved:

Chair	Date
	Date
	Date
	Date

University of California at BERKELEY

Fall 2000

Nonconvex Optimization Problems in H_∞ Optimization and Their Applications

by

Soichi Ibaraki

Abstract

Nonconvex Optimization Problems in H_∞ Optimization and Their Applications

by

Soichi Ibaraki

Doctor of Philosophy in Engineering in Mechanical Engineering

University of California at BERKELEY

Professor Masayoshi Tomizuka, Chair

The LMI (linear matrix inequality)-based H_∞ controller synthesis theory guarantees that if the controller is allowed to have the same order as the plant, and every system matrix of the controller is freely tunable, then the H_∞ optimization problem can be solved by convex optimization and the global optimum can be always found. This dissertation focuses on an extension of H_∞ optimization theories to the problems that cannot be parameterized as a convex optimization problem.

This dissertation first presents an extension of the LMI-based H_∞ controller synthesis algorithm for full-order controllers to fixed structure controllers. A critical limitation of the LMI-based full-order H_∞ controller synthesis algorithm is that it allows no additional constraint to be imposed on the problem; the closed-loop H_∞ norm constraint must be the only constraint imposed on the problem in order for it to be globally solvable by convex optimization. In the case where the controller has a fixed structure and only its parameters are tunable, the problem cannot be reparameterized as a convex optimization problem.

The proposed algorithm starts from the transformation of the fixed-structure H_∞ controller optimization problem into an H_∞ optimization problem of a static output feedback controller. Then, the cone complementarity linearization algorithm is used to locally solve the H_∞ optimization problem of a static output feedback controller.

Based on the proposed H_∞ optimization algorithm, this dissertation demonstrates a tuning method of controller parameters to explicitly design frequency responses of the closed-loop system. The proposed approach offers an intuitive and efficient way to re-tune controller parameters, which were finely tuned by an expert engineer, and improve the control performance. The following three practical application examples are presented: 1) the tuning of a single-input single-output (SISO) PID (Proportional plus Integral plus Derivative) controller for head positioning of a magnetic hard disk drive (HDD), 2) the tuning of a discrete-time observer feedback controller for head positioning of an HDD, and 3) the tuning of a multi-input single-output (MISO) PI (Proportional plus Integral) controller for the lateral control of an automated heavy-duty vehicle (HDV). The effectiveness of the proposed re-tuning method is demonstrated by simulation and experimentation.

Secondly, this dissertation considers the BMI (bilinear matrix inequalities) formulation of H_∞ optimization problems. The BMI framework offers an unified approach to formulate a further general class of H_∞ optimization problems with arbitrary constraints or additional optimization objectives. BMI problems are generally nonconvex optimization problems and are proven to be *NP*-hard. This dissertation proposes a novel local search approach for solving general BMI problems. The proposed algorithm is based on the semidefinite programming (SDP) relaxation approach to BMI problems and the linearization-based local search algorithm, which is analogous to the algorithm employed to solve reduced-order H_∞ controller synthesis problems. Four numerical experiments are conducted to show the search

performance of the proposed approach.

Finally, the proposed fixed-structure H_∞ optimization algorithm is applied to the H_∞ optimization problem of state observers. First, the H_∞ optimization algorithm of Luenberger-type state observers is presented. The proposed approach is applied to the design of fault detection filters for lateral control of automated passenger vehicles. The H_∞ optimization of Luenberger state observers is then extended to the design of more general mismatched state observers (i.e. system matrices of the observer do not necessarily coincide with those of the plant model), and a novel application of H_∞-optimal mismatched state observers to the observer-based feedback control is presented. The mismatched state observer is tuned by using H_∞ optimization such that it not only provides good estimation of state variables of the plant, but also stabilizes the overall closed-loop system under the feedback linearization control scheme. As an application example, the proposed approach is applied to lateral control of HDVs.

Professor Masayoshi Tomizuka
Dissertation Committee Chair

To my parents

Toshihide and Mizuko Ibaraki

and my brother

Koji Ibaraki

Contents

List of Figures **vii**

List of Tables **x**

1 Introduction **1**
1.1 Background 1
1.2 Contributions of the Dissertation 6
1.3 Outline of the Dissertation 9
1.4 Notation 10

2 Preliminaries: Convex Optimization and LMI-based H_∞ Controller Synthesis Theories **13**
2.1 Introduction 13
2.2 Convex Optimization and SDP Problems 14
2.2.1 Convex Optimization Problems 14
2.2.2 Semidefinite Programming (SDP) 17
2.2.3 Algorithms and Softwares for Solving SDPs 19
2.3 LMI-based H_∞ Controller Synthesis Algorithms 21
2.3.1 Problem Statement 21
2.3.2 LMI-based H_∞ State Feedback Controller Synthesis Algorithm . . . 23
2.3.3 LMI-based H_∞ Full-order Controller Synthesis Algorithm 26
2.4 Summary 33

3 H_∞ and Scaled-H_∞ Optimization of Fixed Structure Controllers **35**
3.1 Introduction 35
3.2 Previous Works on Fixed-structure and Reduced-order H_∞ Optimization . 40
3.3 H_∞ Optimization of Fixed-structure Controllers 42
3.3.1 Transformation into a Static Feedback Controller Synthesis Problem 42
3.3.2 H_∞ Optimization of Static Output Feedback Controllers 49
3.4 Scaled-H_∞ Optimization of Static Output Feedback Controllers 54
3.4.1 Scaled-H_∞ Optimization Problem 54
3.4.2 Scaled-H_∞ Optimization of Static Output Feedback Controllers . . . 58
3.4.3 Application of Scaled-H_∞ Optimization 60

3.5 Application Example I: PID Controller Design for Head Positioning of a Magnetic Hard Disk Drive . . . 61
3.5.1 Introduction: Head Positioning Control for a Magnetic Hard Disk Drive 61
3.5.2 Model Description . . . 63
3.5.3 Controller Design Procedure . . . 65
3.5.4 Simulation Results . . . 68
3.5.5 Experimental Results . . . 72
3.6 Application Example II: Digital Observer-based State Feedback Controller Design for Head Positioning of a Magnetic Hard Disk Drive . . . 78
3.6.1 Introduction . . . 78
3.6.2 Plant Model and Controller Structure . . . 79
3.6.3 Controller Design Procedure . . . 80
3.6.4 Simulation Results . . . 83
3.6.5 Experimental Results . . . 86
3.7 Application Example III: MISO PID Controller Design for Lateral Control of Heavy-Duty Vehicles . . . 88
3.7.1 Introduction: Lateral Control of Heavy-Duty Vehicles . . . 88
3.7.2 Model Description . . . 90
3.7.3 Control Objective and Controller Structure . . . 92
3.7.4 Controller Design Procedure . . . 93
3.7.5 Simulation Results . . . 95
3.8 Summary . . . 99

4 Rank Minimization Approach for Solving BMI Problems with Random Search 100
4.1 Introduction . . . 100
4.2 BMI formulation of H_∞ Optimization Problems . . . 103
4.3 Rank Minimization Approach for Solving BMI Problems . . . 105
4.3.1 Rank Minimization Approach for Solving BMI Problems . . . 105
4.3.2 SDP Relaxation Approach to BMI Problems and Combinatorial Problems . . . 107
4.3.3 Random Search Algorithm . . . 110
4.4 Numerical Experiments . . . 111
4.4.1 A Simple BMI Problem over Two Variables . . . 111
4.4.2 Randomly Generated BMI Problems . . . 114
4.4.3 Mixed H_2/H_∞ Controller Design . . . 116
4.4.4 Simultaneous State-Feedback Stabilization . . . 119
4.5 Application to Global Search Algorithms . . . 121
4.6 Summary . . . 124

5 H_∞ State Observers I: H_∞ Optimization of Luenberger State Observers and Its Application to Fault Detection Scheme 125
5.1 Introduction . . . 125
5.1.1 H_∞ Optimization of Luenberger State Observers . . . 125
5.1.2 Application to Fault Detection Filter Design . . . 128

5.2 H_∞ Optimization of Luenberger State Observers with Static Weightings . . 129
5.3 H_∞ Optimization of Luenberger State Observers with Dynamic Weightings 131
5.4 Application Example: Fault Detection Filter Design for Lateral Control of Automated Passenger Vehicles 134
5.4.1 Introduction 134
5.4.2 Model Description 134
5.4.3 Fault Detection Scheme 136
5.4.4 Design Procedure of Dedicated Observers 139
5.4.5 Simulation Results 145
5.5 Summary 148

6 H_∞ State Observers II: Taming Internal Dynamics by Mismatched and H_∞-Optimized State Observer 150
6.1 Introduction 150
6.1.1 Matched and Mismatched State Observers 150
6.1.2 Application of Mismatched State Observers to Feedback Linearization Control Scheme 152
6.2 Feedback Linearization Control Scheme 155
6.3 Mismatched and H_∞-Optimized State Observer 156
6.4 Application Example I: An Illustrative Second-order Plant Example 160
6.5 Application Example II: Application to Lateral Control of HDVs 163
6.5.1 Model Description 163
6.5.2 Controller Design 164
6.5.3 Observer Design 166
6.5.4 Simulation Results 167
6.6 Summary 172

7 Conclusions and Future Research 173
7.1 Conclusions 173
7.2 Future Research 176

Bibliography 179

List of Figures

1.1 Lower and upper linear linear fractional transformations (LFTs) 11

3.1 Extraction of controller parameters 45
3.2 Closed-loop system configuration with modeling uncertainties $\Delta(s)$ 55
3.3 Schematic view of a hard disk drive 62
3.4 Simplified block diagram of tracking control loop 62
3.5 Experimental HDD setup 64
3.6 Simulated and measured frequency responses of the VCM actuator 65
3.7 Design procedure of performance filters 68
3.8 Comparison of closed-loop frequency responses under two manually tuned controllers and the designed PID controller (simulation results) 70
3.9 Measured PES and its frequency spectrums under the conventional controller, $C_2(s)$ 74
3.10 Measured PES and its frequency spectrums under the designed PID controller, $C_{new}(s)$ 75
3.11 Comparison of closed-loop frequency responses under the manually-tuned controller, $C_2(s)$, and the designed PID controller, $C_{new}(s)$ (experimental results) 76
3.12 Transformation into the H_∞ optimization problem of a static output feedback controller 82
3.13 The frequency response of a typical VCM actuator of an HDD 84
3.14 The open-loop responses of the disk drive servo with and without the optimization of controller parameters 85
3.15 The frequency responses of the sensitivity function of the disk drive servo with and without the optimization of controller parameters 85
3.16 Comparison of experimentally measured TMR (Track MisRegistration) spectrums with the original controller setting, $C_{old}(z)$ and the re-designed controller, $C_{new}(z)$ 87
3.17 State variables of the linearized lateral motion model of HDVs 91
3.18 Closed-loop configuration for lateral motion control of HDVs 92
3.19 Multiplicative uncertainties due to parameter perturbations 94

3.20 Frequency responses of the closed-loop transfer functions $T^{cl}_{\dot{\epsilon}_d \to \delta}(s)$, $T^{cl}_{\dot{\epsilon}_d \to y_r}(s)$, and $T^{cl}_{\dot{\epsilon}_d \to \epsilon_r}(s)$ under the designed controller 96
3.21 Scheme of the Crows Landing test site 97
3.22 Closed-loop time-domain simulations under the nominal condition and two perturbed conditions 98

4.1 Contour plot of the greatest eigenvalue of $F(x_1, x_2)$ with the trajectory of the rank minimization approach 112
4.2 Random search after one step of the rank minimization approach 114

5.1 Block diagram of state estimation error dynamics 132
5.2 Extraction of the observer matrix, L 133
5.3 Four-wheel vehicle following a reference path 135
5.4 Block diagram of fault detection scheme based on dedicated observers . . . 137
5.5 Comparison of estimation error dynamics of the Kalman filter, $P_2^{old}(s)$, and the re-tuned setting, $P_2^{new}(s)$ 142
5.6 Block diagram of optimization setting for L_1 143
5.7 Comparison of estimation error dynamics of the Kalman filters, $P_1^{old}(s)$ and $P_2^{old}(s)$, and the re-tuned settings, $P_1^{new}(s)$ and $P_2^{new}(s)$ 144
5.8 Measured and estimated lateral errors at the locations of the front and the rear sensor when the Kalman filters, $\hat{P}_1^{old}(s)$ and $\hat{P}_2^{old}(s)$, are used 146
5.9 The estimation gap profiles, $\hat{y}^1_{fs} - \hat{y}^2_{fs}$ and $\hat{y}^1_{rs} - \hat{y}^2_{rs}$, corresponding to Figure 5.8 146
5.10 The estimation gap profiles, $\hat{y}^1_{fs} - \hat{y}^2_{fs}$ and $\hat{y}^1_{rs} - \hat{y}^2_{rs}$, of the re-tuned observers, $\hat{P}_1^{new}(s)$ and $\hat{P}_2^{new}(s)$, in the nominal condition 147
5.11 The estimation gap profiles, $\hat{y}^1_{fs} - \hat{y}^2_{fs}$ and $\hat{y}^1_{rs} - \hat{y}^2_{rs}$, of the re-tuned observers, $\hat{P}_1^{new}(s)$ and $\hat{P}_2^{new}(s)$, with measurement noise 147
5.12 The estimation gap profiles, $\hat{y}^1_{fs} - \hat{y}^2_{fs}$ and $\hat{y}^1_{rs} - \hat{y}^2_{rs}$, of the re-tuned observers, $\hat{P}_1^{new}(s)$ and $\hat{P}_2^{new}(s)$, in two perturbed conditions 148

6.1 Closed-loop configuration with the outer-loop controller 157
6.2 Closed-loop configuration with the proposed mismatched observer 157
6.3 H_∞ synthesis of the state observer 158
6.4 Closed-loop pole locations with direct state feedback, the Luenberger observer, and the proposed mismatched observer 162
6.5 (a) Step responses of the output, y (left), and (b) step responses of internal modes, x_1 and x_2, and their estimates, $\hat{x}_1$ and $\hat{x}_2$ (right), when the designed observer is applied. 163
6.6 Closed-loop configuration under the assumption that all states are available 165
6.7 Frequency responses from disturbance input, $\dot{\epsilon_d}$, to estimation error vector, $e(t) := x(t) - \hat{x}(t)$ 167
6.8 Closed-loop simulations under the nominal condition and two perturbed conditions 169
6.9 State estimation errors corresponding to Figure 6.8 170

6.10 The closed-loop responses of $y_s(t)$ with direct state feedback and the designed mismatched observer under the perturbed condition 171
6.11 Closed-loop pole locations of the system with direct state feedback and the designed mismatched observer under the same conditions as in Figure 6.10 . 171

List of Tables

3.1 Experimental setup specifications 64
3.2 Performance comparison of two conventional controllers, $C_1(s)$ and $C_2(s)$, and the designed PID controller, $C_{new}(s)$ (simulation results) 72
3.3 The STD of the RPE and NRPE components of measured PES under the original controller, $C_2(s)$, and the designed PID controller, $C_{new}(s)$ 76
3.4 Performance comparison of the conventional controller (C_2) and the designed PID controller (C_{new}) (experimental results) 77

4.1 The average number of iterations and computational time for the BB method and the proposed algorithm to solve randomly generated BMI problems . . 116
4.2 Number of iterations that Algorithm 4 requires to reach the solution at each step of reducing α 120

Acknowledgements

I would like to express my deepest gratitude to my research advisor, Professor Masayoshi Tomizuka, for giving me an opportunity to participate in this research and for his continuous guidance and encouragement throughout my Ph.D. studies at Berkeley. I would also like to thank Professor Laurent El Ghaoui and Professor Andy Packard for not only carefully reviewing the manuscript as my dissertation committee, but also for giving me valuable suggestions and inspirations in the course of the study from various aspects of optimal control theories and numerical optimization theories. I am particularly indebted to Professor El Ghaoui for his contribution to the works presented in Chapters 3 and 4. I would also like to express my sincere gratitude to Professor Seth Sanders for his continuous help to my induction motor control project, which is not included in this dissertation.

Much of applications presented in this dissertation would not have been possible without the help of my friends and colleagues, who are experts on each subject; Hidehiko Numasato at Hitachi, Ltd., Dr. Weiguang Niu at Quantum Co., Jiagen Ding (disk drive control; Sections 3.5 and 3.6), Shashikanth Suryanarayanan (fault management for automated vehicles; Section 5.4), Jeng-Yu Wang and Meihua Tai (automated lateral control of heavy-duty vehicles; Sections 3.7 and 6.5). Experimental hard disk drive setups used in Sections 3.5 and 3.6 are provided by Hitachi, Ltd. and Quantum Co., respectively.

I would like to thank all the members of Mechanical Systems Control Laboratory for their friendship and help in every aspect of my life at Berkeley; Meihua, Jeng-Yu, Shashi, Jiagen, Erwin Satrya Budiman, Ryan Wayne White, Dr. Motoyoshi Ozaki, Dr. Craig Smith, Dong-Jun Lee, Jihua Huang, Lu Guang, Ye Sheng, Dr. Kai-Ten Feng, Dr. Yuping Gu. I particularly acknowledge Ryan, Shashi, and Jeng-Yu for their helpful comments and in-

sightful suggestions on early drafts of this dissertation.

I also would like to express my sincere gratitude to Professor Yoshiaki Kakino at Kyoto University, Japan, and all members in his research group including Professor Atsushi Matsubara, Professor Yukitoshi Ihara, and Mr. Iwao Yamaji, for their encouragement that allowed me to participate in the study at Berkeley.

This research was partially supported by funds contributed to Mechanical Systems Control Laboratory by industrial sponsors.

Finally, and most importantly, I thank to my parents, Toshihide and Mizuko, and my brother, Koji.

Chapter 1

Introduction

1.1 Background

Optimal control has been one of the main research topics in control engineering. In particular, the H_∞ control theories and their applications have attracted numerous research efforts since the mid-1980s. This dissertation focuses on an extension of H_∞ optimization theories to a further general class of problems of practical interest.

In the late-1980s, Doyle et al. [18] stated that the necessary and sufficient condition for the existence of full-order H_∞ (sub-)optimal controllers can be written in the form of two algebraic Ricatti equations (AREs). Furthermore, explicit state-space formulas were given for a particular solution called the "central controller." All solutions are parameterized based on the central controller by using a linear fractional transformation (LFT) involving a free dynamic parameter, $Q(s)$.

This approach offers an efficient and numerically reliable way of computing full-order H_∞ controllers. It has, however, inherent restrictions that limit its applicability. One major drawback of the ARE-based approach is that it overemphasizes the central solution among all possible choices of H_∞ (sub-)optimal controllers. In most cases, there is no explicit connection between the free parameter, $Q(s)$, and the properties of the controller or the closed-loop system. As a result, the diversity of H_∞ controllers is hardly exploited in the ARE-based H_∞ controller synthesis approach, and the central controller is almost exclusively used, despite its certain undesirable properties. For example, the reduced-order H_∞ controller synthesis problem has attracted considerable research interests since the early works on H_∞ control. The central H_∞ controller is typically high order — at least as high as and quite often much higher than the plant model due to dynamic performance weightings augmented in the optimization process to achieve the desired performance. The reduced-order (or fixed-order) H_∞ controller synthesis is, therefore, of interest in practical applications. The Q-parameterization approach seems inadequate for this purpose.

In the mid-1990s, Gahinet and Apkarian [33] and Iwasaki and Skelton [60] proposed an alternative approach to the H_∞ controller synthesis. It was shown that in the full-order controller synthesis case, i.e. the case where the controller is allowed to have the same order as the plant, and every system matrix of the controller is freely tunable, the H_∞ optimization problem can be reparameterized in the semidefinite programming (SDP) form. The AREs that characterize full-order H_∞-optimal controllers are replaced with linear matrix inequalities (LMIs), and the solution set of these inequalities parameterize all (sub-)optimal H_∞ controllers.

The SDP is a convex optimization problem, i.e. a minimization problem of a convex objective function under convex set constraints. In the field of applied mathematics, numerous

research efforts have been devoted to the development of efficient and reliable numerical algorithms to solve convex optimization problems. In particular, SDPs can be solved very efficiently, both in theory and in practice, by using interior-point methods that have been the subject of intense research in this field since the mid-1980s. Recent technical advances in computing capability of computers have made the LMI-based approach particularly attractive. The important roles of SDP formulations have been recognized not only in H_∞ control theories but also in many engineering optimization problems.

Although the LMI-based H_∞ controller synthesis algorithm is generally not as numerically efficient as the ARE-based approach, it has certain crucial advantages from the viewpoint of the extendibility to more general problems. One of its major advantages is that important design parameters in the controller design, such as the controller order or the damping of the closed-loop modes, have a clear interpretation in terms of optimization variables in the LMI formulation. This formulation is, therefore, propitious to the design of "better" H_∞ controllers.

For example, the LMI-based approach offers an explicit formulation of reduced-order H_∞ controller synthesis problems. The constraint on the controller order can be interpreted as a rank constraint imposed in addition to the LMI constraints in the full-order H_∞ controller synthesis case. The reduced-order H_∞ controller synthesis problem is still a hard problem to solve, since the additional rank constraint is not a convex set constraint, and thus the problem is a nonconvex optimization problem. The nonconvexity of the reduced-order H_∞ controller synthesis problem means that it can have multiple local optima. Therefore, it is hard to find the global optimum in an efficient way. It is, however, easier to find a local optimum by applying any descent search approaches. In the mid-90s, several local search algorithms were proposed for reduced-order H_∞ controller synthesis.

This dissertation first considers an extension of reduced-order H_∞ controller synthesis to the H_∞ optimization of fixed-structure controllers. Despite the technical advances in the design and implementation of sophisticated controllers, most industrial controllers still adopt simple structures such as PID (Proportional plus Integral plus Derivative) control. To implement classical full-order H_∞ controllers, one must re-design the entire controller structure, which often requires considerable effort and cost. The extension of the H_∞ optimization to the tuning of parameters of fixed structure controllers is, therefore, of interest and of practical importance. Based on the proposed fixed-structure H_∞ controller optimization algorithm, the re-tuning methodology of controller parameters to improve the control performance is presented.

Besides constraints on the controller order or structure, the practical controller design must often deal with more general constraints or multiple optimization objectives. The following are examples of controller design problems that require additional constraints or optimization objectives to be imposed on the H_∞ optimization problem:

- The classical H_∞ control synthesis theories do not explicitly guarantee the stability of the optimal controller. Although heuristic approaches to avoid the instability of the controller are available, some applications require the constraint on the controller stability to be explicitly imposed.

- Excessively high controller gains are often undesirable for practical implementation. In such cases, constraints must be imposed on the range of each controller parameter.

- Multi-objective optimization is crucial in many practical controller design problems. For example, the controller design for multi-input multi-output (MIMO) plants often requires minimizing H_∞ norms of multiple transfer functions between different in-

put/output channels. In the classical H_∞ optimization approach, multiple H_∞ norm objective functions are approximated by a single H_∞ norm function, which likely introduces a significant conservativeness to the controller design, unless the dynamics of each transfer function is sufficiently decoupled.

- Another practical example of multi-objective optimization is the design of robust controllers for plants with parametric uncertainties. When the ranges of parametric perturbations are known, one of the simplest robust controller design methodologies is to optimize the controller such that it achieves the desirable control performance for multiple plant models corresponding to "extreme" values of uncertain parameters. In fact, this approach offers the least conservative controller when uncertain parameters are assumed to be time-invariant or slowly changing. In such cases, the μ-synthesis approach often results in more conservative controllers.

The conventional H_∞ controller synthesis algorithm cannot be applied to any of the above problems. In fact, any additional constraints that contain the controller dynamics make the H_∞ optimization problem a nonconvex optimization problem.

In the mid-1990s, Goh et al. [39] presented the bilinear matrix inequality (BMI) formulation that offers a unified approach to those problems. Unlike LMI problems, BMI problems are generally nonconvex optimization problems and are proven to be NP-hard, which means any algorithms that globally solve general BMI problems are quite likely non-polynomial time algorithms. The practical importance of solving BMI problems is, however, clear for further generalization of H_∞ optimization theories.

In recent years, considerable research efforts have been devoted to the development of algorithms that solve BMI problems in an efficient and reliable manner. Most of the algorithms

found in literature that claim the applicability to control-related problems of practical size are local search algorithms. It is, however, highly likely for local search approaches to fail to reach the global optimum due to the nonconvex nature of BMI problems. Recent works on this subject also include global search approaches that are guaranteed to find the global optimum. Most of global search algorithms found in the literature are variations of the Branch and Bound (BB) method based on different formulations of BMI problems. Although the computational efficiency is a major focus for all of those works, none of the global search algorithms are polynomial-time algorithms due to the *NP*-hardness of BMI problems. Therefore, their applicability to problems of practical size is questionable.

This dissertation proposes a novel algorithm to solve general BMI problems. Although the proposed algorithm is a local search algorithm, it is based on a completely different formulation of BMI problems from conventional, simpler local search algorithms, and the proposed approach can more likely find the global solution in practice. Considering that any global search algorithm is a non-polynomial time algorithm, the proposed approach is more practical than any existing global search algorithm from the viewpoint of the computational efficiency. It is more reliable than conventional, simpler local search algorithms from the viewpoint of the likelihood of finding the global solution.

The next section summarizes the main contributions of this dissertation in further detail.

1.2 Contributions of the Dissertation

H_∞ and Scaled-H_∞ Optimization of Fixed Structure Controllers

The first contribution of this dissertation is an extension of the LMI-based H_∞ controller

synthesis algorithm for full-order controllers to fixed structure controllers. The proposed algorithm first transforms the original fixed-structure controller optimization problem into an H_∞ synthesis problem of static output feedback controllers, which does not impose any constraints on the controller structure except for the order. Then, the cone complementarity linearization algorithm proposed by El Ghaoui et al. [23] is applied to locally solve this problem. The proposed approach is also applied to the scaled-H_∞ optimization problem of fixed structure controllers, which is often used as an approximation of μ-synthesis problems for mixed real/complex model uncertainties.

Application Examples: As a part of the first contribution, this dissertation demonstrates a tuning method of controller parameters to explicitly design frequency responses of the closed-loop system based on the proposed H_∞ optimization algorithm. The proposed approach offers an intuitive and efficient way to re-tune controller parameters, which were finely tuned by an expert engineer, and improve the control performance. The following three practical application examples are presented: 1) the tuning of a SISO PID controller for head positioning of a magnetic hard disk drive (HDD), 2) the tuning of a discrete-time observer feedback controller for head positioning of an HDD, and 3) the tuning of a multi-input single-output (MISO) PI (Proportional plus Integral) controller for the lateral control of an automated heavy-duty vehicle (HDV). The effectiveness of the proposed re-tuning method is demonstrated by simulation and experimentation.

Rank Minimization Approach for Solving BMI Problems

As a second contribution, this dissertation proposes a novel algorithm to solve general BMI (bilinear matrix inequality) problems. The BMI framework offers an unified approach

to formulate a general class of H_∞ optimization problems with arbitrary constraints or additional optimization objectives. First, it is shown that general BMI problems can be equivalently transformed into a rank minimization problem under LMI constraints. The close analogy of this formulation to the well-known SDP relaxation approach to a certain class of combinatorial problems is also discussed. Then, a linearization-based local search algorithm is proposed to locally solve this formulation. The algorithm is analogous to the one employed to solve the H_∞ optimization problem of static output feedback controllers. The proposed approach is more practically applicable than any existing global search algorithms from the viewpoint of the efficiency, and more reliable than conventional, simpler local search algorithms from the viewpoint of the likelihood of finding the global solution. Four numerical experiments are conducted to show the search performance of the proposed approach.

H_∞ Optimization of Luenberger State Observers

The third contribution of this dissertation is an extension of the H_∞ optimization algorithm of Luenberger state observers. Similarly as the H_2-optimal state observer, which is known as the Kalman filter, the design method of H_∞-optimal Luenberger state observers has been well known in the literature. The conventional formulation of H_∞ state observers does not, however, allow the augmentation of dynamic performance weightings in the optimization setup, since it makes the problem a nonconvex optimization problem. It is shown that the proposed H_∞ optimization algorithm of fixed-structure controllers can be also applied to such cases. This dissertation demonstrates an explicit design method of the estimation error dynamics of Luenberger state observers in the frequency domain by using H_∞ optimization.

Application Example: As an application example in which the frequency-domain es-

timation error performance of a Luenberger state observer is particularly important, the proposed approach is applied to the design of fault detection filters for lateral control of automated passenger vehicles. Simulation results show the effectiveness of the proposed approach in designing the estimation error dynamics of state observers.

H_∞ Optimization of Mismatched State Observers

The final contribution of this dissertation is the extension of the H_∞ optimization of Luenberger state observers to the design of more general mismatched state observers, and a novel application of H_∞-optimal mismatched state observers to the observer-based feedback control. The mismatched state observer is tuned by using H_∞ optimization such that it not only provided good estimation of state variables of the plant, but also stabilized the overall closed-loop system under the feedback linearization control scheme.

Application Example: The proposed approach is applied to the design of a state observer for the lateral control of HDVs. Numerical simulations demonstrate that the feedback linearization control scheme and the proposed mismatched state observer show favorable closed-loop responses for a wide range of longitudinal velocities of the vehicle.

1.3 Outline of the Dissertation

The remainder of this dissertation is organized as follows. Chapter 2 presents a brief review of convex optimization and the LMI-based H_∞ control optimization algorithms, which are essential to understanding the contributions of this dissertation. In Chapter 3, the H_∞ and

scaled-H_∞ optimization algorithms of fixed-structure controllers are proposed. Three application examples of the fixed-structure H_∞ controller optimization are presented. Chapter 4 presents the BMI formulation of H_∞ optimization problems for their further extension to more general problems. The rank minimization approach to solve general BMI problems is proposed. Chapters 5 and 6 discuss design methodologies of H_∞-optimal state observers. First, the H_∞ optimization algorithm of Luenberger state observers is presented in Chapter 5. Chapter 6 presents the H_∞ optimization algorithm of mismatched state observers and its application to state estimation under the feedback linearization control scheme.

1.4 Notation

The following notation will be used throughout the dissertation.

For a square matrix $X \in \mathbb{R}^{n\times n}$, $X \succ 0$, $X \succeq 0$, $X \prec 0$ and $X \preceq 0$ denote that X is symmetric and positive definite, positive semidefinite, negative definite, and negative semidefinite, respectively.

$P(s) : \left[\begin{array}{c|c} A & B \\ \hline C & D \end{array}\right]$ denotes that $P(s)$ is a dynamic system with the following state space representation in the continuous-time domain:

$$\begin{aligned} \dot{x}(t) &= Ax(t) + Bu(t) \\ y(t) &= Cx(t) + Dy(t) \end{aligned} \tag{1.1}$$

where $u(t)$ and $y(t)$ denote the input and output vectors, respectively, and $x(t)$ denotes the state vector.

Consider the interconnected system of two dynamic systems $P(s)$ and $C(s)$ shown in Fig-

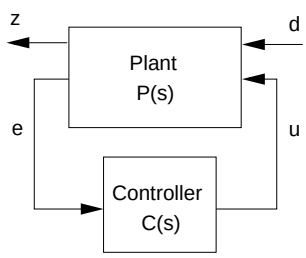

(a) Lower LFT

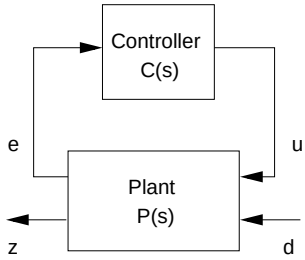

(b) Upper LFT

Figure 1.1: Lower and upper linear linear fractional transformations (LFTs)

ure 1.1 (a). Suppose the plant $P(s)$ is partitioned as follows:

$$P(s) = \begin{bmatrix} P_{11}(s) & P_{12}(s) \\ P_{21}(s) & P_{22}(s) \end{bmatrix} \tag{1.2}$$

where $P_{22}^T(s)$ has the same dimensions as $C(s)$. The lower linear fractional transformation (LFT), $F_L(P(s), C(s))$, is defined as follows:

$$F_L(P(s), C(s)) := P_{11}(s) + P_{12}(s)C(s)(I - P_{22}(s)C(s))^{-1}P_{21}(s)\,. \tag{1.3}$$

Notice that $F_L(P(s), C(s))$ is equal to the closed-loop transfer function from d to z in Figure 1.1 (a).

Similarly, the upper LFT, $F_U(P(s), C(s))$, is defined as follows:

$$F_U(P(s), C(s)) := P_{22}(s) + P_{21}(s)C(s)(I - P_{11}(s)C(s))^{-1}P_{12}(s)\,. \tag{1.4}$$

where $P_{11}^T(s)$ has the same dimensions as $C(s)$. Notice that $F_U(P(s), C(s))$ is equal to the closed-loop transfer function from d to z in Figure 1.1 (b).

$tr(X)$ denotes the trace function of a square matrix X, i.e. the sum of all diagonal entries of X.

$dom\ f$ denotes the domain of a function f.

$\lambda_i(X)$ denotes the i-th eigenvalue of a matrix X. $\lambda_{max}(X)$ and $\lambda_{min}(X)$ denote the maximum and minimum eigenvalues of X, respectively.

Chapter 2

Preliminaries: Convex Optimization and LMI-based H_∞ Controller Synthesis Theories

2.1 Introduction

This chapter presents a brief review of convex optimization and LMI (linear matrix inequality)-based H_∞ controller synthesis theories, which are essential to understanding the contributions of this dissertation. Advanced readers may skip this chapter. The materials presented in this chapter are intended to give a preliminary background to understand the following fundamental facts about H_∞ optimization problems:

1. H_∞ optimization problems of full-order controllers and state feedback controllers can

be reparameterized as convex optimization problems. Therefore, the global optimum can be numerically computed in quite an efficient and reliable manner.

2. When an additional constraint that contains the controller dynamics is imposed, however, the problem becomes a nonconvex optimization problem.

This dissertation focuses on an extension of LMI-based H_∞ optimization approaches to the problems that cannot be parameterized as a convex optimization problem.

This chapter is organized as follows. Section 2.2 gives a brief review of convex optimization and semidefinite programming (SDP). Section 2.3 reviews H_∞ optimization problems of full-order controllers and state feedback controllers. The SDP formulation of each problem is outlined. The proof of each formulation is presented to illustrate the limitations of LMI-based approaches in applying to more general problems.

2.2 Convex Optimization and SDP Problems

2.2.1 Convex Optimization Problems

This section presents a brief overview of convex optimization. See e.g. [11, 86] or any textbooks of mathematical programming for further details.

First, definitions of a convex set, a convex function, and a convex optimization problem are given.

Definition 1 (Convex set) *A set C is* convex *if the line segment between any two points in C lies in C, i.e. if for any x_1,$x_2 \in C$ and any θ with $0 \leq \theta \leq 1$, the following holds:*

$$\theta x_1 + (1-\theta)x_2 \in C\,. \tag{2.1}$$

Definition 2 (Convex function) *A function* $f : \mathbb{R}^n \to \mathbb{R}$ *is* convex *if* dom$f$ *is a convex set and if*

$$f(\theta x + (1-\theta)y) \leq \theta f(x) + (1-\theta)f(y) \tag{2.2}$$

for any x,$y \in$ dom$f$, *and* θ *with* $0 \leq \theta \leq 1$.

Geometrically, this inequality means that the line segment between $(x, f(x))$ and $(y, f(y))$ lies above the graph of f.

Similarly, a function f is called *concave* if $-f$ is convex.

Definition 3 (Convex optimization problem) *The minimization problem of a convex function over the optimization variable* $x \in \mathbb{R}^n$ *subject to inequality constraints on convex functions of* x *and equality constraints on affine functions of* x *is* a convex optimization problem, *i.e.*

$$\begin{aligned} &\min_{x \in \mathbf{R}^n} \ f_0(x) \\ &\text{subject to} \quad f_i(x) \ \leq \ 0 \qquad (i = 1, \cdots, m) \\ &\qquad\qquad a_i^T x \ = \ b_i \qquad (i = 1, \cdots, p) \end{aligned} \tag{2.3}$$

where f_0,$\cdots$,f_m *are convex functions.*

A fundamental property of convex optimization problems is that any local optimum is also globally optimal. The local and global optima for general optimization problems are defined as follows:

Definition 4 (Local and global optima) *Given a general optimization problem,*

$$\begin{aligned} &\min_{x \in \mathbf{R}^n} \ f_0(x) \\ &\text{subject to} \quad f_i(x) \ \leq \ 0 \qquad (i = 1, \cdots, m) \\ &\qquad\qquad h_i(x) \ = \ 0 \qquad (i = 1, \cdots, p) \end{aligned} \tag{2.4}$$

x is locally optimal if x is feasible (i.e. x satisfies all the constraints) and

$$f_0(x) = \inf_{z \in \mathbf{R}^n} \{f_0(z) \mid z \text{ is feasible, } \|z - x\| \leq R\} \tag{2.5}$$

for some $R > 0$. If Eq. (2.5) holds for any feasible z (i.e. $R = \infty$), then x is globally optimal.

Theorem 1 (Global optimum of convex optimization problem) *Suppose x is locally optimal for the convex optimization problem (2.3). Then, x is also globally optimal.*

Consider an unconstrained minimization problem of a convex objective function, $f_0(x)$, over a variable, $x \in \mathbb{R}^n$. When $f_0(x)$ is differentiable, Theorem 1 assures that the global optimum, x^*, can be found by simply computing the solution of $\nabla f(x^*) = 0$, where $\nabla f(x)$ denotes the gradient of f at $x \in \mathbb{R}^n$, i.e. $\nabla f(x) := \left\{ \frac{\partial f}{\partial x_1}, \cdots, \frac{\partial f}{\partial x_n} \right\}^T$. Such a problem can be solved in quite an efficient manner by iterative algorithms, which compute a sequence of points $x^{(0)}, x^{(1)}, \cdots$ with $f(x^{(k)})$ converging to the optimal point as $k \to \infty$. A considerable number of descent methods have been studied, which are guaranteed to generate a decreasing sequence of $f(x^{(k)})$ and to reach the global optimum. The global minimum of convex functions can be always found by simply "going down" from any starting points, unlike nonconvex optimization problems, which can have multiple local minimums.

This fundamental property of convex optimization problems is preserved in constrained problems. The combination of the following two theorems shows that the $m + p$ constraints in the problem (2.3) indeed form a convex set.

Theorem 2 (Sublevel set of a convex function) *Define the α-sublevel set C_α of a function $f : \mathbb{R}^n \to \mathbb{R}$ by*

$$C_\alpha = \{x \in \operatorname{dom} f \mid f(x) \leq \alpha\} \ . \tag{2.6}$$

Sublevel sets of a convex function are convex.

Theorem 3 (Intersection of convex sets) *The intersection of convex sets is also convex, i.e. if sets S_i $(i = 1,\cdots,n)$ are all convex, then their intersection $\cap_{i\in[1,n]}S_i$ is also convex.*

In the field of applied mathematics, numerous research efforts have been devoted to developing efficient numerical algorithms to solve convex optimization problems. In particular, linear programming (LP) and semidefinite programming (SDP), which can be regarded as an extension of LP, have been the subject of intense research due to their obvious applicability to numerous practical problems.

The following sections mainly focus on SDP problems. Section 2.2.2 presents the definition of SDP problems and then briefly discusses their important roles in control-related problems. Section 2.2.3 presents an overview of numerical algorithms to solve SDP problems.

2.2.2 Semidefinite Programming (SDP)

Consider the following problem of minimizing a linear function of a variable $x \in \mathbb{R}^m$ subject to a matrix inequality:

$$\begin{aligned} &\min_{x\in\mathbf{R}^m} \; c^T x \\ &\text{subject to} \quad F(x) \;\preceq\; 0 \end{aligned} \tag{2.7}$$

where

$$F(x) := F_0 + \sum_{i=1}^{m} x_i F_i \; . \tag{2.8}$$

$c \in \mathbb{R}^m$ and $m+1$ symmetric matrices $F_0, \cdots, F_m \in \mathbb{R}^{n\times n}$ are given. Notice that $F(x) \preceq 0$ denotes that $F(x)$ is symmetric and negative semidefinite (see Section 1.4).

Definition 5 (SDPs and LMIs) *The inequality* $F(x) \preceq 0$ *is* a linear matrix inequality (LMI) *and the problem* (2.7) *is* a semidefinite program (SDP).

Since $F(x)$ is symmetric, the necessary and sufficient condition for $F(x)$ to be negative semidefinite is that the largest eigenvalue of $F(x)$ is smaller than or equal to zero. From the fact that the largest eigenvalue of a symmetric matrix $X \in \mathbb{R}^{n\times n}$ is a convex function of X (see [11] for the proof), one can easily see that the constraint, $F(x) \preceq 0$, forms a convex set. LMI constraints are nonlinear and nonsmooth, but convex. Therefore, SDP problems are convex optimization problems.

Many control-related optimization problems can be written in the SDP form. For example, consider the following problem:

$$\begin{aligned} &\text{minimize} \quad \gamma \\ &\text{over} \quad \gamma \in \mathbb{R},\ X \in \mathbb{R}^{n\times n} \\ &\text{subject to} \quad \begin{bmatrix} A^TX + XA & XB & C^T \\ B^TX & -\gamma I & D^T \\ C & D & -\gamma I \end{bmatrix} \prec 0 \\ &\qquad\qquad\qquad\qquad\qquad\qquad\qquad\qquad X \succ 0 \end{aligned} \tag{2.9}$$

where A,B,C, and D are constant matrices with appropriate dimensions. The optimal solution γ^* of the above problem is equal to the H_∞ norm of the continuous system given in the state space representation, $P(s) : \left[\begin{array}{c|c} A & B \\ \hline C & D \end{array}\right]$ (see Lemma 1 in Section 2.3.2). The above problem belongs to the class of SDP; the inequality constraints can be rewritten in the form (2.7) with the optimization variable, $x \in \mathbb{R}^{0.5n(n+1)+1}$, consisting of each entry of $X \in \mathbb{R}^{n\times n}$ (notice that X is constrained to be symmetric) and $\gamma \in \mathbb{R}$.

It implies that the H_∞ norm of a linear system, $P(s)$, can be computed by solving an SDP

problem. Note that this is merely an illustrative example of SDP problems appearing in control problems. In practice, there are more efficient ways to compute the H_∞ norm of a linear system than this approach [9, 12].

The SDP framework has recently attracted great attention in various fields of optimization for the following reasons. First, and most importantly, SDP problems can be solved very efficiently, both in theory and in practice, by using well-developed interior-point methods. Secondly, the SDP framework offers a unified approach to formulate many convex optimization problems, such as LPs and (convex) quadratically constrained quadratic programs (see [110] for more problems that can be formulated in SDP form).

2.2.3 Algorithms and Softwares for Solving SDPs

This section gives an overview of algorithms to solve SDPs. For further details, see [110, 10, 22] and the references therein.

SDP problems can be regarded as extensions of LPs. LPs are generally formulated as follows:

Definition 6 (LP) *The problem of minimizing a linear function of a variable $x \in \mathbb{R}^m$ subject to a componentwise vector inequality is called* linear programming (LP):

$$\begin{aligned} \min_{x \in \mathbf{R}^m} \; & c^T x \\ \text{subject to} \quad & Ax + b \;\; \geq \;\; 0 \end{aligned} \tag{2.10}$$

where $A \in \mathbb{R}^{n \times m}$ and $b \in \mathbb{R}^n$. The inequality denotes the componentwise inequality.

Extensive research has been devoted for decades to develop algorithms to solve general LPs in polynomial time (with respect to the problem size and the required accuracy).

The simplex method, which is still considered the fastest algorithm in practice for solving LP problems of small or medium size, is a non-polynomial time algorithm in theory, i.e. the effort required to solve an LP problem to a given accuracy grows exponentially in worst cases as the problems size becomes larger. The ellipsoid method proposed in the late 1970s by Yudin and Nemirovski [123] and Shor [96] claimed a polynomial worst-case computational complexity. In many practical applications, however, it is much slower than simplex methods. In 1984, Karmarkar introduced the interior-point method for LPs [64], which is guaranteed to solve LPs in polynomial time and, in contrast to the ellipsoid method, is also very effective in practice. Nesterov and Nemirovski [79] showed in the late-1980s that the interior-point method for LPs can be, in principle, generalized to all convex optimization problems. Generalization of interior-point methods from LPs to SDPs was discussed by Alizadeh [1] and Kamath and Karmarkar [61]. Although SDP problems are much more general than LP problems, interior-point methods can be readily applied, and thus are not much harder to solve.

There has been a flurry of papers on development of more efficient interior-point methods to solve SDPs. Several variations of interior-point methods have been implemented on publicly available software. Throughout this dissertation, the following software will be used to solve SDPs.

- **LMI Control Toolbox** developed by Gahinet et al. [34]. It is a commercial software package for use on *MATLAB*. The algorithm is based on Nesterov and Nemirovski's projective algorithm [77].

- **SP** developed by Vandenberghe and Boyd [109] and its *MATLAB* interface **LMI-TOOL** developed by El Ghaoui et al. [36]. The algorithm is based on Nesterov and

Todd's primal-dual potential reduction method [80].

A list of software packages available for SDPs can be found in [22].

2.3 LMI-based H_∞ Controller Synthesis Algorithms

2.3.1 Problem Statement

The H_∞-optimal controller synthesis problem is formulated as follows. Suppose the closed-loop system is given as shown in Figure 1.1 (a) where the plant model, $P(s)$, and the controller, $C(s)$, are assumed to be real, rational and proper continuous-time transfer function matrices. Suppose that the plant model, $P(s)$, can be written in the following continuous-time state space representation:

$$\begin{aligned} \dot{x}(t) &= Ax(t) + B_1 d(t) + B_2 u(t) \\ z(t) &= C_1 x(t) + D_{11} d(t) + D_{12} u(t) \\ e(t) &= C_2 x(t) + D_{21} d(t) + D_{22} u(t)\,. \end{aligned} \tag{2.11}$$

The plant dimensions are summarized by $A \in \mathbb{R}^{n\times n}$, $D_{11} \in \mathbb{R}^{p_1\times m_1}$, and $D_{22} \in \mathbb{R}^{p_2\times m_2}$. The following assumptions are imposed on the plant parameters.

1. $(A,\ B_2,\ C_2)$ is stabilizable and detectable.

2. $D_{22} = 0_{p_2\times m_2}$.

Notice that neither of the assumptions is restrictive in practice; the first assumption is necessary and sufficient to allow for plant stabilization by dynamic output feedback. The second assumption incurs no loss of generality while it considerably simplifies calculations

for H_∞ optimization [37].

Suppose that the controller dynamics, $C(s)$, is given in the following state space representation:

$$\begin{aligned} \dot{x}_K(t) &= A_c x_K(t) + B_c e(t) \\ u(t) &= C_c x_K(t) + D_c e(t) \end{aligned} \tag{2.12}$$

where $A_c \in \mathbb{R}^{k\times k}$, and the dimensions of B_c, C_c, and D_c are compatible with $P(s)$ given in Eq. (2.11).

The objective of the H_∞-optimal controller synthesis problem is to find a controller $C(s)$ (i.e. A_c, B_c, C_c, and D_c) such that: 1) the closed-loop system is internally stable, and 2) the H_∞ norm of $F_L(P(s), C(s))$, i.e. the closed-loop transfer function from d to z in Figure 1.1(a), is minimized.

The discrete-time version of the H_∞-optimal controller synthesis problem is defined in an analogous way.

It is often more convenient to look for a controller, $C(s)$, that achieves the closed-loop H_∞ norm $\|F_L(P(s), C(s))\|_\infty$ less than a given constant level $\gamma > 0$, rather than one that minimizes $\|F_L(P(s), C(s))\|_\infty$. The controller, $C(s)$, that 1) internally stabilizes the closed-loop system, and 2) achieves $\|F_L(P(s), C(s))\|_\infty < \gamma$ for a given $\gamma > 0$, is called the H_∞ γ-suboptimal controller.

The conventional full-order H_∞ (sub-)optimization algorithm, which will be outlined in Section 2.3.3, assumes that: 1) the controller $C(s)$ is full-order, i.e. the order of the controller is the same as that of the plant model $P(s)$ ($k = n$), and 2) every entry of (A_c, B_c, C_c, D_c) is freely tunable.

Numerous theoretical and application works on H_∞ control have been reported since the

1980s. To understand motivation for the introduction of H_∞ optimization to the design of controllers, readers are referred to [125, 41] and many others. The robustness of the closed-loop system against modeling uncertainties or external disturbances is clearly one of the most important motivations. In this dissertation, however, the H_∞ optimization is mainly used as a tool to explicitly design frequency responses of the closed-loop system. Although this approach does not explicitly deal with the robustness of the closed-loop system, it is simple and quite useful for the design of practical controllers, as shown in application examples presented in the later chapters. It should be emphasized that *the H_∞ controller synthesis is merely a mathematical minimization problem, and that the robust controller design is only one of its applications.*

2.3.2 LMI-based H_∞ State Feedback Controller Synthesis Algorithm

The following two special cases of H_∞ optimization problems can be formulated as SDP problems: 1) the state feedback controller synthesis case and 2) the full-order controller synthesis case. Both problems were solved by the ARE-based approaches in the late 1980s by Peterson [87] (state feedback and full-information H_∞ optimal control) and Doyle et al. [18] (full-order H_∞ optimal control), respectively. In the mid-1990s, Gahinet and Apkarian [33] and Iwasaki and Skelton [60] showed that both problems can be reformulated as SDP problems, and thus their numerical solutions can be quite efficiently computed, although an analytical or closed-form solution cannot be offered.

This section presents a brief review of the LMI formulation of the H_∞ optimization problem of state feedback controllers. The materials presented in the following two sections are crucial to understanding the difficulties of applying LMI-based approaches to more general

problems than the above two problems. Although the state feedback controller synthesis problem is not practical in most applications, its LMI formulation is much more straightforward to understand than that of the full-order controller synthesis case. Furthermore, the H_∞ optimization algorithm of Luenberger state observers with static weightings, which will be presented in Section 5.2, is a direct extension of this formulation.

The problem is formulated as follows. All state variables of the plant, $P(s)$, given in Eq. (2.11) are assumed available, i.e. $C_2 = I_n$ and $D_{21} = 0_{p_2 \times m_1}$. The problem is to find the H_∞-optimal state feedback gain matrix, $K \in \mathbb{R}^{m_2 \times n}$, such that $\|F_L(P(s), K)\|_\infty$ is minimized.

The following lemma is crucial to interpret an H_∞ norm constraint as an LMI constraint.

Lemma 1 (Bounded Real Lemma for Continuous-time Systems)

Consider a continuous-time transfer function, $T(s)$, of the (not necessarily minimal) realization $T(s) = D + C(sI - A)^{-1}B$. Then, $\|T(s)\|_\infty < \gamma$ for $\gamma > 0$ and A is asymptotically stable (i.e. $\mathrm{Re}(\lambda_i(A)) < 0$) if and only if there exists a symmetric positive definite matrix, X, that satisfies the following LMI:

$$\begin{bmatrix} A^T X + XA & XB & C^T \\ B^T X & -\gamma I & D^T \\ C & D & -\gamma I \end{bmatrix} \prec 0 \,. \tag{2.13}$$

See e.g. [126] for the proof. By directly applying Lemma 1 to the closed-loop system, $F_L(P(s), K)$, it can be easily observed that the H_∞-optimal solution, K^*, can be computed by solving the following SDP problem.

Lemma 2 (H_∞-optimal State Feedback Controller Synthesis)

The continuous-time H_∞-optimal state feedback gain matrix, K^*, can be obtained by $K^* =$

FX^{-1}, where $(F,\ X)$ is the optimal solution set of the following SDP problem:

$$\begin{aligned}
&\text{minimize} \quad \gamma \\
&\text{over} \quad X \in \mathbb{R}^{n\times n},\ F \in \mathbb{R}^{m_2\times n} \quad \text{and} \quad \gamma \in \mathbb{R} \\
&\text{subject to} \quad \begin{bmatrix} AX + XA^T + B_2F + F^TB_2^T & B_1 & (C_1X + D_{12}F)^T \\ B_1^T & -\gamma I & D_{11}^T \\ C_1X + D_{12}F & D_{11} & -\gamma I \end{bmatrix} \prec 0 \\
&\qquad\qquad\qquad\qquad\qquad\qquad\qquad\qquad\qquad\qquad X \succ 0\,.
\end{aligned} \tag{2.14}$$

Proof: By combining the plant model (2.11), and the state feedback law, $u(t) = Kx(t)$, the closed-loop system dynamics is given as follows:

$$\begin{aligned}
\dot{x}(t) &= (A + B_2K)x(t) + B_1d(t) \\
e(t) &= (C_1 + D_{12}K)x(t) + D_{11}d(t)\,.
\end{aligned} \tag{2.15}$$

Notice that the existence of $X \succ 0$ satisfying Eq. (2.13) is equivalent to that of $X \succ 0$ satisfying:

$$\begin{bmatrix} AX + XA^T & B & XC^T \\ B^T & -\gamma I & D^T \\ CX & D & -\gamma I \end{bmatrix} \prec 0\,. \tag{2.16}$$

Therefore, the H_∞ norm of the closed-loop system (2.15) is less than $\gamma > 0$ if and only if there exists a positive definite symmetric matrix, $X \in \mathbb{R}^{n\times n}$, such that

$$\begin{bmatrix} (A + B_2K)X + X(A + B_2K)^T & B_1 & X(C_1 + D_{12}K)^T \\ B_1^T & -\gamma I & D_{11}^T \\ (C_1 + D_{12}K)X & D_{11} & -\gamma I \end{bmatrix} \prec 0\,. \tag{2.17}$$

Although there are bilinear terms of variables K and X in the constraint (2.17), it can be equivalently transformed into the first LMI constraint in (2.14) by simply introducing the

new variable $F := KX \in \mathbb{R}^{m_2 \times n}$. Since the problem (2.14) is an SDP problem, it has a unique optimal solution. Also notice that X is always invertible, since it is restricted to be strictly positive definite. Therefore, the H_∞ optimal state feedback gain matrix, K^*, can be uniquely obtained. □

The discrete-time version of this problem can be solved in an analogous way. The Bounded Real Lemma for discrete-time systems is given as follows.

Lemma 3 (Bounded Real Lemma for Discrete-time Systems)

Consider a discrete-time transfer function, $T(s)$, of the (not necessarily minimal) realization $T(s) = D + C(zI - A)^{-1}B$. Then, $\|T(z)\|_\infty < \gamma$ for $\gamma > 0$ and A is asymptotically stable in the discrete-time sense (i.e. $|\lambda_i(A)| < 1$) if and only if there exists a symmetric positive definite matrix, X, that satisfies the following LMI:

$$\begin{bmatrix} A^T & C^T \\ B^T & D^T \end{bmatrix} \begin{bmatrix} X & 0 \\ 0 & I \end{bmatrix} \begin{bmatrix} A & B \\ C & D \end{bmatrix} - \begin{bmatrix} X & 0 \\ 0 & \gamma I \end{bmatrix} \prec 0\,. \tag{2.18}$$

The analogous SDP problem for finding the H_∞-optimal state feedback controller for discrete-time systems can be derived in the same way as shown in Lemma 2.

2.3.3 LMI-based H_∞ Full-order Controller Synthesis Algorithm

This section considers the more general case where the controller is a dynamic output feedback controller whose state space representation is given in the form (2.12). The problem is to find (A_c, B_c, C_c, D_c) such that the closed-loop H_∞ norm, $\|F_L(P(s), C(s))\|_\infty$, is minimized, where $P(s)$ is a given plant model in the form (2.11).

The standard LMI-based H_∞ full-order controller synthesis algorithm is based on the following result by Gahinet and Apkarian [33]:

Theorem 4 (Solvability of Continuous-time H_∞ Controller Synthesis Problems) *There exists a dynamic controller, $C(s)$, of order k such that $\|F_L(P_K(s), C(s))\|_\infty < \gamma$ if and only if there exist two symmetric matrices $X \in \mathbb{R}^{n\times n}$ and $Y \in \mathbb{R}^{n\times n}$ such that*

$$\mathcal{N}_1^T \begin{bmatrix} AX + XA^T & XC_1^T & B_1 \\ C_1X & -\gamma I & D_{11} \\ B_1^T & D_{11}^T & -\gamma I \end{bmatrix} \mathcal{N}_1 \prec 0 \tag{2.19}$$

$$\mathcal{N}_2^T \begin{bmatrix} A^TY + YA & YB_1 & C_1^T \\ B_1^TY & -\gamma I & D_{11}^T \\ C_1 & D_{11} & -\gamma I \end{bmatrix} \mathcal{N}_2 \prec 0 \tag{2.20}$$

$$\begin{bmatrix} X & I \\ I & Y \end{bmatrix} \succeq 0 \tag{2.21}$$

$$\operatorname{rank}(XY - I) \leq k \tag{2.22}$$

where $\mathcal{N}_1 = \operatorname{diag}\{N_{12}, I\}, \mathcal{N}_2 = \operatorname{diag}\{N_{21}, I\}$. N_{12} and N_{21} are bases of the null space of $\begin{bmatrix} B_2^T & D_{12}^T \end{bmatrix}$ and $\begin{bmatrix} C_2 & D_{21} \end{bmatrix}$, respectively.

First, notice that in the full-order controller synthesis case, i.e. $k \geq n$, the constraint (2.22) is trivially satisfied for any X and Y. Therefore, the problem for finding X and Y that satisfy the constraints (2.19)$\sim$(2.22) becomes an SDP problem.

The complete proof of Theorem 4 can be found in [33]. However, in order to help readers understand the limitation of the LMI-based approach for the application to the more general class of H_∞ optimization problems, this section presents an outline of the proof of

Theorem 4.

First, recall the following lemmas as well as the Bounded Real Lemma (Lemma 1), which play a central role in the proof.

Lemma 4 (Elimination Lemma) *Given a symmetric matrix $\Psi \in \mathbb{R}^{m\times m}$ and two matrices P, Q of column dimension* m*, consider the problem to find a matrix Θ of compatible dimensions such that*

$$\Psi + P^T\Theta^T Q + Q^T\Theta P \prec 0\,. \tag{2.23}$$

Denote by W_P and W_Q any matrices whose columns form bases of the null space of P and Q, respectively. Then, the problem (2.23) *is solvable for Θ if and only if*

$$\begin{cases} W_P^T\Psi W_P \prec 0 \\ W_Q^T\Psi W_Q \prec 0\,. \end{cases} \tag{2.24}$$

Lemma 5 (Schur Complement) *The block matrix* $\begin{bmatrix} P & M \\ M^T & Q \end{bmatrix}$ *is negative definite if and only if*

$$\begin{cases} Q \prec 0 \\ P - MQ^{-1}M^T \prec 0\,. \end{cases} \tag{2.25}$$

$P - MQ^{-1}M^T$ is called the Schur complement of Q.

Overview of Proof of Theorem 4: From the plant model (2.11) and the controller (2.12), a (not necessarily minimal) state space representation of the closed-loop system, $F_L(P(s), C(s))$, is given as follows:

$$\begin{aligned} \dot{x}_{cl}(t) &= A_{cl}x_{cl}(t) + B_{cl}w(t) \\ z(t) &= C_{cl}x_{cl}(t) + D_{cl}w(t) \end{aligned} \tag{2.26}$$

where $x_{cl}(t) = [x(t)^T \quad x_K(t)^T]^T$ and

$$\begin{aligned} A_{cl} &:= \begin{bmatrix} A + B_2 D_c C_2 & B_2 C_c \\ B_c C_2 & A_c \end{bmatrix}; \quad B_{cl} := \begin{bmatrix} B_1 + B_2 D_c D_{21} \\ B_c D_{21} \end{bmatrix}; \\ C_{cl} &:= \begin{bmatrix} C_1 + D_{12} D_c C_2 \\ D_{12} C_c \end{bmatrix}; \qquad D_{cl} := D_{11} + D_{12} D_c D_{21}. \end{aligned} \tag{2.27}$$

The closed-loop system matrices can be rewritten as

$$A_{cl} = A_0 + \mathcal{B}\Theta\mathcal{D}_{21}; \quad B_{cl} = B_0 + \mathcal{B}\Theta\mathcal{C}; \quad C_{cl} = C_0 + \mathcal{D}_{12}\Theta\mathcal{C}; \quad D_{cl} = D_{11} + \mathcal{D}_{12}\Theta\mathcal{D}_{21}, \tag{2.28}$$

by using the shorthands:

$$\begin{aligned} A_0 &:= \begin{bmatrix} A & 0 \\ 0 & 0_k \end{bmatrix}; \quad B_0 := \begin{bmatrix} B_1 \\ 0 \end{bmatrix}; \qquad C_0 := \begin{bmatrix} C_1 & 0 \end{bmatrix}; \\ \mathcal{B} &:= \begin{bmatrix} 0 & B_2 \\ I_k & 0 \end{bmatrix}; \quad \mathcal{C} := \begin{bmatrix} 0 & I_k \\ C_2 & 0 \end{bmatrix}; \quad \mathcal{D}_{12} := \begin{bmatrix} 0 & D_{12} \end{bmatrix}; \quad \mathcal{D}_{21} = \begin{bmatrix} 0 \\ D_{21} \end{bmatrix}, \end{aligned} \tag{2.29}$$

and

$$\Theta = \begin{bmatrix} A_c & B_c \\ C_c & D_c \end{bmatrix}. \tag{2.30}$$

From the Bounded Real Lemma (Lemma 1), the controller (2.12) is an H_∞ γ-optimal controller if and only if there exists a symmetric positive definite matrix, $X_{cl} \in \mathbb{R}^{(n+k)\times(n+k)}$, that satisfies:

$$\begin{bmatrix} A_{cl}^T X_{cl} + X_{cl} A_{cl} & X_{cl} B_{cl} & C_{cl}^T \\ B_{cl}^T X_{cl} & -\gamma I & D_{cl}^T \\ C_{cl} & D_{cl} & -\gamma I \end{bmatrix} \prec 0\,. \tag{2.31}$$

By using the expression (2.28) of $A_{cl}, B_{cl}, C_{cl}, D_{cl}$, the above relation can be rewritten as:

$$\Psi_{X_{cl}} + \mathcal{Q}^T \Theta^T \mathcal{P}_{X_{cl}} + \mathcal{P}_{X_{cl}}^T \Theta \mathcal{Q} \prec 0 \tag{2.32}$$

where

$$\Psi_{X_{cl}} := \begin{bmatrix} A_0^T X_{cl} + X_{cl} A_0 & X_{cl} B_0 & C_0^T \\ B_0^T X_{cl} & -\gamma I & D_{11}^T \\ C_0 & D_{11} & -\gamma I \end{bmatrix};$$

$$\mathcal{Q} := \begin{bmatrix} \mathcal{C}, & \mathcal{D}_{21}, & 0_{(k+p_2)\times p_1} \end{bmatrix}, \quad \mathcal{P}_{X_{cl}} := \begin{bmatrix} \mathcal{B}^T X_{cl}, & 0, & \mathcal{D}_{12}^T \end{bmatrix}. \tag{2.33}$$

Therefore, the set of γ-suboptimal controllers of order k is nonempty if and only if Eq. (2.32) holds for some $\Theta \in \mathbb{R}^{(k+m_2)\times(k+p_2)}$ and $X_{cl} \succ 0$. Notice that there are bilinear terms in the constraint (2.32) with respect to Θ and X_{cl}. The Elimination Lemma (Lemma 4) can now be invoked to equivalently transform the solvability condition (2.32) into a form depending only on X_{cl} and plant parameters. Let $W_{\mathcal{P}_{X_{cl}}}$ and $W_{\mathcal{Q}}$ denote matrices whose columns form bases of the null space of $\mathcal{P}_{X_{cl}}$ and $\mathcal{Q}$, respectively. Then, by Lemma 4, the constraint (2.32) holds for some Θ if and only if

$$W_{\mathcal{P}_{X_{cl}}}^T \Psi_{X_{cl}} W_{\mathcal{P}_{X_{cl}}} \prec 0\,; \qquad W_{\mathcal{Q}}^T \Psi_{X_{cl}} W_{\mathcal{Q}}^T \prec 0\,. \tag{2.34}$$

Furthermore, it is straightforward to see that the existence of X_{cl} satisfying (2.34) is equivalent to that of X_{cl} satisfying

$$W_{\mathcal{P}}^T \Phi_{X_{cl}} W_{\mathcal{P}} \prec 0\,; \qquad W_{\mathcal{Q}}^T \Psi_{X_{cl}} W_{\mathcal{Q}}^T \prec 0 \tag{2.35}$$

where

$$\Phi_{X_{cl}} := \begin{bmatrix} A_0^T X_{cl}^{-1} + X_{cl}^{-1} A_0 & B_0 & X_{cl}^{-1} C_0^T \\ B_0^T & -\gamma I & D_{11}^T \\ C_0 X_{cl}^{-1} & D_{11} & -\gamma I \end{bmatrix}, \tag{2.36}$$

and $W_{\mathcal{P}}$ is a matrix whose columns form bases of the null space of $\mathcal{P}$. The constraints in (2.35) are still not convex because they involve both X_{cl} and its inverse. Fortunately,

they can be further reduced to a pair of Ricatti inequalities of lower dimension that are convex constraints. First, partition X_{cl} and X_{cl}^{-1} as follows:

$$X_{cl} := \begin{bmatrix} Y & N \\ N^T & * \end{bmatrix}; \qquad X_{cl}^{-1} := \begin{bmatrix} X & M \\ M^T & * \end{bmatrix}, \tag{2.37}$$

where $X, Y \in \mathbb{R}^{n\times n}$ and $M, N \in \mathbb{R}^{n\times k}$.

By using this partition, the condition $W_{\mathcal{P}}^T \Phi_{X_{cl}} W_{\mathcal{P}} \prec 0$ is equivalently reduced to the constraint (2.19) (See [33] for further details of this transformation). Similarly, the condition $W_{\mathcal{Q}}^T \Psi_{X_{cl}} W_{\mathcal{Q}}^T \prec 0$ is reduced to the constraint (2.20). □

Theorem 4 only addresses the existence of a solution and does not include the computation of the optimal controller. The system matrices of the H_∞ γ-suboptimal controller, Θ, can be obtained as follows. Once X and Y satisfying (2.19)∼(2.22) are found, X_{cl} can be reconstructed from Eq. (2.37) by using the singular value decomposition (SVD) (see [33]). Then, Θ can be computed by solving (2.32). Notice that when X_{cl} is given, Eq. (2.32) becomes an LMI with respect to Θ, and thus the problem of finding Θ is a convex optimization problem. In practice, the explicit and numerically more reliable formulas for computing the optimal controller, Θ, are available (Gahinet [32]).

Theorem 4 states that: 1) the controller that achieves the minimum $\|F_L(P(s), C(s)\|_\infty$ is, at most, the same order as the plant $P(s)$, and 2) the H_∞-optimal controller of the same order as the plant, $P(s)$, can be computed by solving convex optimization problems. In the case where the order of the controller is restricted to less than the plant order, however, the problem becomes a nonconvex optimization problem due to the rank constraint (2.22). Furthermore, the SDP formulation of the H_∞ optimization problem clarifies the difficulties of imposing an additional constraint on the controller system matrices, because the SDP

formulation (2.19)$\sim$(2.21) no longer contains the set of controller system matrices, Θ.

This dissertation focuses on solving the problems that cannot be globally solved by convex optimization. Chapter 3 presents an algorithm for solving the H_∞ optimization problem of fixed-structure controllers via the reduced-order H_∞-optimal controller synthesis. In Chapter 4, the BMI formulation is discussed to solve a more general class of H_∞ optimization problems that cannot be parameterized as SDP problems.

The result presented in Theorem 4 for continuous-time cases can be easily transposed to the discrete-time context and leads to the analogous result shown in the following theorem.

Theorem 5 (Solvability of Discrete-time H_∞ Controller Synthesis Problems)

There exists a dynamic discrete-time controller, $C(z)$, of order k such that $\|F_L(P_K(z), C(z))\|_\infty < \gamma$ if and only if there exist two symmetric matrices $X \in \mathbb{R}^{n\times n}$ and $Y \in \mathbb{R}^{n\times n}$ such that

$$\mathcal{N}_1^T \begin{bmatrix} AXA^T - X & AXC_1^T & B_1 \\ C_1XA^T & -\gamma I + C_1XC_1^T & D_{11} \\ B_1^T & D_{11}^T & -\gamma I \end{bmatrix} \mathcal{N}_1 \prec 0 \tag{2.38}$$

$$\mathcal{N}_2^T \begin{bmatrix} A^TYA - Y & A^TYB_1 & C_1^T \\ B_1^TYA & -\gamma I + B_1^TYB_1 & D_{11}^T \\ C_1 & D_{11} & -\gamma I \end{bmatrix} \mathcal{N}_2 \prec 0 \tag{2.39}$$

$$\begin{bmatrix} X & I \\ I & Y \end{bmatrix} \succeq 0 \tag{2.40}$$

$$\operatorname{rank}(XY - I) \leq k \tag{2.41}$$

where $\mathcal{N}_1 = \operatorname{diag}\{N_{12}, I\}, \mathcal{N}_2 = \operatorname{diag}\{N_{21}, I\}$. N_{12} and N_{21} are bases of the null space of

$\begin{bmatrix} B_2^T & D_{12}^T \end{bmatrix}$ *and* $\begin{bmatrix} C_2 & D_{21} \end{bmatrix}$, *respectively.*

Finally, it should be noted that the LMI-based approach to the full-order H_∞ controller synthesis problem is essentially analogous to the classical ARE-based approach proposed by Doyle et al. [18]. The ARE-based approach is often computationally more efficient for "regular" H_∞ optimization problems (i.e. the case where the plant model (2.11) satisfies the following regularity assumptions: 1) D_{12} has full column rank and D_{21} has full row rank, and 2) $P_{12}(s)$ and $P_{21}(s)$ have no invariant zero on the imaginary axis). The LMI-based approach has, however, the following important advantages: 1) it does not require that the plant model satisfies the regularity conditions, and 2) it is easier to see the possibility of extending the algorithm to more general problems, such as the reduced-order controller synthesis. The latter is a strong motivation for the works presented in the following chapters.

2.4 Summary

This chapter has presented a brief review of convex optimization and the LMI-based H_∞ controller synthesis algorithms, which are essential to understanding the contributions of this dissertation. The LMI formulation of the H_∞ optimization problem presented by Gahinet and Apkarian [33] and Iwasaki and Skelton [60] clarifies the following fundamental properties of the H_∞ optimization: 1) H_∞ optimization problems of full-order controllers and state feedback controllers can be reparameterized as convex optimization problems; therefore, the global optimum can be numerically computed in an efficient and reliable manner by using well-developed interior-point methods, and 2) when an additional con-

straint is imposed on the controller, the problem becomes nonconvex, and the LMI-based approach cannot be applied. It is simply because both formulations of the state feedback controller synthesis problem (Lemma 2) and the full-order controller synthesis problem (Theorem 4) no longer include the controller parameters, since they are eliminated in the process of transforming the problem into an SDP problem.

The next chapter will consider the case where the controller has a certain structure, and only its parameters are allowed to be tuned.

Chapter 3

H_∞ and Scaled-H_∞ Optimization of Fixed Structure Controllers

3.1 Introduction

As briefly reviewed in the previous chapter, the LMI (Linear Matrix Inequality)-based H_∞ controller synthesis theory [33, 60] guarantees that if the controller is allowed to have the same order as the plant and every system matrix of the controller is freely tunable, then the H_∞ optimization problem can be solved by convex optimization and thus the global minimum can be always found. This chapter considers the case where the controller has a fixed structure and only its parameters are tunable.

The objective of the H_∞ optimization problem considered in this chapter is to find a linear controller, $C(s)$, whose dynamics has a prescribed fixed structure denoted by $\mathcal{C}$, such that

the following H_∞ norm of the closed-loop transfer function is minimized:

$$\min_{C(s)\in\mathcal{C}} \|F_L(P(s), C(s))\|_\infty \tag{3.1}$$

where $P(s)$ denotes the given plant model. The closed-loop configuration is shown in Figure 1.1 (a).

Applications of the present optimization problem include tuning of SISO (Single-Input Single-Output) PID (Proportional plus Integral plus Derivative) controller gains. Despite of technical advances in the design and implementation of sophisticated controllers, most of industrial controllers still adopt simple structures such as PID control. Application of the H_∞ optimization theory to tuning of parameters of such fixed structure controllers is, therefore, of interest and of practical importance. The conventional H_∞ optimization typically gives a controller of high order — at least as high as and quite often much higher than the plant model due to dynamic performance weightings augmented in the optimization process to achieve the desired performance. To implement such a controller, one must redesign the entire controller structure, which often requires considerable effort and cost. For example, Section 3.5 considers the tuning problem of a PID controller for head positioning control of a magnetic hard disk drive (HDD). In this problem, a PID controller was already implemented on a microprocessor embedded in a commercial HDD system. Although it is not desirable to change the whole controller structure due to time and cost limitations, it is easy to modify the controller parameters (P-gain, I-gain, and D-gain). This chapter presents an intuitive and efficient approach to tune the controller parameters by using H_∞ optimization such that the control performance is further improved.

It should be noted, however, that H_∞ optimization is not the only tuning methodology for PID controllers. Numerous methods for tuning of PID gains have been reported in the

literature over years (see, e.g. [5]) and any fair comparison among those methods is likely to be inconclusive, since their derivations are usually based on different criteria and design philosophy. The H_∞ optimization theory has, however, enjoyed a great attention over years in the field of control and its applicability to practical problems has been reported. Especially when the robustness of the closed-loop system is one of the main concerns of the designer, H_∞ optimization is quite a useful tool. Our subsequent discussion focuses on the algorithm to solve the given H_∞ controller optimization problem.

As discussed in Section 2.3.3, a critical limitation of the LMI-based H_∞ controller synthesis algorithm is that it allows no additional constraint to be imposed on the problem; the closed-loop H_∞ norm constraint must be the only constraint imposed on the problem in order for it to be globally solvable by convex optimization. Therefore, in the case where the controller has a fixed structure and only its parameters are tunable, the problem cannot be reparameterized as a convex optimization problem.

The algorithm proposed in this chapter is outlined as follows. First, the closed-loop system model is reconstructed by using linear fractional transformations (LFTs) presented by Nett et al. [81] such that all tunable controller parameters are "extracted" as a full constant block. Then, the fixed-structure controller optimization problem can be seen as an H_∞ synthesis problem of static output feedback control, which does not impose any constraints on the controller structure except for the order [8, 25].

The H_∞ synthesis problem of static output feedback controllers is still a hard problem to solve. Unlike the full-order controller synthesis case, the H_∞ synthesis problem of static (or more generally, reduced-order) output feedback controllers cannot be reparameterized as a convex optimization problem. The reduced-order H_∞ synthesis problem has, however, received considerable attention in recent years. Several algorithms have been proposed to

solve this problem in an efficient manner (see Section 3.2). In this chapter, the cone complementarity linearization algorithm proposed by El Ghaoui et al. [23] is employed to solve this problem. Although the cone complementarity linearization algorithm is a local search algorithm, and thus there is no guarantee that it finds the global minimum, in most practical applications it performs excellent as shown in [23].

The proposed approach can be also applied to the scaled-H_∞ optimization problem of fixed-structure controllers in a straightforward manner. The scaled-H_∞ optimization problem is strongly related to the μ-synthesis problem, i.e. the controller synthesis problem that guarantees the robust stability and performance for a linear time-invariant (LTI) plant subject to norm-bounded structured uncertainties. Since the general μ-synthesis problem is quite difficult to solve, the scaled-H_∞ optimization problem with a constant scaling matrix is often used as its reasonable "approximation." Since the pioneering works of Doyle [17] and Safonov [91], the practical importance of the scaled-H_∞ optimization problem has been recognized.

The main focus of this chapter is on demonstrating the practical application of H_∞ optimization to the tuning of fixed-structure controllers. The following three practical application examples are presented to show the effectiveness of the proposed approach.

1. *The tuning of a SISO PID controller for head positioning of a magnetic hard disk drive* (*HDD*). The optimal PID controller is obtained as a redesigned version of a second-order compensator tuned manually by an expert servo engineer. The effectiveness of the proposed re-tuning method is demonstrated by simulation and experimentation.

2. *The tuning of an observer feedback controller for head positioning of an HDD.* The H_∞ optimization is carried out in the discrete-time domain due to the discrete-time nature

of the controller structure. Unlike the PID controller case, the optimization problem of parameters of this controller structure cannot be transformed into a static output feedback controller synthesis problem. By using an iterative approach and alternately optimizing a part of the controller parameters, however, a locally optimum solution can be obtained.

3. *The tuning of a multi-input single-output* (*MISO*) *PID controller design for the lateral control of an automated heavy-duty vehicle* (*HDV*). The controller is tuned such that it shows sufficient robust performance against model uncertainties or parametric perturbations without employing complicated controller structures. Simulations have been conducted to show the performance of the designed controller.

The remainder of this chapter is organized as follows. First, previous works on fixed-structure and reduced-order H_∞ optimization problems are briefly reviewed in Section 3.2. The H_∞ optimization algorithm of fixed-structure controllers is proposed in Section 3.3. The scaled-H_∞ optimization of static output feedback controllers is discussed in Section 3.4. In Sections $3.5 \sim 3.7$, three application examples of the proposed fixed-structure H_∞ controller optimization algorithm are presented. A brief summary of this chapter is given in Section 3.8.

Much of what is presented in this chapter can be found in Ibaraki and Tomizuka [54] (including the application example presented in Section 3.5) and Niu et al. [82] (including the application example presented in Section 3.6).

3.2 Previous Works on Fixed-structure and Reduced-order H_∞ Optimization

A number of research efforts on H_∞ optimization of a PID controller have been reported in the literature. Since the standard full-order H_∞ controller synthesis algorithm cannot be applied to this problem, several approaches have been proposed to simplify the problem by imposing certain assumptions on the cost function or the controller structure, which makes it difficult to apply the algorithm to more general problems (Grassi and Tsakalis [40] and Malan et al. [71]). The application of nondeterministic approaches such as the genetic algorithm has been also reported (Kawabe and Tagami [65]).

As will be shown in Chapter 4, the H_∞ optimization problem of general fixed-structure controllers can be formulated as a bilinear matrix inequality (BMI) problem in a straightforward manner. Several variations of local search algrorithm, which can be applied to general BMI problems in principle, have been proposed to solve this problem. The conditional gradient search approaches (e.g. Wenk and Knapp [116] and Takahashi et al. [103]) and successive linearization approaches (e.g. Collins et al. [19]) showed satisfactory search performance in practical applications. More details about the algorithms to solve general BMI problems will be discussed in Chapter 4.

For problems that can be formulated as standard H_∞ optimization problems ("standard" in the sense that the cost function is given by a single H_∞ norm function), the approach presented in this chapter has the following advantages; first, it is a natural extension of the standard full-order H_∞ controller synthesis algorithm and only requires iteration of convex optimization. Since convex optimization problems can be solved in a polynomial time by using well-developed techniques in SDP (See Section 2.2.3), the proposed approach is sub-

stantially faster than any approaches based on nonconvex search algorithms. Furthermore, the proposed approach is not restricted to the tuning of PID controllers. It can be applied to the tuning of a large class of fixed-structure linear controllers that satisfy certain structural conditions, which will be given later.

The proposed algorithm solves the H_∞ optimization problem of fixed structure controllers via the reduced-order H_∞ controller synthesis. The reduced-order H_∞ controller synthesis problem has received considerable attention since the LMI-based approach to H_∞ optimization problems was introduced. Although the reduced-order H_∞ controller optimization problem cannot be repameterized as a convex optimization problem, and thus it is hard to solve globally, several local search algorithms have been proposed for this problem. For example, consider a synthesis problem of the H_∞ (sub-)optimal controller of the minimum order for a continuous-time plant. As discussed in Section 2.3.3, this problem can be rewritten as a minimization problem of $rank(RS - I)$ over R and S under LMI constraints (2.19)$\sim$(2.21). Therefore, the synthesis problem of the H_∞ γ-suboptimal controller of the minimum order can be formulated as follows:

$$\min_{R,S} \lambda_{max}(RS) \qquad \text{subject to (2.19)}\sim\text{(2.21)} . \tag{3.2}$$

The H_∞ γ-suboptimal controller of zeroth order exists if and only if the optimal value of $\lambda_{max}(RS)$ is one. Notice that the constraint (2.21) assures that all eigenvalues of RS are larger than or equal to one (it can be proved by using Lemma 5). The above problem is not a convex optimization problem, since the objective function $\lambda_{max}(RS)$ is not a convex function of R and S. It can be easily seen, however, that if either of R and S is fixed, then the problem becomes a convex optimization problem over the other variable. By alternately fixing R and S at each step, one can reduce the objective value, $\lambda_{max}(RS)$, by iteration

of convex optimization. This is the basic idea of the simplest coordinate descent methods (e.g. Iwasaki and Rotea [59, 90]). Notice that this approach is a local search algorithm and, therefore, is not always guaranteed to find the global minimum. In fact, it is not even guaranteed to converge to a local minimum, due to the non-smoothness of the objective function. Several local search algorithms proposed in the literature claimed better search performance, e.g. the alternating projection method by Grigoriadis and Skelton [42], and the min-max algorithm by Geromel et al. [35] and the descent methods using the analytic center by Iwasaki and Rotea [59, 90]. This chapter employs the cone complementarity linearization algorithm proposed by El Ghaoui et al. [23].

Finally, note that any global search algorithms for BMI problems, which will be discussed in Chapter 4, can be applied to this problem. For example, Yamada and Hara [121] presented a global search algorithm specified to reduced-order H_∞ controller synthesis problems and scaled-H_∞ optimization problems. Any global search algorithms are, however, computationally too expensive in practical applications.

3.3 H_∞ Optimization of Fixed-structure Controllers

3.3.1 Transformation into a Static Feedback Controller Synthesis Problem

Nett et al. [81] showed that a large class of fixed structure controller optimization problems could be equivalently transformed into a synthesis problem of the optimal static output feedback controller. By using this transformation, the constraints on the controller structure implicitly imposed in the problem (3.1) can be avoided except for the constraint on the

controller order. This section presents the transformation procedure for the H_∞ optimization problem of fixed-structure controllers (3.1), although the same transformation can be also applied to scaled-H_∞ optimization problems.

To illustrate the procedure, consider a tuning problem of the following SISO PID controller with approximate derivative and integral actions:

$$C(s) = k_p + k_i \frac{1}{s + \tau_i} + k_d \frac{s}{\tau_d s + 1} \tag{3.3}$$

where k_p, k_i, and k_d are constant parameters that are independently tunable. τ_i and τ_d are small constants for the approximate integral and derivative actions, respectively, and they are assumed to be fixed. A state space representation of the controller dynamics (3.3) is given by:

$$\begin{aligned} \begin{bmatrix} \dot{x}_i(t) \\ \dot{x}_d(t) \end{bmatrix} &= \begin{bmatrix} -\tau_i & 0 \\ 0 & -\frac{1}{\tau_d} \end{bmatrix} \begin{bmatrix} x_i(t) \\ x_d(t) \end{bmatrix} + \begin{bmatrix} 1 \\ \frac{1}{\tau_d} \end{bmatrix} e(t) \\ u(t) &= \begin{bmatrix} k_i & k_d(-\frac{1}{\tau_d}) \end{bmatrix} \begin{bmatrix} x_i(t) \\ x_d(t) \end{bmatrix} + \left[k_p + \frac{k_d}{\tau_d}\right] e(t)\,. \end{aligned} \tag{3.4}$$

Suppose that the plant $P(s)$ is given in the form (2.11) and satisfies the assumptions given in Section 2.3.1. The optimization objective is to tune (k_p, k_i, k_d) in Eq. (3.3) such that the closed-loop H_∞ norm, $\|F_L(P(s), C(s))\|_\infty$, is minimized.

Notice that the controller state variables, $x_i(s)$ and $x_d(s)$, can be written in the s-domain as follows:

$$x_i(s) = \frac{1}{s + \tau_i} e(s); \qquad x_d(s) = \frac{1}{1 + \tau_d s} e(s)\,. \tag{3.5}$$

Therefore, the control law (3.3) can be written as:

$$u(t) = \begin{bmatrix} k_p & k_i & k_d \end{bmatrix} \begin{bmatrix} e(t) \\ x_i(t) \\ -\frac{1}{\tau_d} x_d(t) + \frac{1}{\tau_d} e(t) \end{bmatrix} . \tag{3.6}$$

Then, reconstruct the extended plant $P_K(s)$ as follows:

$$\begin{aligned}
\begin{bmatrix} \dot{x}(t) \\ \dot{x}_i(t) \\ \dot{x}_d(t) \end{bmatrix} &= \begin{bmatrix} A & 0 & 0 \\ C_2 & -\tau_i & 0 \\ \frac{1}{\tau_d} C_2 & 0 & -\frac{1}{\tau_d} \end{bmatrix} \begin{bmatrix} x(t) \\ x_i(t) \\ x_d(t) \end{bmatrix} + \begin{bmatrix} B_1 \\ D_{21} \\ \frac{1}{\tau_d} D_{21} \end{bmatrix} d(t) + \begin{bmatrix} B_2 \\ 0 \\ 0 \end{bmatrix} u(t) \\
z(t) &= \begin{bmatrix} C_1 & 0 & 0 \end{bmatrix} \begin{bmatrix} x(t) \\ x_i(t) \\ x_d(t) \end{bmatrix} + D_{11} d(t) + D_{12} u(t) \\
w(t) &= \begin{bmatrix} C_2 & 0 & 0 \\ 0 & 1 & 0 \\ \frac{1}{\tau_d} C_2 & 0 & -\frac{1}{\tau_d} \end{bmatrix} \begin{bmatrix} x(t) \\ x_i(t) \\ x_d(t) \end{bmatrix} + \begin{bmatrix} D_{21} \\ 0 \\ \frac{1}{\tau_d} D_{21} \end{bmatrix} d(t) .
\end{aligned} \tag{3.7}$$

Notice that $P_K(s)$ contains two controller state variables, $x_i(s)$ and $x_d(s)$. By using the outputs of $P_K(s)$, the control input $u(t)$ is given by:

$$u(t) = \begin{bmatrix} k_p & k_i & k_d \end{bmatrix} w(t) = \begin{bmatrix} k_p & k_i & k_d \end{bmatrix} \begin{bmatrix} e(t) \\ x_i(t) \\ -\frac{1}{\tau_d} x_d(t) + \frac{1}{\tau_d} e(t) \end{bmatrix} \tag{3.8}$$

The entire closed-loop system can be seen as shown in Figure 3.1, where $K := \begin{bmatrix} k_p & k_i & k_d \end{bmatrix}$ is a constant matrix.

This transformation implies that the H_∞ optimization problem of the controller parameters

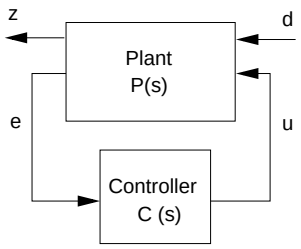

(a) Original closed-loop system configuration

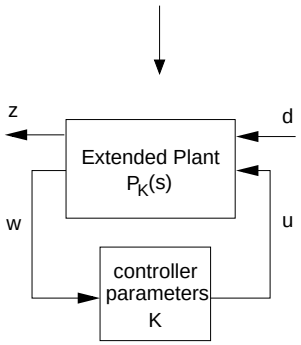

(b) Equivalent closed-loop system with the extended plant $P_K(s)$

Figure 3.1: Extraction of controller parameters

can be seen as an H_∞ synthesis problem of a static output feedback controller for the extended plant model, $P_K(s)$. The algorithm for the H_∞ synthesis of static output feedback controllers will be presented in the next section.

The above transformation procedure is not restricted to PID controllers. The optimization algorithm proposed in this chapter can be applied to any linear controller structures that can be transformed into the form shown in Figure 3.1 (b).

Lemma 6 *Suppose that the the controller has a state space representation* (A_c, B_c, C_c, D_c)

such that the matrix $\begin{bmatrix} A_c & B_c \\ C_c & D_c \end{bmatrix}$ *can be rewritten in the following form:*

$$\begin{bmatrix} A_K & B_K \\ C_K & D_K \end{bmatrix} = P_1 + P_2 K P_3 \tag{3.9}$$

where P_1, P_2 *and* P_3 *are constant* (*i.e. untunable*) *matrices with appropriate dimensions and* K *is a full block of independently tunable controller parameters. Then, the closed-loop system can be transformed into the form shown in Figure* 3.1 (b).

Proof:

Suppose that the controller dynamics, $C(s)$, is given by the state space representation (2.12). The controller dimensions are $A_c \in \mathbb{R}^{k\times k}$ and $D_c \in \mathbb{R}^{m_2\times p_2}$.

Suppose that there exists P_1, P_2 and P_3 that satisfy Eq. (3.9) and $K \in \mathbb{R}^{k_1\times k_2}$. Partition P_1, P_2 and P_3 as follows:

$$\begin{bmatrix} A_c & B_c \\ C_c & D_c \end{bmatrix} = P_1 + P_2 K P_3 = \left[\begin{array}{c|c} P_{11}^1 & P_{12}^1 \\ \hline P_{21}^1 & P_{22}^1 \end{array}\right] + \left[\begin{array}{c} P_1^2 \\ \hline P_2^2 \end{array}\right] K \left[\begin{array}{c|c} P_1^3 & P_2^3 \end{array}\right] \tag{3.10}$$

where $P_{11}^1 \in \mathbb{R}^{k\times k}$, $P_{22}^1 \in \mathbb{R}^{m_2\times p_2}$, $P_1^2 \in \mathbb{R}^{k\times k_1}$ and $P_1^3 \in \mathbb{R}^{k_2\times k}$. Then, A_c, B_c, C_c, and D_c are respectively given by

$$A_K = P_{11}^1 + P_1^2 K P_1^3, \quad B_K = P_{12}^1 + P_1^2 K P_2^3, \quad C_K = P_{21}^1 + P_2^2 K P_1^3, \quad D_K = P_{22}^1 + P_2^2 K P_2^3 . \tag{3.11}$$

Then, the controller dynamics (2.12) can be written as

$$\begin{aligned} \dot{x}_c(t) &= (P_{11}^1 + P_1^2 K P_1^3) x_c(t) + (P_{12}^1 + P_1^2 K P_2^3) e(t) \\ &= P_{11}^1 x_c(t) + P_{12}^1 e(t) + P_1^2 v(t) \\ u(t) &= P_{21}^1 x_c(t) + P_{22}^1 e(t) + P_2^2 v(t) \end{aligned} \tag{3.12}$$

where $v(t) := KP_1^3 x_c(t) + KP_2^3 e(t)$. Define $w(t) := P_1^3 x_c(t) + P_2^3 e(t)$. Then, $v(t)$ is given by $v(t) = Kw(t)$. Suppose that the plant is given by Eq. (2.11). By constructing the extended plant model $P_K(s)$ such that its inputs and outputs are respectively given by $\begin{bmatrix} d(t) \\ v(t) \end{bmatrix}$ and $\begin{bmatrix} z(t) \\ w(t) \end{bmatrix}$ as shown in Figure 3.1 (b), it can be shown that:

$$F_L(P(s), C(s)) = F_L(P_K(s), K) \tag{3.13}$$

where $P_K(s)$ is given by

$$\begin{bmatrix} \dot{x}(t) \\ \dot{x}_c(t) \end{bmatrix} = \begin{bmatrix} A + B_2 P_{22}^1 C_2 & B_2 P_{21}^1 \\ P_1 2^1 C_2 & P_{11}^1 \end{bmatrix} \begin{bmatrix} x(t) \\ x_c(t) \end{bmatrix} + \begin{bmatrix} B_1 + B_2 P_{22}^1 D_{21} \\ P_{12}^1 D_{21} \end{bmatrix} d(t) + \begin{bmatrix} B_2 P_2^2 \\ P_1^2 \end{bmatrix} v(t)$$

$$\begin{bmatrix} z(t) \\ w(t) \end{bmatrix} = \begin{bmatrix} C_1 + D_{12} P_{22}^1 C_2 & D_{12} P_{21}^1 \\ P_2^3 C_2 & P_1^3 \end{bmatrix} \begin{bmatrix} x(t) \\ x_c(t) \end{bmatrix} + \begin{bmatrix} D_{11} + D_{12} P_{22}^1 D_{21} \\ P_2^3 D_{21} \end{bmatrix} d(t)$$

$$+ \begin{bmatrix} D_{12} P_2^2 \\ 0 \end{bmatrix} v(t) . \qquad \square \tag{3.14}$$

Remarks:

1. The PID controller (3.4) satisfies the above condition with

$$P_1 = \begin{bmatrix} -\tau_i & 0 & 1 \\ 0 & -\frac{1}{\tau_d} & \frac{1}{\tau_d} \\ 0 & 0 & 0 \end{bmatrix} ; \qquad P_2 = \begin{bmatrix} 0 \\ 0 \\ 1 \end{bmatrix} ; \qquad P_3 = \begin{bmatrix} 0 & 0 & 1 \\ 1 & 0 & 0 \\ 0 & -\frac{1}{\tau_d} & \frac{1}{\tau_d} \end{bmatrix} ; \tag{3.15}$$

and $K = \begin{bmatrix} k_p & k_i & k_d \end{bmatrix}$.

2. Nett et al. [81] showed nine examples of the controller structures that could be transformed into a static output feedback controller synthesis problem. They satisfy the condition in Lemma 6.

3. If the controller has a state space representation (A_c, B_c, C_c, D_c) such that the full matrix K, the entries of which are all independently tunable, can be obtained by eliminating row(s) and/or column(s) of untunable entries from the matrix $\begin{bmatrix} A_c & B_c \\ C_c & D_c \end{bmatrix}$, then the closed-loop system can be transfered into the form shown in Figure 3.1 (b). This condition is included in the condition in Lemma 6.

4. MIMO PID controllers can be also transformed into the the form shown in Figure 3.1 (b) in the analogous way as the SISO case. Another example of the controller structure transformable into the form in Figure 3.1 (b) is a SISO controller of the following transfer function:

$$G_c(s) = \frac{b_{n-1}s^{n-1} + \cdots + b_1 s + b_0}{s^n + a_{n-1}s^{n-1} + \cdots + a_1 s + a_0} \tag{3.16}$$

where a_i and b_i $(i = 0, \cdots, n-1)$ are independently tunable parameters. Its controllable canonical form is

$$\begin{aligned} \dot{x}_c(t) &= \begin{bmatrix} 0 & 1 & & 0 \\ \vdots & & \ddots & \\ 0 & & & 1 \\ -a_0 & -a_1 & \cdots & -a_{n-1} \end{bmatrix} x_c(t) + \begin{bmatrix} 0 \\ \vdots \\ 0 \\ 1 \end{bmatrix} e(t) \\ u(t) &= \begin{bmatrix} b_0 & b_1 & \cdots & b_{n-1} \end{bmatrix} x_c \,. \end{aligned} \tag{3.17}$$

This representation satisfies the condition in the previous remark. K is given by

$$K = \begin{bmatrix} a_0 & a_1 & \cdots & a_{n-1} \\ b_0 & b_1 & \cdots & b_{n-1} \end{bmatrix}.$$

5. Any controller, the system matrices (A_c, B_c, C_c, D_c) of which are all freely tunable, can be transformed into the form shown in Figure 3.1 (b) with $K = \begin{bmatrix} A_c & B_c \\ C_c & D_c \end{bmatrix}$, no matter what the order of the controller is (i.e. a reduced-order controller synthesis problem can be always transformed into a static output feedback controller synthesis problem).

6. Even if it is not possible to transform the problem to a static output feedback problem where all tunable parameters appear in the static feedback block, a locally optimal solution can be obtained by using an iterative approach and alternately optimizing a part of the controller parameters. In many practical applications, this approach shows sufficient search performance. Section 3.6 presents an example of such cases.

3.3.2 H_∞ Optimization of Static Output Feedback Controllers

This section presents an algorithm to solve the H_∞ optimization problem of static output feedback controllers. Suppose that the original H_∞ optimization problem of fixed structure controller parameters (3.1) can be transformed into the following H_∞ optimization problem of the static output feedback gain matrix K, as shown in the previous section:

$$\min_{K \in \mathbf{R}^{m_2 \times p_2}} \|F_L(P_K(s), K)\|_\infty \tag{3.18}$$

Rewrite the extended plant model $P_K(s)$ as:

$$P_K : \left(\begin{array}{c|cc} A & B_1 & B_2 \\ \hline C_1 & D_{11} & D_{12} \\ C_2 & D_{21} & D_{22} \end{array}\right) \tag{3.19}$$

The plant dimensions are given by $A \in \mathbb{R}^{n\times n}$, $D_{11} \in \mathbb{R}^{p_1\times m_1}$ and $D_{22} \in \mathbb{R}^{p_2\times m_2}$. The objective of this section is to present an algorithm to find an H_∞ sub-optimal solution $K \in \mathbb{R}^{m_2\times p_2}$ for the problem (3.18) (i.e. to find $K \in \mathbb{R}^{m_2\times p_2}$ such that $\|F_L(P_K(s), K)\|_\infty < \gamma$ for given $\gamma > 0$).

Recall the following solvability conditions for continuous-time H_∞ suboptimal controller synthesis problems given in Theorem 4.

Theorem 4 (Solvability of Continuous-time H_∞ Controller Synthesis Problems – Reposted) *There exists a dynamic controller $C(s)$ of order k such that $\|F_L(P_K(s), C(s))\|_\infty < \gamma$ if and only if there exist two symmetric matrices $X \in \mathbb{R}^{n\times n}$ and $Y \in \mathbb{R}^{n\times n}$ such that*

$$\mathcal{N}_1^T \begin{bmatrix} AX + XA^T & XC_1^T & B_1 \\ C_1X & -\gamma I & D_{11} \\ B_1^T & D_{11}^T & -\gamma I \end{bmatrix} \mathcal{N}_1 \prec 0 \tag{3.20}$$

$$\mathcal{N}_2^T \begin{bmatrix} A^TY + YA & YB_1 & C_1^T \\ B_1^TY & -\gamma I & D_{11}^T \\ C_1 & D_{11} & -\gamma I \end{bmatrix} \mathcal{N}_2 \prec 0 \tag{3.21}$$

$$\begin{bmatrix} X & I \\ I & Y \end{bmatrix} \succeq 0 \tag{3.22}$$

$$\text{rank}\,(XY - I) \leq k \tag{3.23}$$

where $\mathcal{N}_1 = \text{diag}\,\{N_{12}, I\}, \mathcal{N}_2 = \text{diag}\,\{N_{21}, I\}$, N_{12} *and* N_{21} *are bases of the null space of* $\begin{bmatrix} B_2^T & D_{12}^T \end{bmatrix}$ *and* $\begin{bmatrix} C_2 & D_{21} \end{bmatrix}$, *respectively.*

In the full-order controller synthesis case, i.e. $k \geq n$, the condition (3.23) is trivially satisfied and the global solution that satisfies the LMI constraints (3.20)$\sim$(3.22) can be computed by convex optimization. For the static controller synthesis problem (3.19), however, X and Y that satisfy (3.20)$\sim$(3.23) with $k = 0$ must be searched. The rank condition (3.23) is not a convex constraint, which makes the reduced-order H_∞ synthesis problem difficult to solve.

Notice that the reduced-order H_∞ controller synthesis problem can be rewritten as a rank minimization problem under LMI constraints [21]:

$$\min_{X,Y} \text{rank}\ (XY - I) \quad \text{subject to (3.20)}\sim\text{(3.22)} \tag{3.24}$$

For the static output feedback controller synthesis, the above rank function can be equivalently replaced by the trace function by using the following lemma.

Lemma 7 *Suppose* $X \in \mathbb{R}^{n\times n}$ *and* $Y \in \mathbb{R}^{n\times n}$ *are symmetric and satisfy* (3.22). *Then,* rank $(XY - I) = 0$ *if and only if* $\text{tr}\,(XY) = n$.

Proof: See Apkarian and Tuan [4].

Lemma 7 implies that there exists a constant matrix, K^*, such that $\|F_L(P_K(s), K^*)\|_\infty < \gamma$ if and only if

$$\min_{X,Y} \text{tr}\,(XY) = n \quad \text{subject to (3.20)}\sim\text{(3.22)} \tag{3.25}$$

This objective function is still not a convex function of X and Y. The cone complementarity linearization algorithm [23] is employed to solve this problem. By linearizing the cost function with respect to X and Y, we have:

$$\min_{X_i, Y_i} \ \mathrm{tr}\,(X_{i-1}Y_i + X_iY_{i-1}) \qquad \text{subject to (3.20)}\sim\text{(3.22)} \tag{3.26}$$

With X_{i-1} and Y_{i-1} fixed, X_i and Y_i that minimize the trace function in (3.26) can be found by convex optimization. This observation suggests the following iterative algorithm to find X and Y that satisfy (3.25).

Algorithm 1 (Continuous-time Static Output Feedback H_∞ Controller Synthesis)

1. *Choose initial* $X_0 = X_0^T \in \mathbb{R}^{n\times n}$ *and* $Y_0 = Y_0^T \in \mathbb{R}^{n\times n}$ *that satisfy* (3.20)$\sim$(3.22). *If there are none, then the problem is infeasible. Set* $i = 1$.

2. *Solve the convex optimization problem* (3.26) *for* X_i *and* Y_i.

3. *Set* $i = i + 1$ *and repeat Step 2 until convergence.*

El Ghaoui et al. [23] showed that the objective function, $t_i := \mathrm{tr}\,(X_{i-1}Y_i + X_iY_{i-1})$, was monotonically non-increasing at each step, i.e. $t_i \le t_{i-1}$. Since t_i is lower bounded by $2n$, the algorithm converges.

Although this algorithm is a local search algorithm and thus is not always guaranteed to find the global minimum, in most practical applications it shows excellent search performance, as reported in [23] with extensive numerical examples.

Once the optimal X and Y that satisfy (3.25) are found, the sub-optimal output feedback gain matrix K^*, which makes the closed-loop H_∞ norm (3.18) less than γ, can be

computed by solving the following convex optimization problem for K^* (See Eq. (2.32) in Section 2.3.3).

$$\begin{bmatrix} A^T X_{cl} + X_{cl} A & X_{cl} B_1 & C_1^T \\ B_1^T X_{cl} & -\gamma I & D_{11}^T \\ C_1 & D_{11} & -\gamma I \end{bmatrix} + \begin{bmatrix} C_2^T \\ D_{21}^T \\ 0 \end{bmatrix} K^{*T} \begin{bmatrix} B_2^T X_{cl} & 0 & D_{12}^T \end{bmatrix} + \begin{bmatrix} X_{cl} B_2 \\ 0 \\ D_{12} \end{bmatrix} K^* \begin{bmatrix} C_2 & D_{21} & 0 \end{bmatrix} \prec 0 \qquad (3.27)$$

where $X_{cl} = X^{-1} = Y$. Theorem 4 guarantees the existence of a solution K^* of this problem.

The discrete-time version of the H_∞ sub-optimal static output feedback controller synthesis algorithm can be derived in an analogous way based on Theorem 5.

Algorithm 2 (Discrete-time Static Output Feedback H_∞ Controller Synthesis)

1. *Choose initial* $X_0 = X_0^T \in \mathbb{R}^{n \times n}$ *and* $Y_0 = Y_0^T \in \mathbb{R}^{n \times n}$. *Set* $i = 1$.

2. *Solve the following convex optimization problem for* X_i *and* Y_i:

$$\min_{X_i, Y_i} \operatorname{tr}(X_{i-1} Y_i + X_i Y_{i-1}) \qquad \text{subject to (2.38)}\sim\text{(2.40)}\,. \qquad (3.28)$$

3. *Set* $i = i + 1$ *and repeat Step 2 until convergence.*

Similarly as the continuous-time problem case, once the optimal X and Y that satisfy $\operatorname{tr}(XY) = n$ subject to (2.38)$\sim$(2.40) are found, the H_∞ γ-suboptimal output feedback

gain matrix K^* can be computed by solving the following problem for K^*.

$$\begin{bmatrix} -X_{cl}^{-1} & A & B_1 & 0 \\ A^T & -X_{cl} & 0 & C_1^T \\ B_1^T & 0 & -\gamma I & D_{11}^T \\ 0 & C_1 & D_{11} & -\gamma I \end{bmatrix} + \begin{bmatrix} 0 \\ C_2^T \\ D_{21}^T \\ 0 \end{bmatrix} K^{*T} \begin{bmatrix} B_2^T & 0 & 0 & D_{12}^T \end{bmatrix} + \begin{bmatrix} B_2 \\ 0 \\ 0 \\ D_{12} \end{bmatrix} K^* \begin{bmatrix} 0 & C_2 & D_{21} & 0 \end{bmatrix} \prec 0 \qquad (3.29)$$

where $X_{cl} = X^{-1} = Y$.

3.4 Scaled-H_∞ Optimization of Static Output Feedback Controllers

3.4.1 Scaled-H_∞ Optimization Problem

The algorithm presented in Section 3.3 can be also applied to locally solve the scaled-H_∞ optimization problem of fixed-structure controllers. First, this section reviews the scaled-H_∞ optimization problem. See e.g. [90, 17, 91] for further details.

Suppose that the closed-loop system can be represented by using LFTs in the form shown in Figure 3.2, where $P(s)$ and $C(s)$ denote the nominal plant model and controller, respectively, and $\Delta(s)$ denotes modeling uncertainties. Suppose $\Delta(s) \in \mathbf{\Delta}$, where $\mathbf{\Delta}$ is a set of norm-

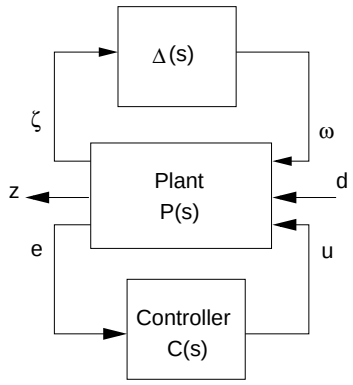

Figure 3.2: Closed-loop system configuration with modeling uncertainties $\Delta(s)$

bounded structured uncertainties defined by:

$$\mathbf{\Delta} := \{\Delta = \mathrm{diag}(\delta_1 I_{q_1}, \cdots, \delta_l I_{q_l}, \Delta_{l+1}, \cdots, \Delta_p) \mid \|\Delta\|_\infty \leq 1\} \tag{3.30}$$

where $\delta_i I_{q_1}$ $(i = 1, \cdots, l)$ denotes a real parametric perturbation $(\delta_i \in \mathbb{R})$ and Δ_i $(i = l+1, \cdots, p)$ is a q_i-input, q_i-output linear (possibly time-varying) operator, which usually denotes unmodeled dynamics.

The robust performance of this uncertain closed-loop system is defined by:

$$J(C(s)) := \sup_{\Delta \in \mathbf{\Delta}} \|F_U(F_L(P(s), C(s)), \Delta(s))\|_\infty \tag{3.31}$$

Notice that $F_U(F_L(P(s), C(s)), \Delta(s))$ represents the closed-loop transfer function from d to z in Figure 3.2.

The *μ-synthesis problem* is defined as

$$\min_{C(s)} \ \gamma \qquad \text{subject to} \ \ J(C(s)) < \gamma \,. \tag{3.32}$$

The objective of the μ-synthesis problem is to find a controller $C(s)$ that guarantees the closed-loop H_∞ norm of the transfer function from d to z less than the given value γ under

the existence of any modeling uncertainties $\Delta(s) \in \mathbf{\Delta}$. The general μ-synthesis problem is a hard problem to solve (it is proven to be NP-hard with respect to the problem size [105]). The scaled-H_∞ problem is often used as its reasonable "approximation." Define:

$$J_b(C(s)) := \inf_{\gamma>0, D\in\mathcal{D}} \gamma \tag{3.33}$$

$$\text{subject to} \quad \left\| \begin{bmatrix} D & 0 \\ 0 & \gamma I \end{bmatrix}^{-\frac{1}{2}} F_L(P(s), C(s)) \begin{bmatrix} D & 0 \\ 0 & \gamma^{-1} I \end{bmatrix}^{\frac{1}{2}} \right\|_\infty < 1 \,.$$

The set of scaling matrices, $\mathcal{D}$, is defined as follows.

$$\mathcal{D} := \{D = \text{diag}(D_1, \cdots, D_l, d_1 I_{q_{l+1}}, \cdots, d_{k-l} I_{q_p})\} \tag{3.34}$$

where $D_i \in \mathbb{R}^{q_i \times q_i}$, $D_i \succ 0$, $d_j \in \mathbb{R}$, and $d_j > 0$. The dimensions of each diagonal block of D depend on those of the corresponding block of the uncertainty structure $\mathbf{\Delta}$ (see e.g. [125, Chapter 11]). Note that $F_L(P(s), C(s))$ represents the closed-loop transfer function from $[\omega, d]^T$ to $[\zeta, z]^T$ in Figure 3.2.

The *scaled-H_∞ controller synthesis problem* is defined as

$$\min_{C(s)} \; J_b(C(s)) \,. \tag{3.35}$$

It is known that for any proper controller $C(s)$ that stabilizes the nominal plant $P(s)$, $J_b(C(s))$ gives an upper bound for $J(C(s))$, i.e. $J(C(s)) \leq J_b(C(s))$. That is, a solution for the scaled-H_∞ controller synthesis problem always gives the upper bound for the general μ-synthesis problem defined in (3.32). In the special case where the model perturbation $\Delta(s)$ is arbitrary fast time-varying, it was shown by Shamma [94] that the scaled-H_∞ optimization problem (3.35) gave the exact solution for the μ-synthesis problem (3.32), i.e. did not introduce any conservativeness.

Since the pioneer works of Doyle [17] and Safonov [91], the practical importance of the scaled-H_∞ optimization problem has been recognized and considerable research efforts have been devoted to this problem. If the controller is a state feedback controller [83, 20], or the plant satisfies a simplifying condition called the rank-one assumption [58], then the problem can be reparameterized as a convex optimization problem. In general output feedback controller synthesis cases, however, the problem cannot be formulated as a convex optimization problem.

A widely used approach to obtain a local solution for the scaled-H_∞ (full-order) controller synthesis problem (3.35) is the D-K iteration [17, 91]. If the scaling matrix D is fixed, the problem becomes the standard H_∞ controller synthesis problem, which can be solved by convex optimization. If the controller $C(s)$ is fixed, the problem becomes a convex optimization problem on D. The D-K iteration method is a coordinate descent method to locally solve the problem (3.35) by iterating these two steps.

The D-K iteration is a local search algorithm and thus is not always guaranteed to find the global solution. Furthermore, a major disadvantage of the D-K iteration is its convergence speed; the convergence speed of the D-K iteration can be very slow, even when the iteration is still far from any of local minimums [120]. Several alternative local search approaches to scaled-H_∞ optimization problems have been proposed (Iwasaki and Rotea [59, 90] and Yamada and Hara [120]). As will be discussed in the following section, nonconvex constraints appeared in the scaled-H_∞ optimization problem and the reduced-order H_∞ controller synthesis problem are of an analogous form. Therefore, any approaches to solve reduced-order H_∞ controller synthesis problems can be straightforwardly applied to scaled-H_∞ optimization problems as well [21].

3.4.2 Scaled-H_∞ Optimization of Static Output Feedback Controllers

The approach presented in Section 3.3.2 can be also applied to locally solve the scaled-H_∞ optimization problem in a straightforward manner.

The objective of the scaled-H_∞ (sub-)optimization problem for a continuous-time plant, $P(s)$, is to find a controller, $C(s)$, and a scaling matrix, $D \in \mathcal{D}$, such that

$$\left\| \begin{bmatrix} D & 0 \\ 0 & \gamma I \end{bmatrix}^{-\frac{1}{2}} F_L(P(s), C(s)) \begin{bmatrix} D & 0 \\ 0 & \gamma^{-1} I \end{bmatrix}^{\frac{1}{2}} \right\|_\infty < 1 \tag{3.36}$$

for given $\gamma > 0$. From Theorem 4, the necessary and sufficient condition for the existence of the γ-suboptimal controller $C(s)$ of order k satisfying the above inequality can be derived as follows [90]:

Theorem 6 (Solvability of Scaled-H_∞ Controller Synthesis Problems)

For the given continuous-time plant $P(s)$ (in the form (3.19)) and $\gamma > 0$, there exists a dynamic controller $C(s)$ of order k and a scaling matrix $D \in \mathcal{D}$ satisfying the inequality (3.36) if and only if there exist $X \in \mathbb{R}^{n\times n}$, $Y \in \mathbb{R}^{n\times n}$, $R \in \mathcal{D}$, and $S \in \mathcal{D}$ such that

$$\mathcal{N}_1^T \begin{bmatrix} AX + XA^T & XC_1^T & B_1 \\ C_1 X & -R_\gamma & D_{11} \\ B_1^T & D_{11}^T & -S_\gamma \end{bmatrix} \mathcal{N}_1 \prec 0 \tag{3.37}$$

$$\mathcal{N}_2^T \begin{bmatrix} A^T Y + YA & YB_1^T & C_1^T \\ B_1^T Y & -S_\gamma & D_{11}^T \\ C_1 & D_{11} & -R_\gamma \end{bmatrix} \mathcal{N}_2 \prec 0 \tag{3.38}$$

(3.22) and (3.23)

$$R_\gamma := \begin{bmatrix} R & 0 \\ 0 & \gamma I \end{bmatrix} \tag{3.39}$$

$$S_\gamma := \begin{bmatrix} S & 0 \\ 0 & \gamma I \end{bmatrix} \tag{3.40}$$

$$R = S^{-1} \tag{3.41}$$

where $\mathcal{N}_1$ and $\mathcal{N}_2$ are defined in the same way as in Theorem 4.

Similarly as in the H_∞ controller synthesis case (Theorem 4), the constraint (3.23) is automatically satisfied for the full-order controller synthesis case (i.e. $k \geq n$). Even in full-order synthesis case, however, the scaled-H_∞ optimization problem remains as a nonconvex optimization problem due to the inverse constraint (3.41).

Notice that in the static controller synthesis case (i.e. $k = 0$), the rank constraint (3.23) can be seen as an inverse constraint, i.e. $X = Y^{-1}$. This observation suggests that the same approach presented in Section 3.3.2 can be also applied to deal with the constraint (3.41).

Algorithm 3 (Scaled-H_∞ Optimization of Static Output Feedback Controller)

1. *Choose initial $X_0 = X_0^T \in \mathbb{R}^{n\times n}$, $Y_0 = Y_0^T \in \mathbb{R}^{n\times n}$, $R_0 \in \mathcal{D}$, and $S_0 \in \mathcal{D}$. Set $i = 1$.*

2. *Solve the following convex optimization problem:*

$$\begin{aligned} \min_{X_i,\, Y_i \in \mathbf{R}^{n\times n},\, R_i,\, S_i \in \mathcal{D}} \quad & \mathrm{tr}(X_i Y_{i-1} + X_{i-1} Y_i) + \mathrm{tr}(R_i S_{i-1} + S_i R_{i-1}) \\ \text{subject to} \quad & (3.37)(3.38)(3.22)(3.39)(3.40) \\ \textit{and} \quad & \begin{bmatrix} R_i & I \\ I & S_i \end{bmatrix} \succeq 0 \,. \end{aligned} \tag{3.42}$$

3. *Set $i = i + 1$ and repeat Step 2 until convergence.*

For given $\gamma > 0$, there exists a constant matrix, K^*, and a scaling matrix, $D \in \mathcal{D}$, satisfying the inequality (3.36) (replace $C(s)$ with K^*) if and only if the global minimum of

$tr(X_iY_i)+tr(R_iS_i)$ is $n+N$, where $N := \sum_{i=1}^{p} q_i$ (the size of a matrix in $\mathcal{D}$, see Eq. (3.34)). Notice that the constraint (3.42) is added to ensure that $tr(R_iS_i) \geq N$.

Once such a solution set (X_i, Y_i, R_i, S_i) is found, the optimal output feedback gain K^* can be computed in a similar way as presented in Section 3.3.2.

The discrete-time version of this algorithm can be derived in an analogous way based on Theorem 5.

3.4.3 Application of Scaled-H_∞ Optimization

The objective of the μ-synthesis problem (and its approximate version, the scaled-H_∞ optimization problem) is to find a controller that guarantees a certain closed-loop H_∞ norm performance under the existence of any modeling uncertainties that belong to the given uncertainty structure denoted by $\mathbf{\Delta}$. Therefore, they are more "natural" approaches than the H_∞ optimization from the viewpoint of the robust control. It should be noted, however, that the μ-synthesis approach is likely to result in too conservative controllers in practical applications. This conservativeness problem is even more crucial for the scaled-H_∞ optimization approach, since it is a conservative approximation of the μ-synthesis problem. Therefore, the applicability of the scaled-H_∞ optimization to practical problems is sometimes questionable, especially when the robustness is not a critical issue.

In the following sections, three practical application examples of the H_∞ optimization of fixed structure controllers are presented. From the computational point of view, the difference between the algorithms to solve the scaled-H_∞ optimization problem and the fixed structure H_∞ optimization problem is not significant. See e.g. [59, 58] for application examples of the scaled-H_∞ optimization.

3.5 Application Example I: PID Controller Design for Head Positioning of a Magnetic Hard Disk Drive

3.5.1 Introduction: Head Positioning Control for a Magnetic Hard Disk Drive

This section considers the tuning problem of a SISO PID controller for track-following control of a head positioning servo system of a magnetic hard disk drive (HDD).

An HDD storage technology continues to experience a dramatic areal density growth of 60% every year [43]. As the storage capacity of HDDs increases dramatically, the demand for positioning control accuracy of the read/write head of HDD is becoming more stringent. Figure 3.3 shows the schematic view of an HDD. The head positioning servo system consists of the magnetic read/write head, the arm, and the voice coil motor (VCM) actuator. Fixed servo bursts written on the disks provide information on the deviation of the head from the center of a track. A simplified block diagram of the tracking control loop for head positioning of an HDD is depicted in Figure 3.4. The position error signal (PES) is measured at the head tip. The objective of this section is to design the controller, $C(s)$, by using the frequency-domain loop-shaping technique based on the fixed-structure H_∞ optimization algorithm proposed in Section 3.3.

The head positioning control for an HDD has attracted considerable attention in the literature (e.g. [99, 15]). Normal operation of an HDD requires quick access to many different tracks. Furthermore, the sensitivity of the head position to external disturbances, such as

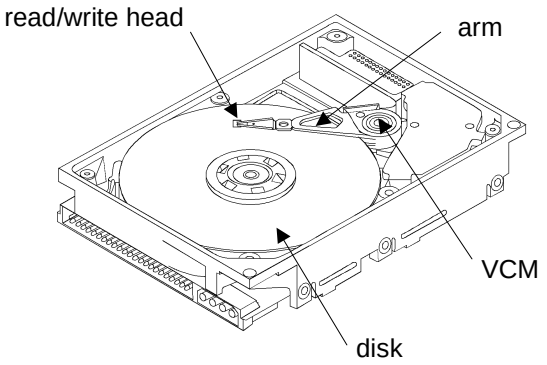

Figure 3.3: Schematic view of a hard disk drive

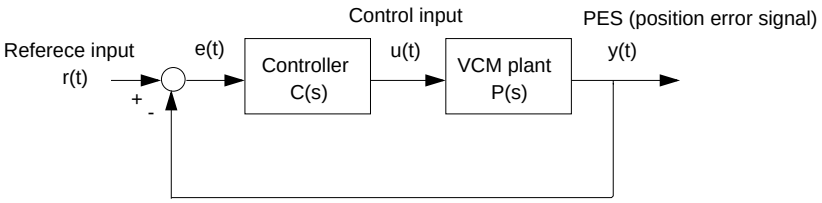

Figure 3.4: Simplified block diagram of tracking control loop

the vibrations due to the spindle motor rotation, track irregularities, position sensing noise, mechanical vibrations and shocks, is also an important issue in the design of controllers. To satisfy these two different requirements, the controller for the head positioning servo system usually has two modes; the track-seeking mode and the track-following mode. This section focuses on the design of a feedback controller for the track-following mode. Track-to-track pitches determine the required accuracy of positioning the head; the smaller the pitch, the smaller the error specification. This is a strong technological trend exploited by all HDD manufacturers.

In recent years, HDD manufacturers devote considerable research effort into dual stage ac-

tuators for head positioning control of an HDD (see [16] and the references therein). With this technology, the servo bandwidth can be as wide as about 2.0 kHz compared to 600 Hz to 900 Hz, typical bandwidths under single stage actuation with a VCM. However, the dual-stage actuator technique is not yet mature enough for mass production. Also, the cost associated with it is still high. Therefore, it is an important problem to tune a controller for a VCM actuator such that it achieves the optimal performance to meet the demanded areal density. In this section, the fixed-structure H_∞ controller optimization is applied to the tuning of a head positioning controller of an HDD. The proposed method succeeds to further improve the performance of a PID controller, which has been finely tuned by an experienced servo engineer.

The standard full-order H_∞ controller synthesis and the μ-synthesis have been applied to this problem by Hirata et al. [50] and Hernandez et al. [46], respectively. For those approaches, the order of the designed controller is always one of the major issues. Furthermore, it is often undesirable to re-implement the whole controller structure due to time and cost limitations.

3.5.2 Model Description

Figure 3.5 shows the experimental HDD setup. The VCM controller is implemented on a microprocessor embedded in a commercial disk drive system. The specifications of the experimental HDD system are shown in Table 3.1.

The VCM actuator dynamics is modeled as follows:

$$P(s) = K_{vcm}\frac{\omega_1^2}{s^2+2\zeta_1\omega_1 s+\omega_1^2}\cdot\frac{\omega_2^2}{s^2+2\zeta_2\omega_2 s+\omega_2^2}\cdot\frac{-0.5D_1 s+1}{0.5D_1 s+1}\,. \tag{3.43}$$

Figure 3.5: Experimental HDD setup

Table 3.1: Experimental setup specifications

Capacity	18.4 GB
Disks	5/3.5”
TPI	13,000
Spindle Speed	7,208 rpm
Sampling Period	99.1 μm
Average Seek Time	6.5/7.5 ms (Read/Write)

The first term represents the gain, and the second term represents the double integrator characteristics at high frequencies and flattening characteristics at low frequencies due to the pivot friction. The high resonant mode is also included in the model. The last term $\frac{-0.5D_1s+1}{0.5D_1s+1}$ represents the Pade approximation of computational delay of the controller. The parameters in the model (3.43) are identified based on the measured frequency responses of the experimental setup. The simulated frequency response of the model (3.43) and the measured frequency response are shown in Figure 3.6. The high mechanical resonant mode

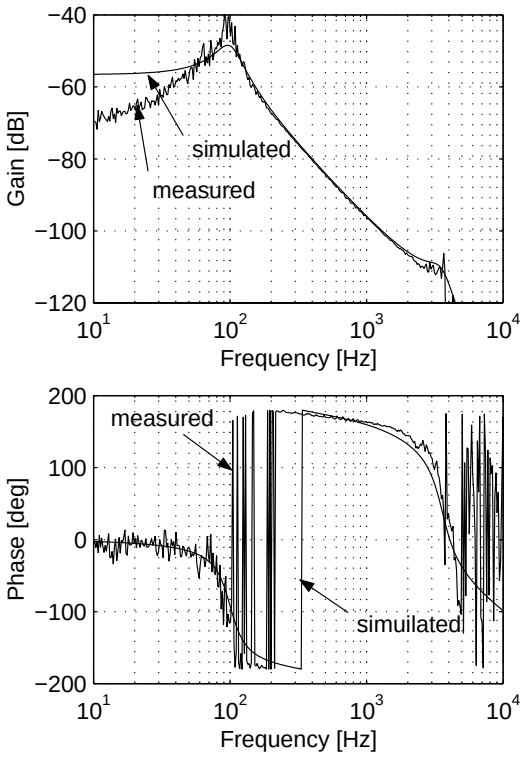

Figure 3.6: Simulated and measured frequency responses of the VCM actuator

appears at 3.6 *kHz*.

3.5.3 Controller Design Procedure

The objective of this section is to design the PID controller (3.3) for this plant based on the proposed fixed-structure H_∞ optimization algorithm. The optimal PID controller is obtained as a re-designed version of a second order compensator tuned manually by an experienced servo engineer.

The design requirements are given as follows. 1) The open-loop cross-over frequency should

be larger than $f_c = 600\ Hz$ to secure a sufficient bandwidth of the closed-loop system. 2) The gain and phase margin should be larger than 5 dB and 40 *degrees*, respectively, for the robustness of the closed-loop system. 3) The peak gain of the closed-loop sensitivity transfer function should be as low as possible to reduce the resonant vibrations.

The followings are two controllers conventionally used in industrial applications:

$$C_1(s) = K_1 \frac{(s+\omega_{n1})(s+\omega_{n2})}{(s+\omega_{d1})(s+\omega_{d2})} \tag{3.44}$$

$$C_2(s) = K_2 \frac{(s+\omega_{n1})(s+\omega_{n2})(s+\omega_{n3})}{(s+\omega_{d1})(s+\omega_{d2})(s+\omega_{d3})} \tag{3.45}$$

where $\omega_{n1} = 170 \times 2\pi$, $\omega_{d1} = 2 \times 10^{-4} \times 2\pi$, $\omega_{n2} = 170 \times 2\pi$, $\omega_{d2} = 7000 \times 2\pi$, $\omega_{n3} = 750 \times 2\pi$, $\omega_{d3} = 1190 \times 2\pi$, $K_1 = 8.334 \times 10^4$, and $K_2 = 10.061 \times 10^4$. These controller parameters are designed by an experienced servo control engineer based on manual loop-shaping such that the closed-loop system achieves given performance requirements. Note that $C_2(s)$ is designed to reduce the peak gain of the sensitivity transfer function by adding the term $(s+\omega_{n3})/(s+\omega_{d3})$ to introduce additional phase lead around the cross-over frequency. The frequency responses of $C_1(s)$ and $C_2(s)$ are shown in Figure 3.8 (a).

The PID controller (3.3) is re-tuned to improve the control performance (with respect to the above design requirements) than is provided by $C_1(s)$ and $C_2(s)$. Notice that the second order controller, $C_1(s)$, is equivalent to the PID controller in the form (3.3) ($k_p = 1.147 \times 10^4$, $k_i = 6.200 \times 10^6$, $k_d = 5.173$, $\tau_i = 0.0002 \times 2\pi$ and $\tau_d = 1/(7000 \times 2\pi)$), which implies that the optimized PID controller should be at least better than $C_1(s)$.

First, the above design objectives are interpreted as the following H_∞ (sub-)optimization problem:

$$\text{Find } K = (k_p, k_i, k_d) \quad \text{such that} \quad \left\| \begin{array}{c} T(s)W_u(s) \\ S(s)W_p(s) \end{array} \right\|_\infty < 1 \tag{3.46}$$

where $T(s)$ is the closed-loop complementary sensitivity function and $S(s)$ is the closed-loop sensitivity transfer function defined respectively by

$$T(s) = \frac{P(s)C(s)}{1+P(s)C(s)} \tag{3.47}$$

$$S(s) = \frac{1}{1+P(s)C(s)}\,. \tag{3.48}$$

The constants, τ_i and τ_d, in Eq. (3.3) are selected as $\tau_i = 0.0002 \times 2\pi$ and $\tau_d = 1/(7000 \times 2\pi)$ such that the PID controller has the same poles as $C_1(s)$.

The performance filters, $W_u(s)$ and $W_p(s)$, in Eq. (3.46) respectively specify the desired shape of $|T(j\omega)|$ and $|S(j\omega)|$. *$W_u(s)$ and $W_p(s)$ are designed based on the actual closed-loop frequency responses of $T(j\omega)$ and $S(j\omega)$ under the conventional controller, $C_2(s)$ (or $C_1(s)$), such that the solution of the problem* (3.46) *achieves better performance than the conventional controllers.*

Figure 3.7 illustrates the design procedure of performance filters, $W_u(s)$ and $W_p(s)$. For example, $W_p(s)$ is designed based on the frequency response of the sensitivity transfer function with $C_1(s)$ (or $C_2(s)$) used in the feedback loop (Figure 3.7(b)). Then, suppose that the optimal set of controller parameters achieves $\|S_{new}(j\omega)W_p(j\omega)\| < 1$, where $S_{new}(s)$ denotes the sensitivity transfer function under the new controller setting. This means that the gain of the sensitivity transfer function is reduced over the specified frequency range (Figure 3.7(c)).

$W_u(s)$ and $W_p(s)$ are given as follows:

$$W_u(s) = \frac{2.45 \times 10s + 4.62 \times 10^3}{s + 4.05 \times 10^5}\,, \tag{3.49}$$

$$W_p(s) = \frac{3.25 \times 10^{-1}s^2 + 1.67 \times 10^3 s + 4.09 \times 10^6}{s^2 + 3.90 \times 10^2 s + 3.62 \times 10^4}\,. \tag{3.50}$$

Their inverse frequency responses are shown in Figure 3.8 (c) and (d), respectively.

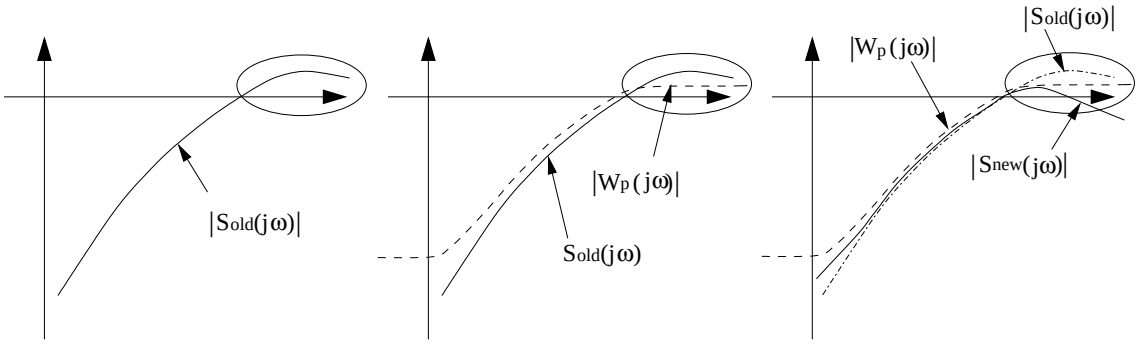

(a) Suppose the closed-loop frequency response $|S_{old}(j\omega)|$ under the original controller $C_1(s)$ is given as above.

(b) Design the performance filter $W_p(s)$ based on $|S_{old}(j\omega)|$. The circle denotes the frequency range where $|S(j\omega)|$ must be particularly reduced.

(c) If $\|S_{new}(s)W_p(s)\|_\infty < 1$ under the new controller, then $|S_{new}(j\omega)| < |S_{old}(j\omega)|$ in the specified frequency range.

Figure 3.7: Design procedure of performance filters

3.5.4 Simulation Results

The problem (3.46) can be transformed into an H_∞ optimization problem of static output feedback controllers as shown in Section 3.3.1. It can be solved by applying the algorithm presented in Section 3.3.2.

All computations have been carried out on *MATLAB* by using the SDP solver package *LMI Control Toolbox* [34] (see Section 2.2.3). The (sub-)optimal set of controller parameters was 'obtained after 31 iterations over X_i and Y_i (Step 2 in Algorithm 1). The iteration was terminated when $\mathrm{tr}(X_iY_i)$ became less than 10.001. Note that the overall plant $P_K(s)$ is tenth order (the original plant, $P(s)$, is fifth order, the controller adds two state variables, and the filters have totally three state variables). The optimal gains, $k_p = 4.607 \times 10^3$, $k_i = 5.932 \times 10^6$, and $k_d = 5.864$, achieve the closed-loop H_∞ gain (3.46) of 1.1130.

Figure 3.8 (a)$\sim$(d) show simulated frequency responses of (a) the controller dynamics, $C(s)$, (b) the open-loop transfer function, $P(s)C(s)$, (c) the closed-loop complementary sensitivity transfer function, $T(s)$, and (d) the sensitivity transfer function, $S(s)$, under two manually-tuned controllers ($C_1(s)$ given in Eq. (3.44) and $C_2(s)$ given in Eq. (3.45)) and the designed PID controller (denoted by $C_{new}(s)$). The controllers were discretized by using the Tustin transformation with the sampling time shown in Table 3.1. All frequency responses shown in Figure 3.8 are simulated in the discrete-time domain.

It can be observed from Figure 3.8 (d) that the peak gain of the sensitivity transfer function is reduced compared to the cases where $C_1(s)$ and $C_2(s)$ are used. Table 3.2 shows the order, cross-over frequency, gain margin, phase margin, and the peak gain of the sensitivity transfer function for each of three controllers. It shows that the designed PID controller satisfies all of the given performance specifications. Notice that the order of $C_{new}(s)$ is less than that of $C_2(s)$.

The superiority of the designed PID controller to $C_1(s)$ and $C_2(s)$, which were finely tuned by an experienced servo engineer, can be explained by two complex zeros of the designed PID controller at $s = -3.97 \times 10^2 \pm 9.14 \times 10^2 j$. They introduce additional gain drop at the corresponding frequency and phase lead at higher frequencies to the controller frequency response (see Figure 3.8 (a)), which leads to desirable drop of the peak gain of the sensitivity transfer function. It is generally difficult to deal with complex zeros/poles by the manual loop-shaping. The "automatic" loop-shaping by the H_∞ optimization has advantages to find a controller that achieves better performance.

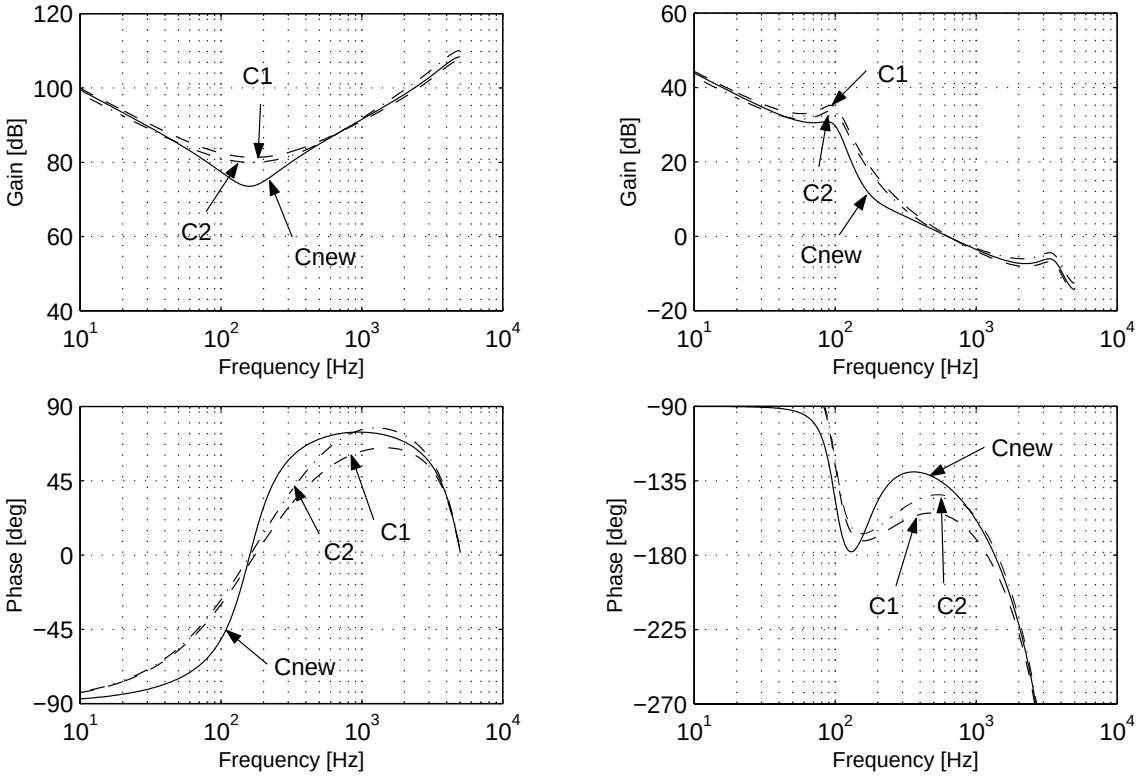

(a) Controller, $C(s)$

(b) Open-loop transfer function, $C(s)P(s)$

Figure 3.8: Comparison of closed-loop frequency responses under two manually-tuned controllers ("C1": $C_1(s)$ and "C2": $C_2(s)$) and the designed PID controller ("Cnew") (simulation results)

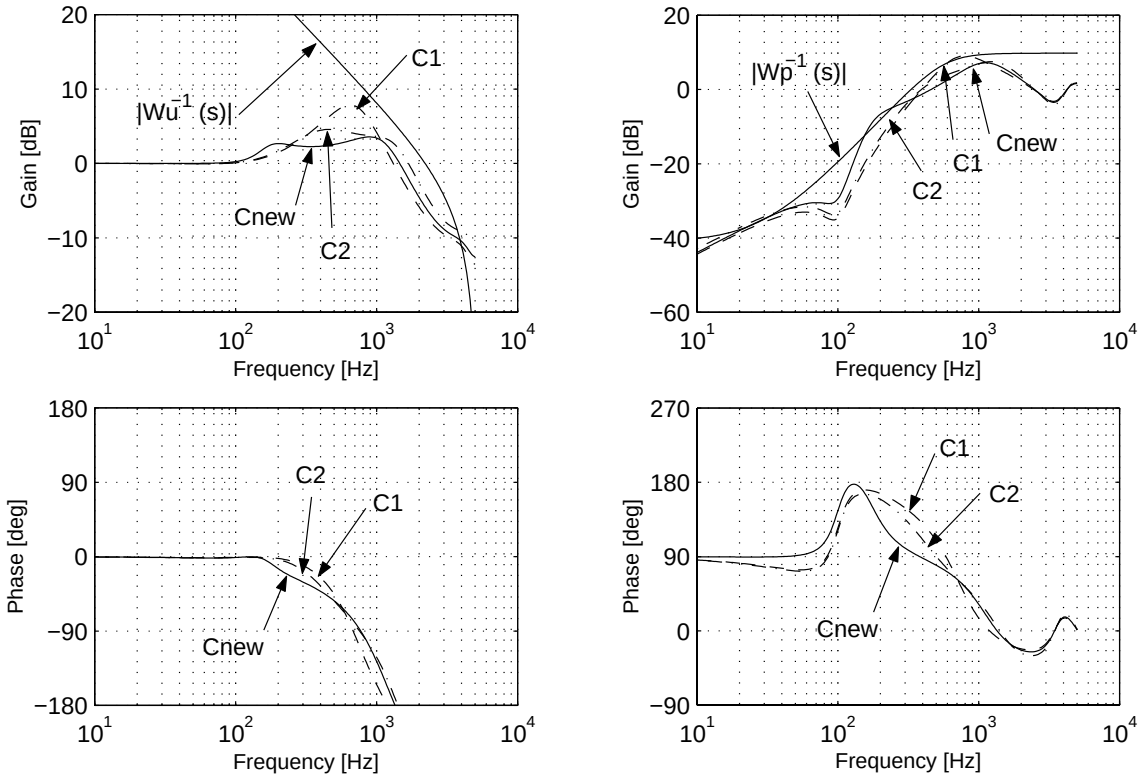

(c) Complementary sensitivity transfer function, $T(s)$ (d) Sensitivity transfer function, $S(s)$

Figure 3.8 (continued): Comparison of closed-loop frequency responses under two manually-tuned controllers ("C1": $C_1(s)$ and "C2": $C_2(s)$) and the designed PID controller ("Cnew") (simulation results)

Table 3.2: Performance comparison of two conventional controllers, $C_1(s)$ and $C_2(s)$, and the designed PID controller, $C_{new}(s)$ (simulation results)

	C_1	C_2	C_{new}
Order	2	3	2
Cross-over frequency (Hz)	636	622	625
Gain margin (dB)	5.32	5.02	5.53
Phase margin (deg)	23.36	35.82	41.63
Sensitivity function peak (dB)	9.04	7.50	7.20

3.5.5 Experimental Results

The control performance of the designed PID controller was also evaluated in experimentation. First, the control performance of the manually-tuned third-order controller, $C_2(s)$, and the designed PID controller, $C_{new}(s)$, were compared by PES measurement. The PES was logged for $1,000$ rotations of the disk with the read/write head fixed on the innermost track of the disk.

Figures 3.9 and 3.10 show PES measurements and their frequency spectrums under the original controller, $C_2(s)$, and the designed PID controller, $C_{new}(s)$, respectively. The PES can be decomposed into the repeatable position error (RPE) component and the nonrepeatable position error (NRPE) component. In (a) of each figure, the maximum deviation of the measured PES profile to the positive and negative directions ("maxPES" and "minPES", respectively) and its RPE component ("RPE") are plotted. In (b), the maximum deviation of the NPES component to the positive and negative directions ("maxNRPE", "minNRPE") are plotted, as well as the the $\pm 5\sigma$ profile of the NRPE component ("+5std" and "-5std"), where σ denotes the standard deviation (STD). (c) and (d) show frequency spectrums of the measured PES and its NRPE component, respectively.

"std(RPE)," "min(RPE)," and "max(RPE)" represent the standard deviation, the maximum value, and the minimum value of the RPE profile, respectively. "min(std)," "max(std)," and "ave(std)" represent the minimum value, the maximum value, and the average of the standard devision profile of the NRPE component, respectively.

Table 3.4 compares the STD of the measured PES, which is composed of the RPE and the NRPE components, between two controllers. The reduction in the STD of the NRPE component observed in this experiment was about 15%. In the PES spectrum shown in Figures 3.9 (c) and 3.10 (c), the gain drop around the peak frequency at about 1000 *Hz* and the gain rise at lower frequencies can be observed, which validate the simulation results shown in Figure 3.8 (d).

To further validate the simulation results, the closed-loop frequency responses were measured by using the frequency-sweep method imposing sinusoidal disturbances of the frequency varying from 0.01 *Hz* to 25 *kHz*. Figure 3.11 (a)$\sim$(d) respectively show the measured frequency responses of (a) the controller dynamics, $C(s)$, (b) the open-loop transfer function, $C(s)P(s)$, (c) the complementary sensitivity transfer function, $T(s)$, and (d) the sensitivity transfer function $S(s)$, under $C_2(s)$ and $C_{new}(s)$. Table 3.4 shows the order, cross-over frequency, gain margin, phase margin, and the peak gain of the sensitivity transfer function for each controller.

The experimental results clearly validate the simulation results shown in the previous section. The gain drop of the sensitivity transfer function around the crossover frequency brought the performance improvement observed in PES responses, even though the order of $C_{new}(s)$ is less than that of $C_2(s)$.

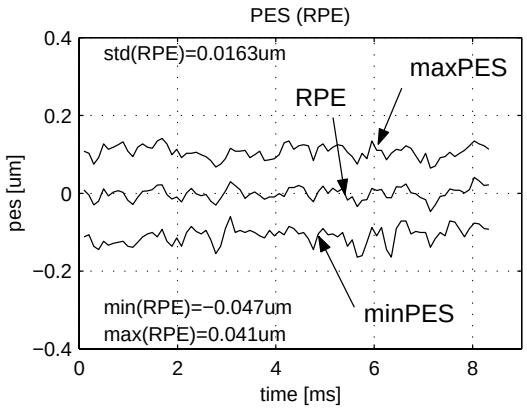

(a) PES and its RPE component

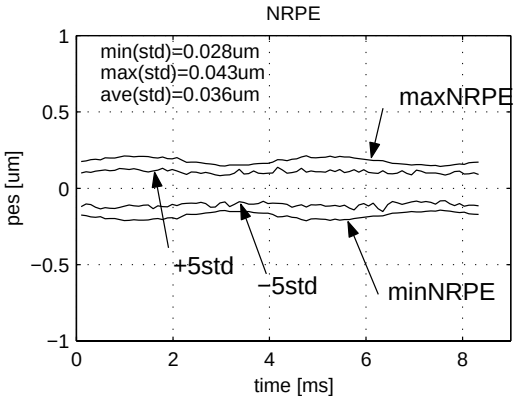

(b) NRPE component

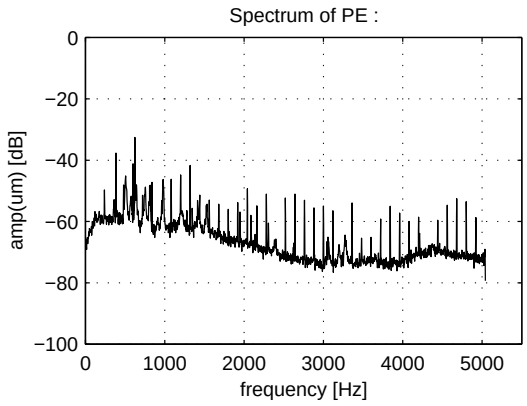

(c) Frequency spectrum of PES

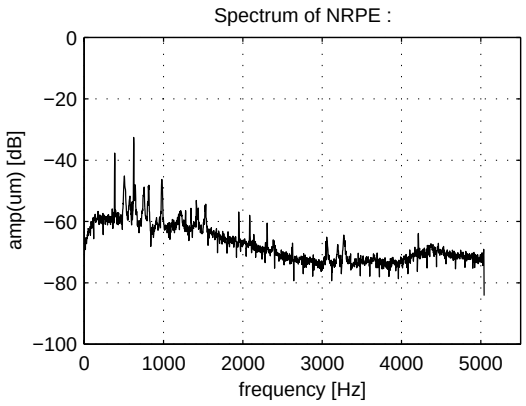

(d) Frequency spectrum of NRPE component

Figure 3.9: Measured PES and its frequency spectrums under the conventional controller, $C_2(s)$

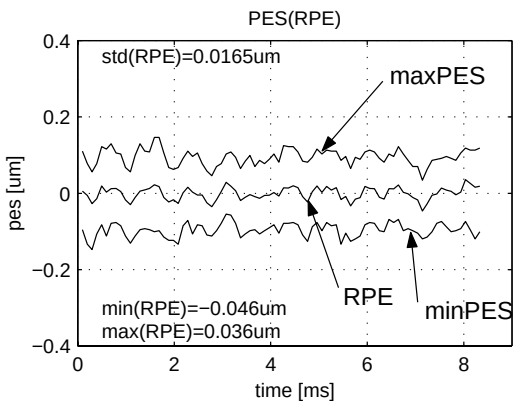

(a) PES and its RPE component

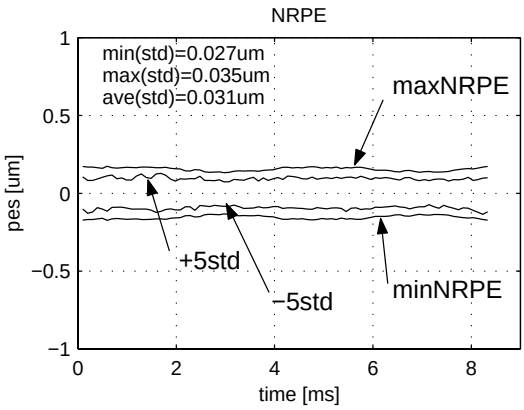

(b) NRPE component

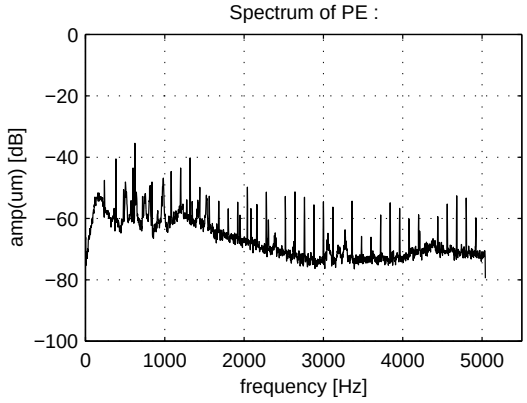

(c) Frequency spectrum of PES

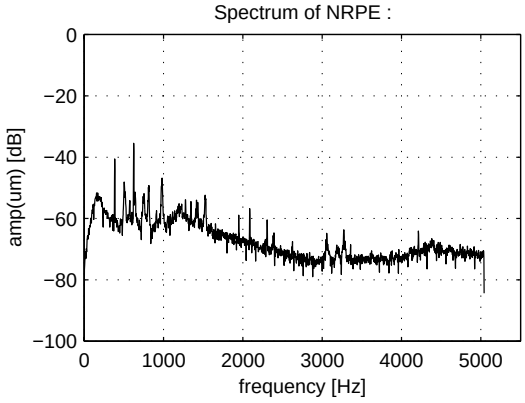

(d) Frequency spectrum of NRPE component

Figure 3.10: Measured PES and its frequency spectrums under the designed PID controller, $C_{new}(s)$

Table 3.3: The STD of the RPE and NRPE components of measured PES under the original controller, $C_2(s)$, and the designed PID controller, $C_{new}(s)$

	$C_2(s)$	$C_{new}(s)$	improvement
NRPE	0.036 μm	0.031 μm	13.9%
RPE	0.0163 μm	0.0165 μm	-1.2%

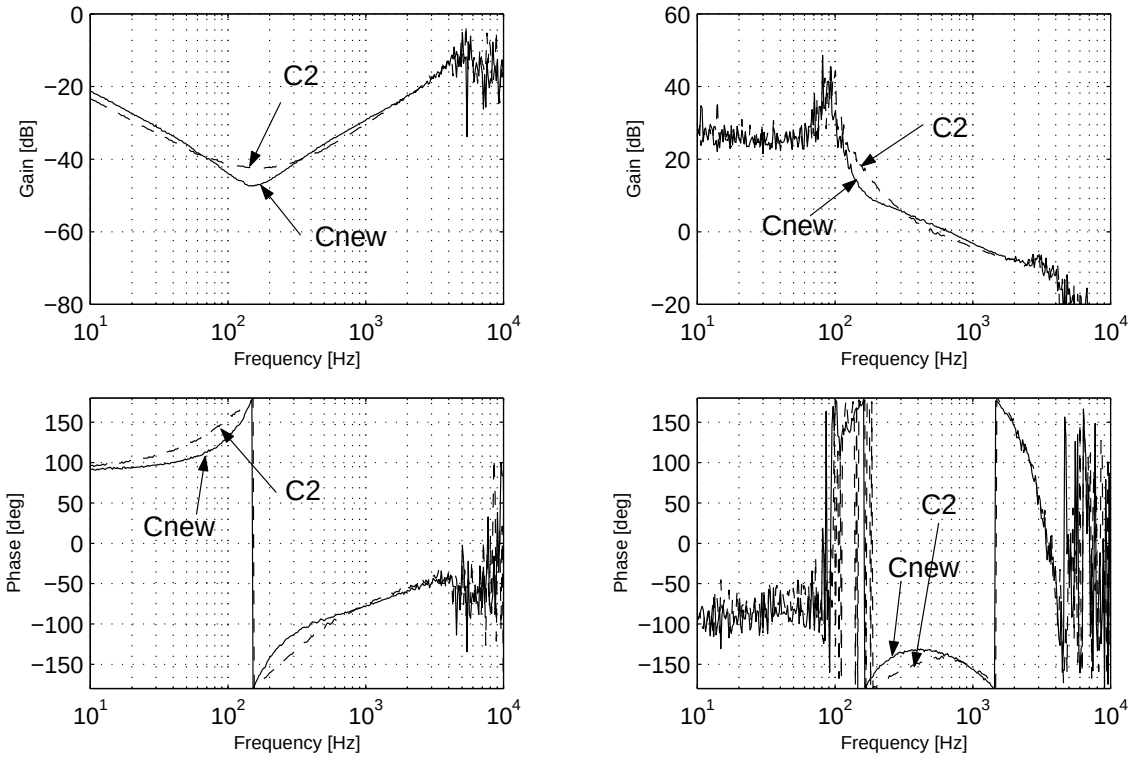

(a) Controller, $C(s)$

(b) Open-loop transfer function, $C(s)P(s)$

Figure 3.11: Comparison of closed-loop frequency responses under the manually-tuned controller, $C_2(s)$ ("C2"), and the designed PID controller, $C_{new}(s)$ ("Cnew") (experimental results)

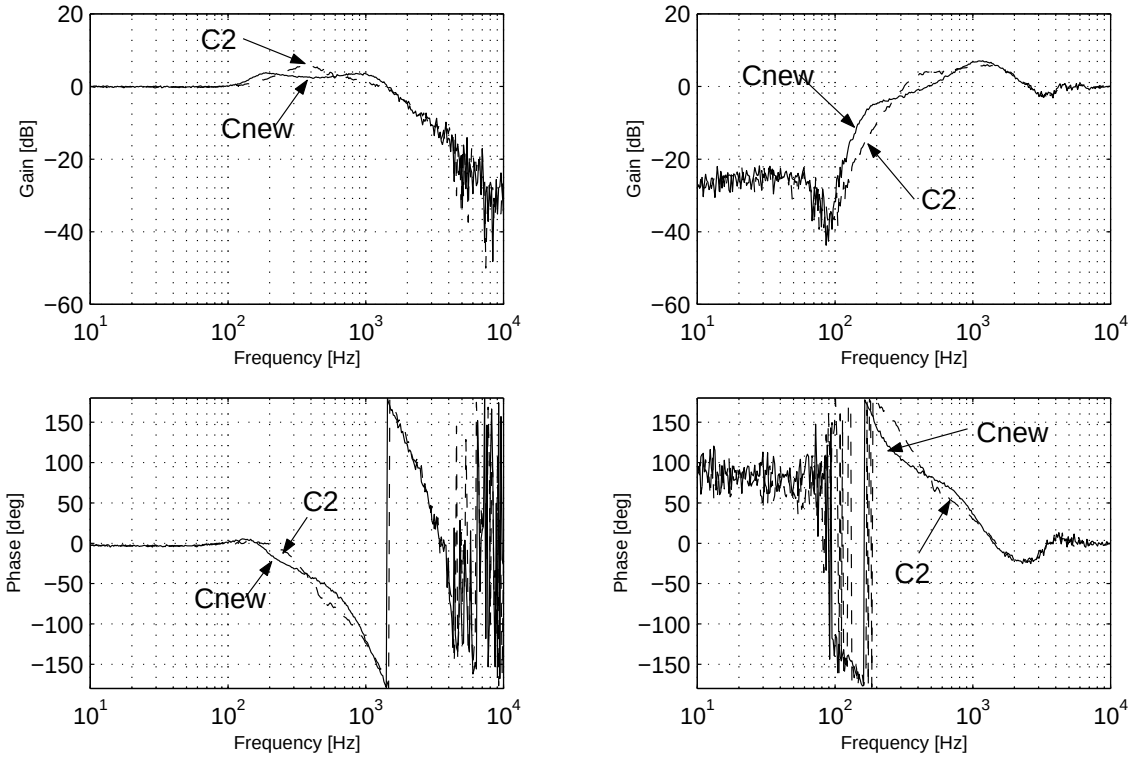

(c) Complementary sensitivity transfer function, $T(s)$ (d) Sensitivity transfer function, $S(s)$

Figure 3.11 (continued): Comparison of closed-loop frequency responses under the manually-tuned controller $C_2(s)$ ("C2") and the designed PID controller $C_{new}(s)$ ("Cnew") (experimental results)

Table 3.4: Performance comparison of the conventional controller (C_2) and the designed PID controller (C_{new}) (experimental results)

	C_2	C_{new}
Order	3	2
Cross-over frequency (Hz)	510	668
Gain margin (dB)	6.70	5.70
Phase margin (deg)	37.5	41.0
Sensitivity function peak (dB)	6.0	7.1

3.6 Application Example II: Digital Observer-based State Feedback Controller Design for Head Positioning of a Magnetic Hard Disk Drive

3.6.1 Introduction

This section also considers the tuning problem of a fixed-structure track-following controller for head positioning of an HDD. The differences from the previous problem are summarized as follows.

1. The plant model is based on a different product by a different manufacturer. The plant dynamics is approximated by a simple double-integrator model.

2. An observer-based state feedback controller is employed instead of a PID controller. The design objective is to tune its observer and state feedback matrices by using the fixed-structure H_∞ controller optimization. Unlike the PID controller case, this problem cannot be transformed by using LFTs into a static output feedback H_∞ controller synthesis problem. By using an iterative approach and alternately optimizing a part of controller parameters, however, a locally optimal solution can be obtained. This approach can be applied to almost any fixed-structure linear controllers and shows sufficient search performance in many practical applications.

3. The H_∞ optimization is performed in the discrete-time domain due to the discrete-time nature of the controller structure.

4. To show the flexibility of the proposed approach to some extent, slightly different

tuning objectives are considered. The controller tuning focuses more on the gain reduction of the sensitivity transfer function at low frequencies than that at the peak frequency.

3.6.2 Plant Model and Controller Structure

The VCM actuator dynamics is modeled under the assumption that the power-amplifier is ideal and the actuator is perfectly rigid, without any friction or mechanical resonances. In other words, the plant dynamics, $G(z)$, is approximated by a double-integrator model and is represented by the following discrete-time state equations:

$$\begin{aligned} x(k) &= \Psi_p x(k-1) + \Gamma_p u(k-1) \\ y(k) &= h_p x(k-1) \end{aligned} \tag{3.51}$$

where $u(k) \in \mathbb{R}$ and $y(k) \in \mathbb{R}$ denote the control input to the VCM actuator and the measured PES, respectively, and $x(k) \in \mathbb{R}^2$ is the state vector, which consists of the position and velocity of VCM actuator as state variables. The matrices in Eq. (3.51) are $\Psi_p \in \mathbb{R}^{2\times 2}$, $\Gamma_p \in \mathbb{R}^{2\times 1}$, and $h_p \in \mathbb{R}^{1\times 2}$.

Consider the VCM controller, $C(z)$, of the following well-known observer-based state feedback controller structure (Franklin et al. [29]):

$$\begin{aligned} \hat{x}(k) &= \bar{x}(k) + L(y(k) - h\hat{x}(k)) \\ \bar{x}(k) &= \Psi\hat{x}(k-1) + \Gamma u(k-1) \\ u(k) &= -\begin{bmatrix} K & 1 \end{bmatrix} \hat{x}(k) \end{aligned} \tag{3.52}$$

where $\Psi = \begin{bmatrix} \Psi_p & \Gamma_p \\ 0_{1\times 2} & 1 \end{bmatrix}$, $\Gamma = \begin{bmatrix} \Gamma_p \\ 0 \end{bmatrix}$ and $h = \begin{bmatrix} h_p & 0 \end{bmatrix}$. $K \in \mathbb{R}^{1\times 2}$ and $L \in \mathbb{R}^{3\times 1}$ are the state feedback and the state estimator gain matrices, respectively. $\bar{x}(k)$ and $\hat{x}(k)$ are the predicted and corrected system state estimates. Notice that the third state variable represents the bias force of the actuator, i.e. the controller has an integrator in addition to the observer-based state feedback structure.

3.6.3 Controller Design Procedure

Controller Tuning by using H_∞ Optimization

The objective of this section is to tune the controller parameters (K, L) in Eq. (3.52). Similarly as in Section 3.5, it is assumed that a set of controller parameters conventionally used for the given plant were tuned by an experienced servo engineer using any standard approaches, such as the pole assignment technique presented in [29]. The controller design requirements are summarized as follows: 1) the open-loop cross-over frequency and gain/phase margins should be larger than given certain levels to secure a sufficient bandwidth and the robustness of the closed-loop system, and 2) the gain of the closed-loop sensitivity transfer function should be as low as possible to achieve the desirable disturbance rejection performance. In particular, the gain at low frequencies should be reduced to reject low-mid frequency external disturbances. A high peak gain around the cross-over frequency should be also avoided not to induce vibrations.

The objective is to re-tune the controller parameters (K, L) to improve the control performance (with respect to the above design requirements) than is provided by the conventional

controller setting (denoted by $C_{old}(z)$).

The above design objectives are interpreted as the following H_∞ (sub-)optimization problem:

$$\text{Find } (K,\ L) \quad \text{such that} \quad \left\| \begin{array}{c} T(z)W_u(z) \\ S(z)W_p(z) \end{array} \right\|_\infty < 1 \tag{3.53}$$

where $T(z)$ is the closed-loop complementary sensitivity function and $S(z)$ is the sensitivity transfer function defined in Eqs. (3.47) and (3.48), respectively.

The performance filters, $W_u(z)$ and $W_p(z)$, in Eq. (3.53) respectively specify the desired shape of $|T(e^{j\omega})|$ and $|S(e^{j\omega})|$. They can be designed in the similar way as presented in Section 3.5.3.

H_∞ Optimization of Observer and State Feedback Matrices

It can be easily seen that it is not possible to transform the problem (3.53) into a static output feedback synthesis problem, where both K and L appear in the static block as optimization parameters. Thus, K and L are optimized in an alternating manner to obtain a locally optimal solution. In many practical cases, it shows a sufficient search performance and results in improvement of the control performance.

Consider the problem of finding K, with L fixed, to achieve the closed-loop H_∞ norm constraint given in Eq. (3.53). This fixed-structure H_∞ controller synthesis can be equivalently transformed into the synthesis problem of the H_∞ (sub-)optimal static output feedback controller using LFTs as follows.

1. Rewrite the plant dynamics, $P(s)$, such that $\left[\begin{array}{c} T(z)W_u(z) \\ S(z)W_p(z) \end{array} \right]$ becomes equal to $F_L(P(z), C(z))$ (see Figure 3.12 (a)).

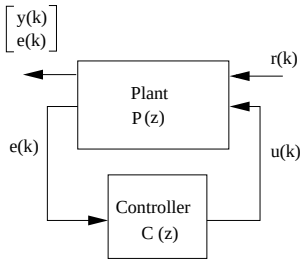

(a) Closed-loop system configuration of the problem (3.53)

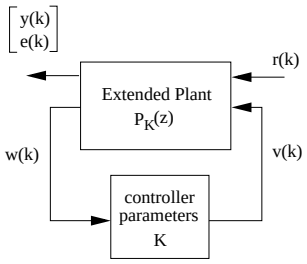

(b) Extraction of controller parameters K

Figure 3.12: Transformation into the H_∞ optimization problem of a static output feedback controller

2. By defining $w(k) := \begin{bmatrix} \hat{x}_1(k-1), & \hat{x}_2(k-1) \end{bmatrix}^T$ and $v(k) := Kw(k)$, the third equation in (3.52) can be rewritten as $u(k) = -v(k) - \hat{x}_3(k)$, where $\hat{x}_i(k)$ denotes the i-th component of $\hat{x}(k)$.

3. Reconstruct the combined model $P_K(z)$ of the plant (3.51) and the controller (3.52) such that its inputs are $r(k)$ and $v(k)$ and its outputs are $\begin{bmatrix} y(k) & e(k) \end{bmatrix}^T$ and $w(k)$ (see Fig. 3.12 (b)). Notice that $P_K(z)$ does not include K.

4. It is easy to see that $F_L(P_K(z), K)$ is equivalent to $F_L(P(z), C(z))$.

The "extraction" of L (with K fixed) can be done in an analogous way.

By using the above transformation, the fixed-structure H_∞ controller optimization problem can be seen as the following H_∞ (sub-)optimization problem of a static output feedback gain matrix K:

$$\text{Find} \quad K \quad \text{such that} \quad \|F_L(P_K(z), K)\|_\infty < 1\,. \tag{3.54}$$

Algorithm 2 can be applied to locally solve this discrete-time H_∞ optimization problem of

static output feedback controllers.

3.6.4 Simulation Results

First, the state feedback gain matrix, K, was re-tuned by solving the problem (3.53) with the performance filters, $W_p(z)$ and $W_u(z)$, designed based on the closed-loop frequency responses under $C_{old}(z)$. Then, the observer gain matrix, L, was re-designed by slightly modifying the performance filters based on the optimization result of K. Since no significant improvement was achieved by further iterations, the design procedure was terminated at this point. All computations have been carried out on *MATLAB* by using *LMI Control Toolbox* [36] (see Section 2.2.3).

The frequency response of a typical HDD's VCM actuator is shown in Figure 3.13. Even though the optimization was based on the rigid body model, the simulation model of the plant includes three mechanical resonance modes for more accurate simulations.

Figures. 3.14 and 3.15 show the frequency responses of the open-loop transfer function, $P(z)C(z)$, and the sensitivity transfer function, $S(z)$, under the original controller $C_{old}(z)$ and the re-tuned controller $C_{new}(z)$, respectively. In Figure 3.14, it can be observed that the open-loop bandwidth was increased to 940 Hz from 800 Hz by the optimization scheme. Figure 3.15 shows that the gain of the sensitivity transfer function has been reduced up to 3 dB at low frequencies, which implies better disturbance rejection at those frequencies. However, the peak gain is a little higher than the case where $C_{old}(z)$ is used.

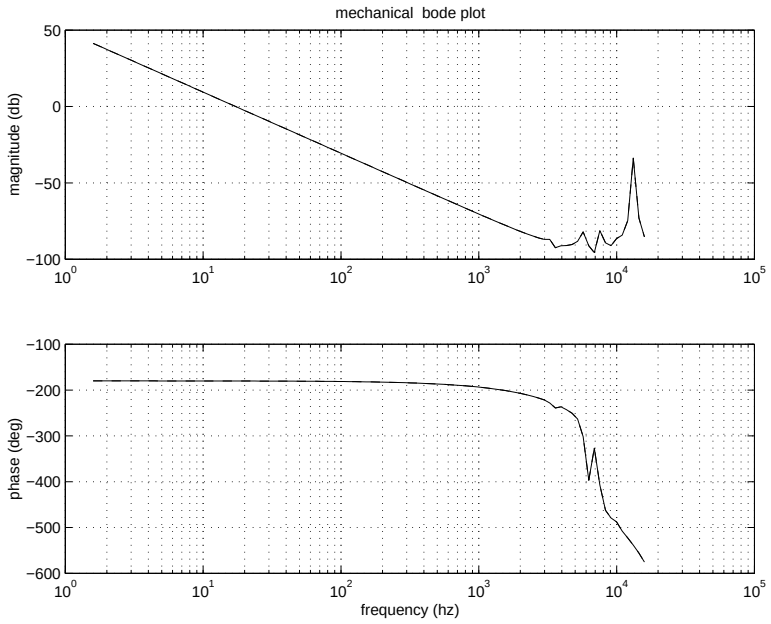

Figure 3.13: The frequency response of a typical VCM actuator of an HDD

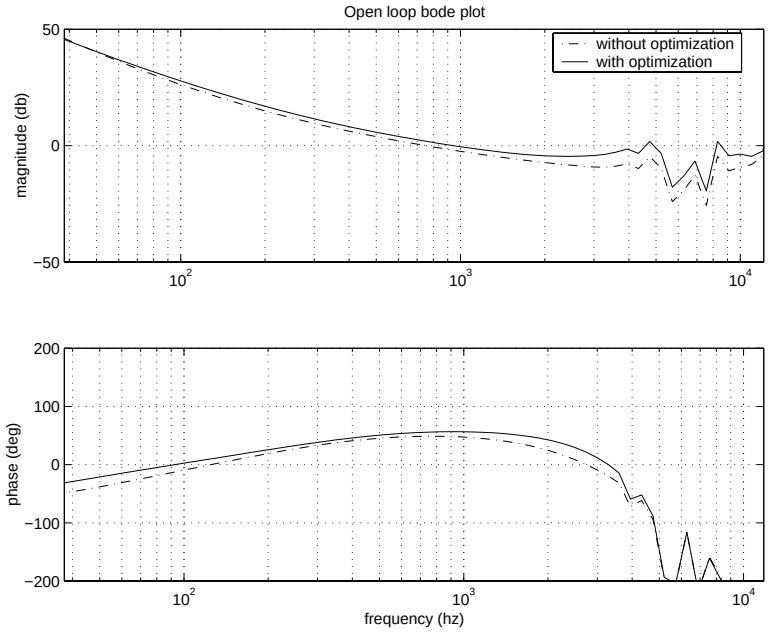

Figure 3.14: The open-loop responses of the disk drive servo with and without the optimization of controller parameters

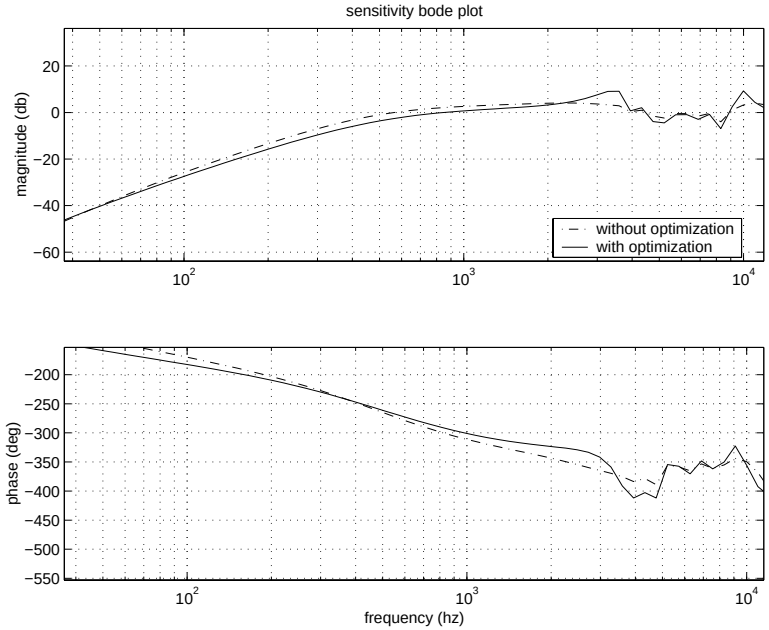

Figure 3.15: The frequency responses of the sensitivity function of the disk drive servo with and without the optimization of controller parameters

3.6.5 Experimental Results

The two controllers, $C_{old}(z)$ and $C_{new}(z)$, were implemented on a laboratory prototype drive to verify the effectiveness of the optimization scheme. The track density of the drive was about $780,000$ *tracks/m* ($20,000$ *TPI*, or Tracks Per Inch).

Figure 3.16 shows a portion of the measured PES spectrum with $C_{old}(z)$ (three plots in the left column) and $C_{new}(z)$ (three plots in the right column). Notice that the PES spectrum with $C_{new}(z)$ is lower than that with $C_{old}(z)$.

The standard deviation of the measured TMR (Track MisRegistration) signal for each controller also shows the effectiveness of the re-design of the controller. The net reduction in overall TMR observed in this experiment was about 20% (the track RMS TMR was reduced from 2.2% to 1.8%). The net reduction for the RRO (Repeated Run-Out) and NRRO (Non-Repeated Run-Out) were about the same.

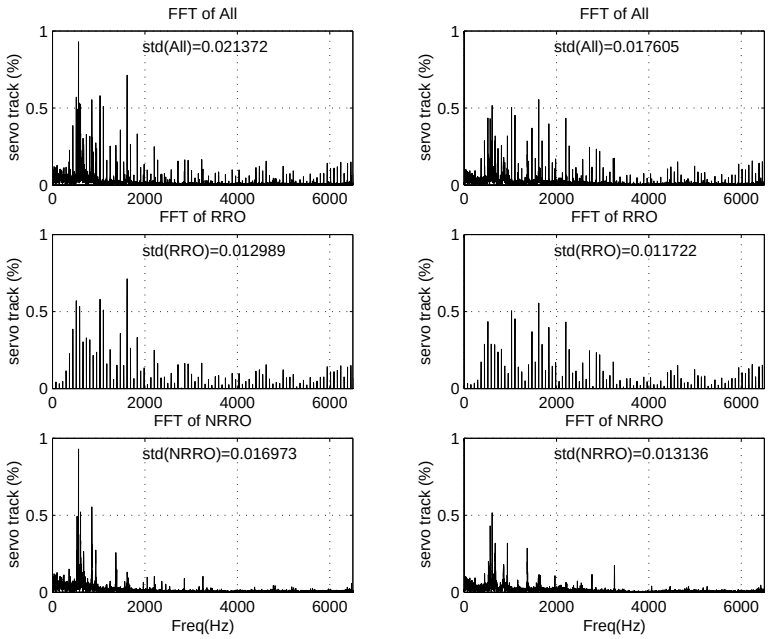

Figure 3.16: Comparison of experimentally measured TMR (Track MisRegistration) spectrums with the original controller setting, $C_{old}(z)$ (left column) and the re-designed controller, $C_{new}(z)$ (right column) ("All": measured TMR signal, "RRO": Repeated Run-Out component of TMR signal, "NRRO": Non-Repeated Run-Out component of TMR signal, "std": standard deviation)

3.7 Application Example III: MISO PID Controller Design for Lateral Control of Heavy-Duty Vehicles

3.7.1 Introduction: Lateral Control of Heavy-Duty Vehicles

Automatic Highway System (AHS) technologies have attracted growing attention among researchers throughout the world in the past several years. AHS technologies offer a number of benefits including the saving of fuel cost and the reduction of driver's stress. The ratio of automation cost to vehicle cost is significantly lower for heavy-duty vehicles (HDVs) than for passenger vehicles. These aspects make AHS technologies particularly attractive for HDVs. A comprehensive review of automated control of HDVs can be found in Kanellakopoulos and Tomizuka [62], and Tomizuka et al. [106].

This section considers the steering control problem for lateral control of a single-unit HDV (tractor-semitrailer type). For the lateral control purpose, Chen and Tomizuka [13] have developed a nonlinear control model of a single-unit HDV. A dynamic model of more general multi-unit HDVs has been developed by Tai and Tomizuka [101]. The controller design presented in this section is based on the linearized steering control model of a single-unit HDV developed by Wang and Tomizuka [113].

The steering input has to be determined in accordance with a controller that offers the stability, adequate tracking performance, and robustness to uncertainties. The challenges in designing such a controller arise from [47]:

1. Perturbations or uncertainties in vehicle model parameters (such as inertia and its distribution) and environment (such as changes in road friction). In particular, the

variation of vehicle's longitudinal velocity has a significant effect on the vehicle dynamics, as shown by Patwardhan et al. [85].

2. Nonlinearities in the vehicle dynamics model. If the vehicle's longitudinal velocity is considered as a state variable of the model, it becomes an important source of the nonlinearity. Another significant source of model nonlinearities is tire force saturation.

3. Smoothness requirement of steering action for cabin comfort and longer actuator life.

Considerable research efforts have been devoted in recent years to address the above issues in the design of lateral motion controllers for HDVs. Many of the proposed controllers are based on sophisticated linear or nonlinear control theories, such as the full-order H_∞ controller by Wang and Tomizuka [113], the back stepping control by Chen and Tomizuka [14], and the chattering-free sliding mode control by Hingwe and Tomizuka [48]. Since the vehicle's longitudinal velocity has a significant effect on the vehicle dynamics and is measurable or easy to estimate, the controllers whose dynamics is dependent on the vehicle velocity, as well as lateral displacement measurements of the vehicle, have shown promising results. Such controllers include the gain-scheduled linear H_∞ controller by Wang and Tomizuka [114], the linear parameter varying (LPV) H_∞ controller by Hingwe et al. [47], the gain-scheduled H_∞ controller based on the μ-synthesis by Hingwe [49, Chapter 5], the nonlinear adaptive robust control by Tai and Tomizuka [102], and the feedback linearization controller, which will be presented in Section 6.5.

This section presents the H_∞ optimization of a multi-input single-output (MISO) PI (Proportional plus Integral) controller for lateral control of HDVs. Since most of sophisticated controllers found in the literature have a complicated and high-order structure, and thus require a higher installation cost, it is of interest to evaluate the optimal performance that

simple PI controllers can achieve. In particular, the controller design focuses on the robustness of the closed-loop system against the model uncertainties and perturbations, since it is generally a more important issue in the automated vehicle control than the transient response performance.

3.7.2 Model Description

The controller design presented in this section is based on the lateral motion model of a single-unit HDV developed by Chen and Tomizuka [13]. It is a nonlinear model based on the following assumptions: 1) the roll motion is negligible, 2) the longitudinal acceleration is small, 3) the tire slip angles of the left and right wheels are the same, and 4) the tire force can be linearly modeled. By further assuming that 1) the yaw angle of the tractor relative to the road is small, and 2) the articulation angle between the tractor and semi-tractor is small, the following linearized model can be derived [113]:

$$\ddot{q} + A_{22}\dot{q} + A_{21}q = B_1\delta + B_2\dot{\epsilon}_d + B_3\ddot{\epsilon}_d \tag{3.55}$$

where

$$\begin{aligned} &A_{21} = M^{-1}K,\ A_{22} = M^{-1}D, \\ &b_1 = M^{-1}F,\ b_2 = M^{-1}E_2,\ b_3 = M^{-1}E_2\ . \end{aligned} \tag{3.56}$$

and $q = [\ y_r \quad \epsilon_r \quad \epsilon_f\ ]^T$ is the generalized coordinate vector: y_r is the lateral displacement of the tractor's center of gravity (CG) relative to the road centerline, ϵ_r is the yaw angle of the tractor relative to the road centerline, ϵ_f is the articulation angle between the tractor and semi-tractor (See Figure 3.17). δ is the steering angle and it is the control input. $\dot{\epsilon}_d$ and

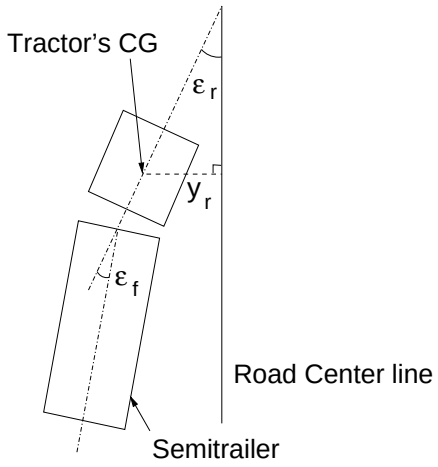

Figure 3.17: State variables of the linearized lateral motion model of HDVs

$\ddot{\epsilon}_d$ are the yaw rate and yaw acceleration of the road frame, respectively. They are regarded as disturbances. See [113] for detailed descriptions of the inertial matrix M, the damping matrix D, the stiffness matrix K, the coefficient matrices F, E_1, and E_2. The linearized model used in this section is based on the lateral motion model of a Freightliner FLD 120 class-8 tractor with a Grate-Dane semitrailer.

Note that 1) M is a function of m_2 (cargo load in the trailer), 2) D is a function of v (longitudinal velocity of the vehicle), m_2 and μ (road adhesion coefficient), and 3) F and K are functions of μ. Variations of these parameters are the main cause of model uncertainties. y_r and ϵ_r are measured by using the sensing system, which consists of magnets buried under the road surface and on-board magnetometers attached at the front and rear bumpers of the tractor.

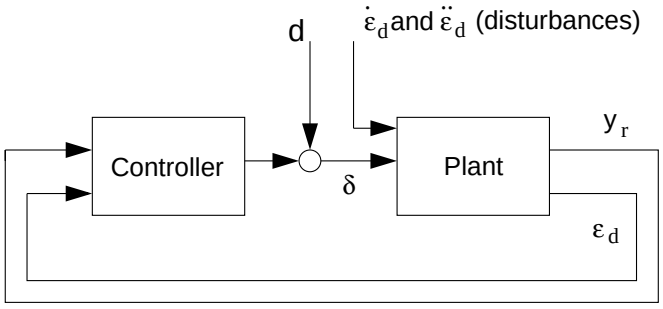

Figure 3.18: Closed-loop configuration for lateral motion control of HDVs

3.7.3 Control Objective and Controller Structure

This section focuses on the controller design for the lane following maneuver. The control objective is to keep the lateral tracking errors at the tractor's CG and the rear of the trailer to be small in lane-following maneuvers.

Suppose that a two-inputs single-output PI controller of the following transfer function is used to control the lateral motion of the vehicle:

$$\delta(s) = \left(k_{p1} + \frac{k_{i1}}{s+\tau_1}\right)(-y_r(s)) + \left(k_{p2} + \frac{k_{i2}}{s+\tau_2}\right)(-\epsilon_r(s)) \tag{3.57}$$

where k_{p1}, k_{i1}, k_{p2}, and k_{i2} are tunable controller parameters. τ_1 and τ_2 are added to avoid a pure integrator. They are set to $\tau_1 = \tau_2 = 10^{-6}$.

The closed-loop block diagram is shown in Figure 3.18. The design objective is to tune the controller parameters (k_{p1}, k_{i1}, k_{p2}, k_{i2}) such that the closed-loop system is stable and shows the desirable disturbace rejection perforamance for the lane-following maneuver.

3.7.4 Controller Design Procedure

The above design objectives can be interpreted as the following H_∞ (sub-)optimization problem:

$$\text{Find } K = (k_{p1},\ k_{i1},\ k_{p2},\ k_{i2}) \quad \text{such that} \quad \left\| \begin{array}{c} T^{cl}_{\dot{\epsilon}_d \to y_r}(s) W_{p1}(s) \\ T^{cl}_{\dot{\epsilon}_d \to \epsilon_r}(s) W_{p2}(s) \\ T^{cl}_{\dot{\epsilon}_d \to \delta}(s) W_u(s) \end{array} \right\|_\infty \leq 1 \tag{3.58}$$

where $T^{cl}_{\dot{\epsilon}_d \to y_r}(s)$, $T^{cl}_{\dot{\epsilon}_d \to \epsilon_r}(s)$, and $T^{cl}_{\dot{\epsilon}_d \to \delta}(s)$ denote the closed-loop transfer function from the disturbance, $\dot{\epsilon}_d$, to the plant outputs, y_s and ϵ_r, and the control input, δ, respectively. The plant dynamics is assumed to be in the nominal condition ($v = 18\ m/s$, $\mu = 0.8$ and $m_2 = 10670\ kg$).

$W_{p1}(s)$ and $W_{p2}(s)$ are the performance filters designed based on the desired dynamics of $T^{cl}_{\dot{\epsilon}_d \to y_r}(s)$ and $T^{cl}_{\dot{\epsilon}_d \to \epsilon_r}(s)$, respectively. $W_u(s)$ is the uncertainty filter that is designed based on the "acceptable" range of model uncertainties. The parametric uncertainties in the plant model are assumed to be within the following ranges. The speed range for HDVs is assumed to be $v = 0 \sim 25\ m/s$ ($0 \sim 90\ km/hour$). Cargo load in the trailer varies from $m_2 = 5000 \sim 2400\ kg$. The road adhesion coefficient is within $\mu = 0.5 \sim 1.0$. Figure 3.19 shows multiplicative uncertainties, $\Delta(j\omega)$, of the plant model, caused by parametric perturbations of v, μ and m_2 (dotted lines). The lateral motion model (3.55) does not include the steering actuator dynamics. Since the steering actuator dynamics is nonlinear and it is generally difficult to identify its accurate model, it is treated as model uncertainty. The dashed line shows the multiplicative error introduced by the actuator dynamics, when it is approximated by an second order model. The robustness filter, $W_u(s)$, is designed by considering the range of those "acceptable" uncertainties. The solid line

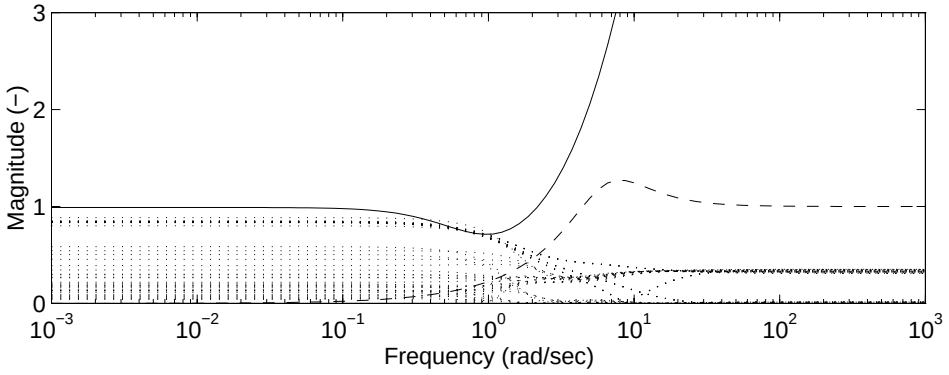

Figure 3.19: Multiplicative uncertainties due to parameter perturbations (dotted lines: $v(0 \sim 25m/s)$, $\mu(0.5 \sim 1.0)$ and $m_2(5000 \sim 2400kg)$) and the actuator model (dashed line). The solid line is the frequency response of the uncertainty filter $W_u(s)$.

shows the frequency response of the uncertainty filter $W_u(s)$.

$W_{p1}(s)$, $W_{p2}(s)$, and $W_u(s)$ are chosen as follows:

$$\begin{aligned} W_{p1}(s) &= \frac{300(s + 5 \times 10^{-4})}{s + 0.1}, \\ W_{p2}(s) &= \frac{20(s + 6.667 \times 10^{-4})}{s + 0.1}, \\ W_u(s) &= \frac{9.8s^2 + 19.002s + 13.248}{s^2 + 24.090s + 13.380}. \end{aligned} \tag{3.59}$$

By using the transformation presented in Section 3.3.1, the extended plant, $P_K(s)$, can be constructed such that $F_L(P_K(s), K)$ forms the closed-loop system given in Eq. (3.58) with $K = [k_{p1}\ k_{i1}\ k_{p2}\ k_{i2}]$.

The optimal set of the controller parameters, K^*, which minimizes the closed-loop H_∞ norm (3.58), can be computed by using the algorithm presented in Section 3.3.2. All computations have been carried out on *MATLAB* by using *LMI Control Toolbox* [36] (see Section 2.2.3). After 15 iterations over X_i and Y_i (Step 2 in Algorithm 1), $tr(X_iY_i) = 12.000$ can be achieved (the weighted plant model, $P_K(s)$, is 12th order; the original plant is 6th

order, the controller adds two states and the filters are totally 4th order). The optimal gains, $k_{p1} = 0.1997$, $k_{i1} = 0.0059$, $k_{p2} = 0.9546$, and $k_{i2} = -2.7723$ achieve the closed-loop H_∞ gain of 0.9992.

3.7.5 Simulation Results

Figure 3.20 shows the closed-loop frequency responses of $T^{cl}_{\dot{\epsilon}_d \to \delta}(s)$ (upper), $T^{cl}_{\dot{\epsilon}_d \to y_r}(s)$ (middle) and $T^{cl}_{\dot{\epsilon}_d \to \epsilon_r}(s)$ (lower), under the designed controller. The plant is assumed to be in the nominal condition. The dotted lines in each figure indicate the inverse frequency responses of the performance filters, $W_u(s)$, $W_{p1}(s)$, and $W_{p2}(s)$, respectively. The controller parameters were optimized such that each frequency response gain stays "under" that of the inverse of the corresponding performance filter. Since the controller design focuses more on the robustness of the closed-loop system than the disturbance rejection performance, the filter $W_u(s)$ was designed more tightly than $W_{p1}(s)$ and $W_{p2}(s)$.

Time-domain simulations were conducted to show the closed-loop performance of the designed controller. The road curvature scenario used in numerical simulations was designed based on the test track at Crows Landing test site [113] (Figure 3.21). In simulations, the road curvature was treated as a disturbance to the plant dynamics by way of $\dot{\epsilon}_d$ and $\ddot{\epsilon}_d$. Figure 3.22 shows the simulation results in the nominal condition ($v = 18\,m/s$, $\mu = 0.8$, $m_2 = 10670\,kg$) and two perturbed conditions ($v = 25\,m/s$, $\mu = 1.0$, $m_2 = 24000\,kg$) ($v = 15\,m/s$, $\mu = 0.6$, $m_2 = 5000\,kg$). The maneuver was accomplished with an overshoot from the lane centerline about 0.5 m at the tractor's CG (y_r) in the nominal condition, about 2.5 m in the perturbed conditions. The maximum overshoots are observed when the vehicle is entering curved sections at 825 m and 1375 m, where the road curvature changes from

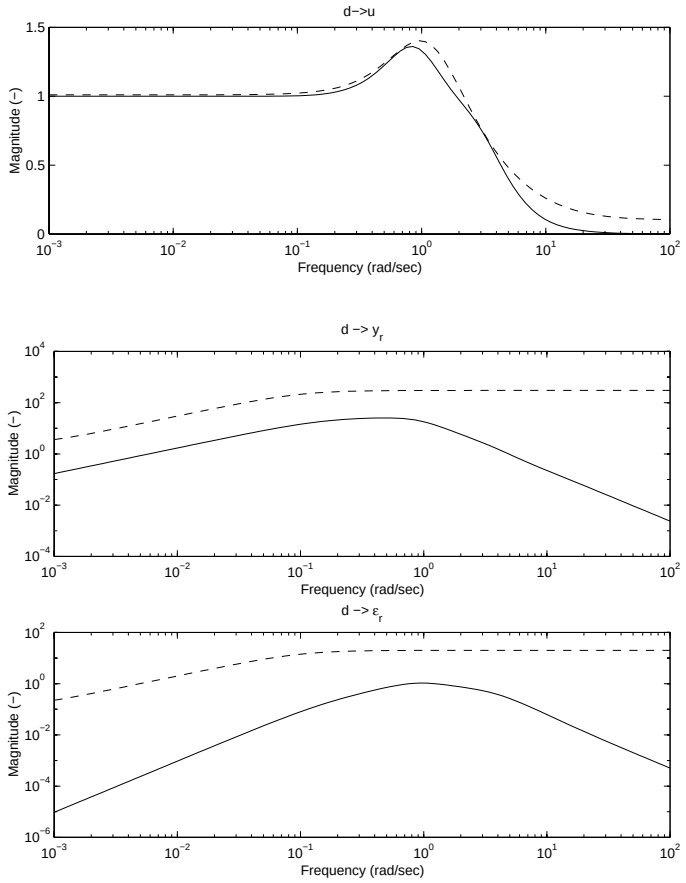

Figure 3.20: Frequency responses of the closed-loop transfer functions $T^{cl}_{\dot{\epsilon}_d \to \delta}(s)$ (upper), $T^{cl}_{\dot{\epsilon}_d \to y_r}(s)$ (middle), and $T^{cl}_{\dot{\epsilon}_d \to \epsilon_r}(s)$ (lower) under the designed controller. The dashed lines are inverse frequency responses of the performance filters, $W_u(s)$ (upper), $W_{p1}(s)$ (middle), and $W_{p2}(s)$ (lower), respectively.

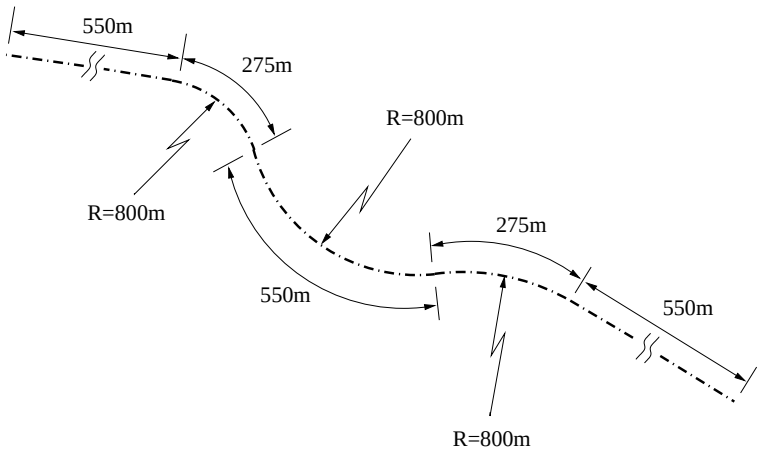

Figure 3.21: Scheme of the Crows Landing test site

$\rho = \mp 1/800\ 1/m$ to $\rho = \mp 1/800\ 1/m$. Steering actions were sufficiently smooth both on curved and straight sections.

It is noted that the lane-following performance of the designed controller is not as good as more complicated controllers found in the literature [113, 72]. However, it stabilizes the closed-loop system even under the existence of model uncertainties within the prescribed range, despite its quite simple structure.

In particular, the simulation results validated that the variation of the vehicle's longitudinal velocity had a significant effect on the closed-loop performance. Therefore, the application of gain-scheduled controllers, whose dynamics is dependent also on the vehicle velocity, is critical to further improve the lane-following performance. From this point of view, Section 6.5 will present the application of the feedback linearization control scheme to this problem.

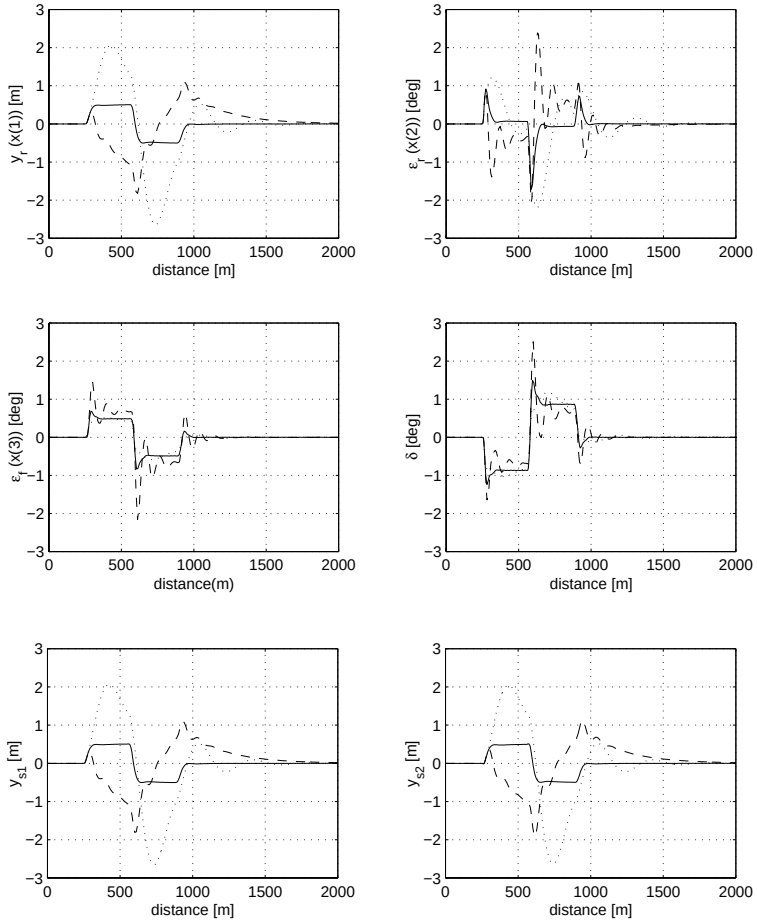

Figure 3.22: Closed-loop time-domain simulations under the nominal condition (solid:$v = 18$ m/s, $\mu = 0.8$, $m_2 = 10670$ kg) and two perturbed conditions (dashed:$v = 25$ m/s, $\mu = 1.0$, $m_2 = 24000$ kg) (dotted:$v = 15$ m/s, $\mu = 0.6$, $m_2 = 5000$ kg)

3.8 Summary

In this chapter, the H_∞ optimization algorithm for parameters of a fixed structure linear controller was presented. The proposed algorithm consists of two steps: 1) "Extraction" of controller parameters from the closed-loop system as a full constant block by using LFTs, and 2) H_∞ synthesis of a static output feedback controller. Unlike the full-order H_∞ controller synthesis case, the H_∞ optimization of static output feedback controllers cannot be solved by convex optimization. The cone complementarity linearization algorithm is employed to locally solve the problem by iteration of convex optimization.

Even if the controller structure does not satisfy the condition required for the problem to be equivalently transformed into a static output feedback synthesis problem, an iterative approach similar to the one presented in Section 3.6 can be applied to obtain a locally optimal solution. This approach can be applied to almost any fixed-structure linear controllers. In many practical applications, it exhibits an adequate search performance and results in improved control performances.

Three practical application examples of the fixed-structure H_∞ controller optimization were presented. The present approach offers an intuitive and efficient method to explicitly design the frequency responses of the closed-loop system. In Section 3.5 and 3.6, the present method was applied to re-tune fixed-structure controllers for head positioning of an HDD. In these applications, the weighting functions were chosen such that the optimal controller achieves better performance than the controller conventionally used for the plant. Simulation and experimental results showed the effectiveness of the proposed approach as a fine tuning method to improve controller performance without requiring profound knowledge and experiences in manual loop-shaping.

Chapter 4

Rank Minimization Approach for Solving BMI Problems with Random Search

4.1 Introduction

This chapter considers an algorithm to solve BMI (bilinear matrix inequality) problems of following form (Safonov et al. [92]):

$$\begin{aligned} &\text{Find} \quad x = \{x_i\}_{i=1,\cdots,N} \in \mathbb{R}^N \\ &\text{such that} \quad F_0 + \sum_{i=1}^{N} x_i F_i + \sum_{i=1}^{N}\sum_{j=1}^{N} x_i x_j F_{ij} \prec 0 \end{aligned} \tag{4.1}$$

where F_0, F_i $(i = 1,\cdots,N)$, and F_{ij} $(i, j = 1,\cdots,N)$ are constant symmetric matrices. General BMI problems are not convex optimization problems due to the bilinear terms in the constraint (4.1) and, therefore, can have multiple local solutions. BMI problems are proven to be *NP*-hard (Toker and Özbay [104]), which means that any algorithms that globally

solve general BMI problems are quite likely non-polynomial time algorithms.

In recent years, considerable research efforts have been devoted to the development of algorithms to solve general BMI problems. Most of the algorithms found in the literature that claim the applicability to control-related problems of practical size are local search algorithms. One of the simplest approaches is an iterative algorithm solving alternating LMIs at each step, making use of the bilinear property of the problem. Another simple approach is based on the linearization; under an assumption of small search steps, one can approximate a BMI problem by an LMI problem by using the first-order perturbation approximation [45]. It is, however, highly likely for such local search approaches to fail to reach the global optimum due to the nonconvex nature of BMI problems. Goh et al. [39] showed this aspect by using a small BMI problem as an example (see Section 4.4.1).

Most of global search algorithms found in the literature are variations of the Branch and Bound (BB) method based on different formulations of BMI problems [39, 112, 51, 6, 121, 69, 74, 107]. Although the computational efficiency is a major focus for all of those works, none of global search algorithms are polynomial-time algorithms due to the *NP*-hardness of BMI problems. Therefore, their applicability to problems of practical size is questionable.

The approach proposed in this chapter is outlined as follows. First, it is shown that general BMI constraints can be reformulated as a combination of LMI constraints and a rank constraint. If the rank constraint is dropped, the problem becomes a convex optimization problem, whose optimal objective value gives a lower bound for the original BMI problem. This approach is analogous to the well-known SDP relaxation approach to a certain class of combinatorial problems. Although the approximate solution of the relaxed problem can be used with BB methods for global search, this chapter employs a linearization-based local search algorithm to reduce the relaxation gap, which is analogous to the algorithm used

in Chapter 3 to solve the H_∞ optimization problem of static output feedback controllers. Furthermore, a random search approach can be straightforwardly applied along with the deterministic approach. In recent years, random searches have attracted more attention in the field of general nonconvex optimization as a tool that has a potential to substantially enhance the computational efficiency [75, 30]. The proposed formulation of BMI problems is propitious to the introduction of random search approaches.

The proposed approach is a local search algorithm and, therefore, there is no guarantee that it finds the global solution. It is, however, based on a completely different formulation of BMI problems from conventional, simpler local search algorithms, and it is claimed that the proposed approach can more likely find the global solution than conventional local search approaches in practice. Considering that any global search algorithm is a non-polynomial time algorithm due to the *NP*-hardness of BMI problems, the proposed approach is more practical than any existing global search algorithm from the viewpoint of the computational efficiency. It is more reliable than conventional, simpler local search algorithms from the viewpoint of the likelihood of finding the global solution.

The remainder of this chapter is organized as follows. First, the next section briefly reviews a crucial role that the BMI formulation plays for generalization of H_∞ optimization problems. The proposed algorithm is presented in Section 4.3. Section 4.4 presents four numerical experiments to show the search performance of the proposed approach. Section 4.5 briefly discusses the application of the proposed approach to global search. A summary is given in Section 4.6. Much of what is presented in this chapter can be found in Ibaraki and Tomizuka [53].

4.2 BMI formulation of H_∞ Optimization Problems

Chapter 3 presented an extension of the LMI-based H_∞ optimization algorithm for full-order controllers to fixed-structure controllers. The BMI framework offers an unified approach to formulate a further general class of H_∞ optimization problems with arbitrary constraints or additional optimization objectives. This section briefly reviews a crucial role that the BMI formulation plays for generalization of H_∞ optimization problems.

The classical H_∞ controller synthesis theory focuses on the following problem.

$$\min_{C(s)} \gamma \qquad \text{such that} \quad \|F_L(P(s), C(s))\|_\infty < \gamma \tag{4.2}$$

where $C(s)$ is a rational and proper transfer function matrix of controller dynamics and $P(s)$ is the given plant model. As discussed in Section 2.3.3, the full-order H_∞ controller synthesis problem can be formulated as an SDP problem and the global optimum can be always found by using convex optimization. A critical limitation of the LMI-based H_∞ controller synthesis algorithm is that it allows no additional constraint containing the controller dynamics, $C(s)$, to be imposed on the problem; the closed-loop H_∞ norm constraint (4.2) must be the only constraint imposed to the problem in order for it to be globally solvable by convex optimization. This can be explained as follows.

Recall the SDP formulation of the continuous-time H_∞ controller synthesis problem (Theorem 4 in Section 2.3.3). The direct application of the Bounded Real Lemma (Lemma 1) to the closed-loop system (2.26) does not formulate the problem as an SDP problem. As shown in Eq. (2.32), the formulation contains bilinear terms of the optimization variables. The problem to find Θ and X_{cl} that satisfy the constraint (2.32) can be seen as a BMI problem of the form (4.1).

In the case of the full-order H_∞ controller synthesis, the problem can be equivalently trans-

formed into an LMI problem by using variable transformations (see the proof of Theorem 4). This approach cannot be, however, applied when additional constraints, which contain the controller dynamics, $C(s)$, are imposed. The previous chapter considered the special case where the controller had a structural constraint. In this case, the problem can be equivalently transformed into an H_∞ optimization problem of a static output feedback controller. In general, a constraint that contains the controller system matrices, Θ, cannot be imposed on the LMI formulation (2.19)$\sim$(2.21), since the LMI formulation no longer contains the original variable, Θ. It must be imposed on the BMI formulation (2.32). This strongly motivates to introduce the BMI formulation for the further extension of H_∞ optimization algorithms.

The following are examples of controller design problems that require additional constraints or optimization objectives to be imposed on the H_∞ optimization problem:

1. *Controller synthesis with constraints on the controller structure.* Examples include the fixed order/structure controller design problem, the controller design problem with limits on controller gains [78], and the sparse feedback gain design problem [44].

2. *Multi-objective optimization.* Examples include the mixed H_2/H_∞ optimization problem (e.g. [122]) and simultaneous controller optimization problem for multiple plant models (e.g. [66]).

3. *Robust optimization.* Examples include the μ-synthesis problem [92] and the scaled-H_∞ optimization problem with constant scaling matrices (see Section 3.4).

The BMI framework offers a unified approach to formulate these problems.

4.3 Rank Minimization Approach for Solving BMI Problems

4.3.1 Rank Minimization Approach for Solving BMI Problems

Consider the problem given in Eq. (4.1). The problem in fact belongs to the class of indefinite quadratic programming, which includes BMI problems. First, the following lemma shows that the problem (4.1) can be equivalently rewritten as a rank minimization problem subject to LMI constraints.

Lemma 8 *The indefinite quadratic programming problem* (4.1) *is equivalent to the following problem*:

$$\begin{aligned}
&\text{Find} \quad x = \{x_i\}_{i=1\cdots N} \in \mathbb{R}^N \quad \text{and} \quad X = \{X_{ij}\}_{i,j=1\cdots N} \in \mathbb{R}^{N\times N} \\
&\text{such that} \quad F_0 + \sum_{i=1}^{N} x_i F_i + \sum_{i=1}^{N}\sum_{j=1}^{N} X_{ij} F_{ij} \prec 0 \qquad (4.3) \\
&\qquad\qquad \begin{bmatrix} X & x \\ x^T & 1 \end{bmatrix} \succeq 0 \qquad (4.4) \\
&\qquad\qquad \text{rank}(X) = 1\,. \qquad (4.5)
\end{aligned}$$

The above problem can be seen as a minimization problem of the objective function, $rank(X)$, under LMI constraints (4.3) and (4.4). The rank minimization problems are generally quite hard to solve (a special case which can be equivalently transformed into an SDP problem is discussed in Mesbahi [73]). The rank minimization problems appear, however, in many control-related optimization problems such as reduced-order H_∞ controller synthesis and scaled-H_∞ optimization with constant scaling matrices, as discussed in Sections 3.3.2 and 3.4.2, respectively.

Analogous to these cases, a linearization-based local search approach is employed to solve

the problem (4.3)$\sim$(4.5). Since the constraint (4.4) assures that $tr(X) - x^T x \geq 0$ and $tr(X) - x^T x = 0$ if and only if $X = xx^T$, there exists a solution, (x, X), that satisfies the constraints (4.3)$\sim$(4.5) if and only if the optimal value of the following problem is zero:

$$\min_{x,X} \ \mathrm{tr}(X) - x^T x \qquad \text{subject to (4.3) and (4.4)}\,. \tag{4.6}$$

By linearizing the objective function, the following descent method to find a local optimum of the problem (4.6) is obtained.

Algorithm 4 (Rank minimization approach to solve BMI problems)

1. *Find a feasible set* $(x^{(0)}, X^{(0)})$ *that satisfies the constraints* (4.3) *and* (4.4). *Set* $k = 1$. *If there is no feasible solution, then the problem is infeasible.*

2. *Solve the following convex optimization problem for* $x^{(k)} \in \mathbb{R}^N$ *and* $X^{(k)} \in \mathbb{R}^{N \times N}$:

$$\min_{x^{(k)}, X^{(k)}} \ \mathrm{tr}(X^{(k)}) - 2x^{(k-1)\,T} x^{(k)} \qquad \text{subject to (4.3) and (4.4)}\,. \tag{4.7}$$

3. *Set* $k = k + 1$ *and repeat Step 2 until convergence.*

It is easy to show that this algorithm converges.

Lemma 9 *The sequence* $t_k := tr\left(X^{(k)}\right) - 2x^{(k-1)\,T} x^{(k)} + x^{(k-1)\,T} x^{(k-1)}$ $(k = 1, 2, \cdots)$ *is bounded below by zero and non-increasing. Thus, the sequence* $\{t_k\}$ $(k = 1, 2, \cdots)$ *converges to some value,* $t_{opt} \geq 0$. *Equality holds if and only if* $X^{(k)} = x^{(k)} x^{(k)\,T}$ *as* $k \to \infty$.

Proof:

Since $tr\left(X^{(k)}\right) \geq x^{(k)\,T} x^{(k)}$ due to the constraint (4.5),

$$t_k \ = \ \mathrm{tr}\left(X^{(k)}\right) - 2x^{(k-1)\,T} x^{(k)} + x^{(k-1)\,T} x^{(k-1)}$$

$$\begin{aligned} &\geq x^{(k)\,T}x^{(k)} - 2x^{(k-1)\,T}x^{(k)} + x^{(k-1)\,T}x^{(k-1)} \\ &= \left(x^{(k)} - x^{(k-1)}\right)^T \left(x^{(k)} - x^{(k-1)}\right) \\ &\geq 0\,. \end{aligned} \tag{4.8}$$

Furthermore, since $tr\left(X^{(k)}\right) - 2x^{(k-1)\,T}x^{(k)} \geq tr\left(X^{(k-1)}\right) - 2x^{(k-1)\,T}x^{(k-1)}$,

$$\begin{aligned} t_k &= \mathrm{tr}\left(X^{(k)}\right) - 2x^{(k-1)\,T}x^{(k)} + x^{(k-1)\,T}x^{(k-1)} \\ &\leq \mathrm{tr}\left(X^{(k-1)}\right) - x^{(k-1)\,T}x^{(k-1)} \\ &\leq \mathrm{tr}\left(X^{(k-1)}\right) - 2x^{(k-2)\,T}x^{(k-1)} + x^{(k-2)\,T}x^{(k-2)} \\ &= t_{k-1}\,. \qquad \square \end{aligned} \tag{4.9}$$

4.3.2 SDP Relaxation Approach to BMI Problems and Combinatorial Problems

Consider the following minimization problem subject to BMI constraints:

$$\begin{aligned} &\min_{x\in\mathbf{R}^N} \ \gamma \\ &\text{such that} \quad F_0 + \sum_{i=1}^{N} x_i F_i + \sum_{i=1}^{N}\sum_{j=1}^{N} x_i x_j F_{ij} - \gamma I \prec 0 \end{aligned} \tag{4.10}$$

where I denotes the identity matrix of the same size as F_0. Then, compare with the following problem:

$$\begin{aligned} &\min_{x\in\mathbf{R}^N, X\in\mathbf{R}^{N\times N}} \ \gamma \\ &\text{such that} \quad F_0 + \sum_{i=1}^{N} x_i F_i + \sum_{i=1}^{N}\sum_{j=1}^{N} X_{ij} F_{ij} - \gamma I \ \prec \ 0 \\ &\qquad\qquad \begin{bmatrix} X & x \\ x^T & 1 \end{bmatrix} \ \succeq \ 0\,. \end{aligned} \tag{4.11}$$

Notice that the above problem is an LMI problem and, therefore, can be globally solved by convex optimization. From Lemma 8, it is clear that the optimal solution for the problem (4.11) gives a lower bound for the original BMI problem (4.10) (Notice that if the rank constraint, $rank(X) = 1$, is added to the problem (4.11), then the problem (4.11) becomes equivalent to the original problem (4.10)).

An analogous relaxation approach is well known to find an approximate solution for a certain class of combinatorial optimization problems. The Max-Cut problem is to find a cut of maximum total weight in an edge-weighted undirected graph (see e.g. [88]). This problem is one of the original *NP*-complete problems and thus hard to solve. It can be formulated as an indefinite quadratic problem in binary variables as follows:

$$\max_{x} \; x^T Q x + 2b^T x + d \qquad \text{subject to} \quad x \in \{-1, 1\}^N \tag{4.12}$$

where $Q = Q^T \in \mathbb{R}^{N \times N}$ and $b, d \in \mathbb{R}^N$ are given. Using the fact that $x \in \{-1, 1\}^N$ can be written as $x_i^2 = 1$ ($i = 1,\ldots,N$), the above problem can be equivalently transformed to:

$$\begin{aligned} &\max_{x \in \mathbf{R}^N, X \in \mathbf{R}^{N \times N}} \operatorname{tr}(QX) + 2b^T x + d \\ &\text{subject to} \quad \begin{bmatrix} X & x \\ x^T & 1 \end{bmatrix} \succeq 0, \quad \operatorname{diag}(X) = e, \quad \operatorname{rank}(X) = 1 \end{aligned} \tag{4.13}$$

where $e \in \mathbb{R}^N$ is the vector of all ones. If the rank constraint in the problem (4.13) is dropped, then the problem can be solved by convex optimization, and it gives an upper bound for the original problem (4.12). This SDP relaxation approach method proposed by Goemans and Williamson [38] is widely accepted as the best current approximation approach to the Max-Cut problem. Goemans and Williamson [38] have also proposed to introduce a randomized algorithm to recover the optimal solution from the approximate

solution (x, X). It is guaranteed to produce a solution with the expected value at worst 14% smaller than the true optimum.

The clear similarity of the formulation (4.13) of the Max-Cut problem and the formulation (4.3)$\sim$(4.5) of the BMI problem implies that the analogous SDP relaxation approach also offers a good approximation for BMI problems. The mathematical justification of the SDP relaxation approach to BMI problems can be found in Konishi and Shin [68], where three relaxation approaches (the Lagrange relaxation, the relaxation using nonconvex quadratic inequalities, and the SDP relaxation) are applied to the problem (4.1), and it is shown that the SDP relaxation gives the best lower bound among them. This strongly justifies the approach presented in this chapter.

Notice that the application of the SDP relaxation approach (4.11) to BB methods is straightforward; the SDP relaxation approach gives a tight lower bound at each region of the branching space. More details will be discussed in Section 4.5. However, this chapter employs the local search algorithm presented in Algorithm 4 to reduce the relaxation gap, considering that any variations of the BB method are non-polynomial time algorithms due to the *NP*-hardness of BMI problems. The proposed algorithm is more practically applicable than any existing global search algorithms from the viewpoint of the computational efficiency. Furthermore, analogous to the algorithm proposed by Goemans and Williamson [38], a random search can be also applied along with the proposed deterministic approach to enhance the computational efficiency, as will be discussed in the next section. Although the proposed approach is a local search, the combination of the linearization-based descent method and random searches can find the global solution in many practical applications.

4.3.3 Random Search Algorithm

The algorithm proposed by Goemans and Williamson [38] to solve the Max-Cut problem includes random searches. Other nontrivial examples of randomized algorithms based on the SDP relaxation include the application to the Graph Coloring problem [63]. In both cases, the SDP relaxation is followed by an algorithm examining several random draws from the distribution defined by the solution of the relaxed problem.

The proposed formulation of BMI problems is propitious to the introduction of random search approaches. A simple random search approach, which is analogous to the one used in Frazzoli et al. [30], can be applied in Algorithm 4 along with the deterministic approach. After each step of solving the problem (4.7), random samples are drawn from the Gaussian distribution with the mean $x^{(k)}$ and covariance $\alpha \left(X^{(k)} - x^{(k)} x^{(k)\,T} \right)$, where $(x^{(k)},\ X^{(k)})$ is the solution for the problem (4.7) at the k-th step, and $\alpha > 0$ is a scalar constant. Notice that if $X = xx^T$, then the distribution consists of a unique point, which is the optimal solution of the original BMI problem (4.1). If a solution of the original problem (4.1) is found by this search, then the algorithm is terminated. Otherwise, Step 2 is repeated.

A major disadvantage of the formulation (4.3) is that it introduces a slack variable matrix X, which has $\frac{1}{2}N(N+1)$ parameters. When N is large, the increase of the number of variables may significantly slow down the algorithm. On the other hand, the direct applicability of random searches is a strong advantage of the proposed formulation, and so is the fact that the SDP relaxation approach generally gives a very good lower bound for the original problem.

4.4 Numerical Experiments

In this section, four numerical experiments are presented to show the search performance of the proposed algorithm for solving BMI problems. All experiments were carried out by using MATLAB on a PC with CPU Pentium 450 *MHz*. The SDP solver engine *SP* [109] and its MATLAB interface *LMITOOL* [36] (see Section 2.2.3) were used for SDP problems.

4.4.1 A Simple BMI Problem over Two Variables

The first problem is a very simple BMI problem over two variables, which was shown in Goh et al. [39] as an example of BMI problems that had multiple local minimums. The problem is given as follows:

$$\begin{aligned} &\min_{x=[x_1,\,x_2]^T} \gamma \\ &\quad \text{subject to} \quad F(x) - \gamma I \prec 0, \quad x_1 \in [-0.5,\, 2]\,, \quad x_2 \in [-3,\, 7]\,, \end{aligned} \tag{4.14}$$

where $F(x) = F_0 + x_1F_1 + x_2F_2 + x_1x_2F_{12}$ and F_0, F_1, F_2, and F_{12} are constant 3×3 symmetric matrices given as follows:

$$\begin{aligned} F_0 &= \begin{bmatrix} -10 & -0.5 & -2 \\ -0.5 & 4.5 & 0 \\ -2 & 0 & 0 \end{bmatrix}; \quad F_1 = \begin{bmatrix} 9 & 0.5 & 0 \\ 0.5 & 0 & -3 \\ 0 & -3 & -1 \end{bmatrix}; \\ F_2 &= \begin{bmatrix} -1.8 & -0.1 & -0.4 \\ -0.1 & 1.2 & -1 \\ -0.4 & -1 & 0 \end{bmatrix}; \quad F_{12} = \begin{bmatrix} 0 & 0 & 2 \\ 0 & -5.5 & 3 \\ 2 & 3 & 0 \end{bmatrix}. \end{aligned} \tag{4.15}$$

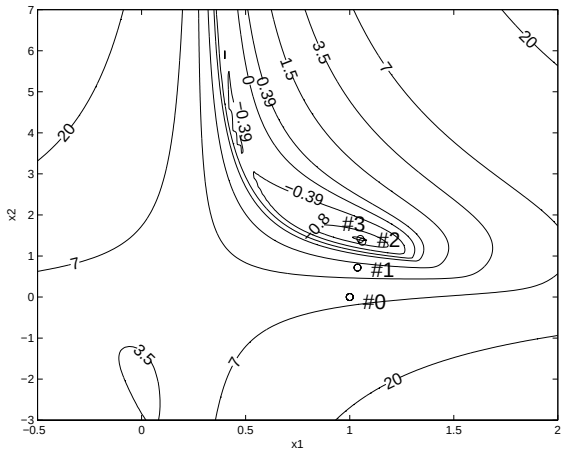

Figure 4.1: Contour plot of the greatest eigenvalue of $F(x_1, x_2)$ with the trajectory of the rank minimization approach ($\bigcirc$ #0 $\sim$ $\bigcirc$ #3)

There are three local minimums in the domain, as can be observed from the contour plot of the greatest eigenvalue of $F(x_1, x_2)$ (denoted by $\bar{\lambda}\{F(x_1, x_2)\}$) shown in Figure 4.1. Therefore, conventional local search algorithms may not be able to find the global optimum, depending on the initial point.

First, the SDP relaxation approach presented in Section 4.3.2 was applied to compute the lower bound for this problem. The relaxed problem (4.11) gave the optimal objective value $\gamma^{(0)} = -1.000$ with the solution $(x_1^{(0)},\ x_2^{(0)}) = (1.00,\ 0.00)$ (shown in Figure 4.1 by $\bigcirc$ #0). The global optimum of the problem (4.14) is known to be $(x_1^*, x_2^*) = (1.0488, 1.4179)$ with the corresponding optimal objective value $\gamma^* = \bar{\lambda}\{F(x_1^*, x_2^*)\} = -0.9565$ (see [39]). Notice that the SDP relaxation approach gave quite a tight lower bound. Its solution $x^{(0)} = (x_1^{(0)},\ x_2^{(0)})$ achieved, however, only $\bar{\lambda}\{F(x_1^{(0)}, x_2^{(0)})\} = 5.919$, which is not sufficiently close to the global optimum.

Then, Algorithm 4 was applied starting from this initial point, $x^{(0)}$, to reduce $tr(X^{(k)}) -$

$x^{(k)\,T}x^{(k)}$ to zero. Notice that the proposed approach can be only applied to the feasibility problem in the form (4.1). For this problem, the objective index, γ, in the problem (4.14) is fixed to -0.9565, which is equal to the global optimum. The objective is to find the global solution, $x^* = (x_1^*,\ x_2^*)$, that satisfies the constraint (4.14) with γ fixed to this value.

$\bigcirc$ #1 $\sim$ $\bigcirc$ #3 in Figure 4.1 indicate the optimal solutions, $x^{(k)}$, after the k-th step of the rank minimization approach (4.7). After three iterations, $tr(X^{(k)}) - x^{(k)\,T}x^{(k)}$ became approximately zero and $x^{(3)}$ achieved $\bar{\lambda}\{F(x^{(3)})\} = -0.9565$. The total computational time for the initial search and three iterations was only 0.14 *sec.*

Since the problem is small and thus each step of solving the problem (4.7) did not computationally cost much, a random search was not used. To show the effectiveness of the random search presented in Section 4.3.3, however, 50 random samples were drawn from the Gaussian distribution with the mean $x^{(1)}$ and the covariance $X^{(1)} - x^{(1)}x^{(1)\,T}$ after the first iteration (see Figure 4.2). The best objective value among 50 random samples was $\bar{\lambda}\{F(x)\} = -0.9555$ (the mean value, $x^{(1)}$, gave $\bar{\lambda}\{F(x^{(1)})\} = 2.113$). Although it did not reach the global optimum, this result shows the effectiveness of random search to some extent. The computational time to compute $\bar{\lambda}\{F(x)\}$ for 50 random samples was only 0.14 *sec.*

Finally, it should be noted that it is not necessarily because the initial point, $x^{(0)}$, was already close to the global optimum that the sequence $\{x^{(k)}\}$ converged to the global optimum. Notice that the objective function in the rank minimization approach (4.7) is not $\bar{\lambda}\{F(x)\}$ and, therefore, the existence of multiple local minimums for $\bar{\lambda}\{F(x)\}$ does not necessarily mean that the problem (4.7) also has multiple local minimums. For this particular problem, Algorithm 4 found the global minimum by at most four iterations for any of 36 different initial points in the domain.

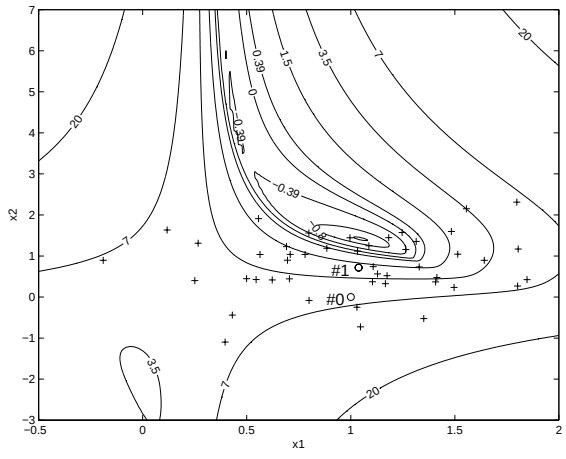

Figure 4.2: Random search after one step of the rank minimization approach

4.4.2 Randomly Generated BMI Problems

The proposed algorithm was then tested to solve randomly generated BMI problems of the following form:

$$\min_{x\in\mathbf{R}^{N_1},\, y\in\mathbf{R}^{N_2}} \gamma \qquad \text{such that}$$
$$F_0 + \sum_{i=1}^{N_1} x_i F_{i0} + \sum_{j=1}^{N_2} y_j F_{0j} + \sum_{i=1}^{N_1}\sum_{j=1}^{N_2} x_i y_j F_{ij} - \gamma I \quad \prec \quad 0 \tag{4.16}$$

where F_0, F_{i0}, F_{0j}, and F_{ij} $(i = 1, \cdots, N_1;\ j = 1, \cdots, N_2) \in \mathbb{R}^{m\times m}$ are randomly generated constant symmetric matrices. Similar tests were conducted by Tuan et al. [107]. Notice that there is no quadratic term in the constraint (4.16), i.e. the above problem is strictly a BMI problem and less general than the class of indefinite quadratic programming problems given in Eq. (4.1).

First, for each given problem, the global minimum was computed by using the BB method proposed by Tuan et al. [107]. A major advantage of this method is that it only performs the branching operations on either x-space of N_1 dimension or y-space of N_2 dimension that has less dimension than the other. By making use of the bilinear property of BMI problems, it reduces the dimension of the branching space significantly than conventional general-purpose BB methods such as the one presented by Goh et al. [39]. The BB operations were iterated until the global minimum is found with 1% tolerance.

Then, Algorithm 4 was applied to solve the same problem (4.16) with γ fixed to the global optimum. This test was conducted for three different problem settings: 1) F_0, $F_{ij} \in \mathbb{R}^{3\times 3}$ and x, $y \in \mathbb{R}^3$ (100 problems), 2) F_0, $F_{ij} \in \mathbb{R}^{6\times 6}$ and x, $y \in \mathbb{R}^3$ (100 problems), and 3) F_0, $F_{ij} \in \mathbb{R}^{3\times 3}$ and x, $y \in \mathbb{R}^5$ (35 problems). In all cases, each entry of the coefficient matrices are randomly generated from -10 to 10. All variables, x_i $(i = 1,\cdots,N_1)$ and y_j $(j = 1,\cdots,N_2)$, are restricted to $[0.01,\ 100]$.

Table 4.1 shows the average number of iterations and computational time that the BB method and Algorithm 4 respectively had to perform to reach the global optimum in total 235 problems. In 40 problems (17.0% of all problems), Algorithm 4 failed to reach the global minimum. The approach proposed in this chapter is a local search algorithm, and thus there is no guarantee that it finds the global minimum. For practical control-related problems, however, it can be used at least to improve the control performance, as will be shown in the next experiment. Although the BB method proposed by Tuan et al. [107] is more efficient for solving BMI problems than conventional general-purpose BB methods, it still requires excessively heavy computations. Computational loads increase exponentially as the size of problem becomes larger.

Table 4.1: The average number of iterations and computational time for the BB method and the proposed algorithm to solve randomly generated BMI problems

Size Number	$F_{ij} \in \mathbb{R}^{3\times 3}$, $x, y \in \mathbb{R}^3$ 100			$F_{ij} \in \mathbb{R}^{6\times 6}$, $x, y \in \mathbb{R}^3$ 100		
BB method	number of successes	average iterations	average time (sec)	number of successes	average iterations	average time (sec)
	100(100%)	32.20	3.103×10^2	100(100%)	100.85	1.138×10^3
Algorithm 4	number of successes	average iterations*	average time* (sec)	number of successes	average iterations*	average time* (sec)
	84(84%)	14.95	8.900	81(81%)	54.69	80.97

Size Number	$F_{ij} \in \mathbb{R}^{3\times 3}$, $x, y \in \mathbb{R}^5$ 35		
BB method	number of successes	average iterations	average time (sec)
	100(100%)	40.24	2.874×10^4
Algorithm 4	number of successes	average iterations*	average time* (sec)
	30(85.7%)	8.100	18.52

*: does not include cases that failed.

4.4.3 Mixed H_2/H_∞ Controller Design

The next example presents the application of the proposed algorithm to more practical control-related optimization problems. The problem is taken from [45].

Consider the following plant model:

$$\dot{x} = Ax + Bu + B_1 w, \quad z_1 = C_1 x + D_1 u, \quad z_2 = C_2 x + D_2 u \tag{4.17}$$

where

$$A = \begin{bmatrix} -1.40 & 0.49 & -1.93 \\ -1.73 & -1.69 & -1.25 \\ 0.99 & 2.08 & -2.49 \end{bmatrix}; \quad B = \begin{bmatrix} 0.25 \\ 0.41 \\ 0.65 \end{bmatrix};$$

$$B_1 = \begin{bmatrix} -0.16 & -1.29 \\ 0.81 & 0.96 \\ 0.41 & 0.65 \end{bmatrix}; \quad C_1 = \begin{bmatrix} -0.41 & 0.44 & 0.68 \end{bmatrix};$$

$$C_2 = \begin{bmatrix} -1.77 & 0.50 & -0.40 \end{bmatrix}; \quad D_1 = D_2 = 1\,. \tag{4.18}$$

The objective is to design a state feedback control, $u = Kx$, such that the closed-loop H_2 norm from w to z_2 is minimized, while the H_∞ norm from w to z_1 is kept less than the given level, $\gamma > 0$. This problem can be formulated as a BMI problem as follows.

$$\begin{aligned} &\min \ \eta^2 \\ &\text{over} \quad P_1,\, P_2 \in \mathbb{R}^{3\times 3},\, K \in \mathbb{R}^{1\times 3},\, Z \in \mathbb{R}, \text{ and } \eta \in \mathbb{R} \quad \text{such that} \\ &\begin{bmatrix} (A+BK)^T P_1 + P_1(A+BK) & P_1 B_1 & (C_1+D_1K)^T \\ B_1^T P_1 & -\gamma I & 0 \\ C_1 + D_1 K & 0 & -\gamma I \end{bmatrix} \prec 0 \\ &\begin{bmatrix} (A+BK)^T P_2 + P_2(A+BK) & P_2 B_1 \\ B_1^T P_2 & -I \end{bmatrix} \prec 0 \\ &\begin{bmatrix} P_2 & (C_2+D_2K)^T \\ C_2 + D_2 K & Z \end{bmatrix} \succ 0 \\ &\mathrm{tr}(Z) < \eta^2, \quad P_1 \succ 0, \quad P_2 \succ 0\,. \end{aligned} \tag{4.19}$$

First, the above constraints were transformed into the form given in Eq. (4.1). Then, the initial point, $x^{(0)}$, was computed. For this problem, instead of using the rank relaxation

approach given in Section 4.3.2, the following heuristic method was used to find a "better" initial point.

Most of practical control-related optimization problems can be solved by convex optimization if the design objective is relaxed. For this problem, if a common Lyapunov matrix for the H_2 and H_∞ problems is assumed (i.e. $P_1 = P_2$), then the problem can be equivalently transformed into an LMI problem (see e.g. [67]). This LMI approach gave the suboptimal solution that achieved $\eta^2 = 2.545$. This solution was used as the initial point for Algorithm 4. Notice that it is highly likely that this point is not even feasible once the objective index, η, is reduced. This approach does not guarantee a faster convergence to a global solution. In many practical applications, however, it significantly reduces the number of iterations required to reach a global solution.

Recall that the proposed approach can be applied only to the feasibility problem to find the solution set, $(P_1,\ P_2,\ K,\ Z)$, that satisfy all constraints in the problem (4.19) with both η and γ fixed. Therefore, iterations over η are required to solve the minimization problem (4.19). Starting from $\eta^2 = 2.545$, η was reduced at each step and Algorithm 4 was applied to find a solution set for each given η.

After three iterations over η (totally 11 iterations of solving the problem (4.7)), the solution set was found that achieved $\eta^2 = 1.875$. The total computational time was 228.23 sec. The optimal feedback gain matrix was $K = \begin{bmatrix} 1.2123 & -0.0713 & 0.5021 \end{bmatrix}$.

This solution may or may not be the global optimum. Although there is no guarantee that the proposed approach finds the global optimum, it can be at least used to to improve the controller performance, as shown in this experiment. This "path-following" approach is commonly used in most of local search algorithms to solve control-related BMI problems (see e.g. [45]).

4.4.4 Simultaneous State-Feedback Stabilization

The next problem is also taken from [45]. The objective is to stabilize three different linear time-invariant systems using the common state feedback control with limits on the feedback gains. Consider the following three plants:

$$\dot{x} = A_k x + B_k u, \quad k = 1, 2, 3 \tag{4.20}$$

where

$$\begin{aligned} A_1 &= \begin{bmatrix} 1 & -1 & 0 \\ 1 & 1 & 0 \\ 0 & 0 & -0.5 \end{bmatrix}; \quad A_2 = \begin{bmatrix} 1.5 & -7 & 0 \\ 7 & 1.5 & 0 \\ 0 & 0 & 1 \end{bmatrix}; \\ A_3 &= \begin{bmatrix} -0.5 & -3 & 0 \\ 3 & -0.5 & 0 \\ 0 & 0 & 2 \end{bmatrix}; \quad B_1 = B_2 = B_3 = \begin{bmatrix} 0.2477 & -0.1645 \\ 0.4070 & 0.8115 \\ 0.6481 & 0.4083 \end{bmatrix}. \end{aligned} \tag{4.21}$$

The goal is to find $K = \{K_{ij}\}_{i=1,2;\, j=1,2,3} \in \mathbb{R}^{2\times 3}$ satisfying $|K_{ij}| \leq K_{ij,max}$ $(i = 1,\ 2;\ j = 1,\ 2,\ 3)$ such that the state feedback control, $u = Kx$, stabilizes all three plants and that the decay rate of each closed-loop system is maximized, where $K_{ij,max}$ $(i = 1, 2;\ j = 1, 2, 3) > 0$ are constant. This problem is known to be *NP*-hard (Nemirovskii [78]). This problem can be written as the following BMI problem:

$$\begin{aligned} &\max \ \alpha \\ &\text{over} \quad P_k \in \mathbb{R}^{3\times 3} \ (k = 1, 2, 3), \ \text{and} \ K \in \mathbb{R}^{2\times 3} \\ &\text{such that} \qquad\qquad |K_{ij}| \ \leq \ K_{ij,max}, \quad i = 1, 2;\ j = 1, 2, 3 \end{aligned}$$

Table 4.2: Number of iterations that Algorithm 4 requires to reach the solution at each step of reducing α ("+" denotes that the solution was obtained by random searches)

α	-2.05	-1.85	-1.50	-1.00	-0.50	-0.10	0	0.10	0.30	0.50
iterations	-	1	1+	2+	4	10	3+	2+	8+	12+

α	0.60	0.70	0.75	0.80	0.85	0.90	0.95	1.00	1.05	total
iterations	7+	9+	5	6	5	5+	5+	4	5+	94

$$
\begin{aligned}
(A_k + B_k K)^T P_k + P_k (A_k + B_k K) &\prec -2\alpha P_k \\
P_k &\succ 0, \quad k = 1, 2, 3\,.
\end{aligned} \tag{4.22}
$$

The similar "path-following" method as presented in the previous section was used to reduce α. Starting from $\alpha = -2.05$ (if $K = 0_{2\times 3}$, then the problem (4.22) has trivially a feasible solution for $\alpha \geq -2.05$), α is reduced at each step. The feasible solution set, (K, P_1, P_2, P_3), is computed for each given α by using Algorithm 4. The optimal solution set is used as an initial point for the next step of reducing α.

Table 4.2 shows the number of iterations required at each step. For this problem, random searches proposed in Section 4.3.2 were performed after each iteration (100 points were sampled after each iteration of Step 2 in Algorithm 4). "+" in Table 4.2 indicates that the solution was obtained by random searches. Unlike the previous problem, the proposed algorithm required too many iterations (94 iterations) to reach the optimum, $\alpha = 1.05$. This result is the same as the one obtained in [45].

4.5 Application to Global Search Algorithms

The proposed algorithm showed satisfactory search performance in Sections 4.4.1 and 4.4.3. There is, however, no guarantee that it finds the the global minimum, as can be observed in the results in Section 4.4.2. In Sections 4.4.3 and 4.4.4, only a suboptimal solution was obtained, which may or may not be the global optimum. Furthermore, the result in Section 4.4.4 was not satisfactory from the viewpoint of the convergence speed.

This section presents the BB method based on the SDP relaxation and the rank minimization approach presented in Section 4.3. When the proposed local search approach does not give a satisfactory result, one can alternatively apply this global search approach, which utilizes the results of the local search. It should be emphasized, however, that the main focus of this chapter is on the local search approach. As briefly reviewed in Section 4.1, considerable research efforts have been devoted to global search algorithms for BMI problems. Due to the *NP*-hardness of BMI problems, any global search algorithms are most likely non-polynomial time algorithms.

The basic concept of BB methods is summarized as follows. At each iteration, the variable space is partitioned into smaller regions ("branching" operation). In each region, the lower and upper bounds of the objective index are computed ("bounding" operation). If the lower bound at one region is higher than the upper bound at another regions, then this region does not contain the global optimum, and thus is discarded from further operations. The region that is most likely to contain the global optimum is further subdivided into smaller regions. The branching and bounding operations are iterated until the global optimum is obtained.

The SDP relaxation approach and the rank minimization approach proposed in this chapter

can be applied to the bounding operations. Note that this approach is analogous to the ones suggested by Tuan et al. [107] and Konishi and Shin [68]. This section focuses only on bounding operations. See e.g. [51, 107, 39] for further details about branching operations.

Bounding: Lower Bound Estimation

Consider a hyper-rectangular region, $x \in M \subset \mathbb{R}^N$, where

$$M := [p_1,\ q_1] \times [p_1,\ q_1] \times \cdots \times [p_N,\ q_N]\ . \tag{4.23}$$

The objective of the bounding operation is to estimate the upper and lower bound for the objective index, γ, of the BMI problem (4.10) within this region. As discussed in Section 4.3.2, the SDP relaxation approach (4.11) can be applied to compute the lower bound by imposing an additional constraint, $x \in M$.

Tuan et al. [107] proposed to alternatively impose a constraint on X to obtain a tighter lower bound. It is based on the following lemma.

Lemma 10 (Tuan et al. [107])

Suppose that $p_i < q_i$ *and* $p_j < q_j$. $x_i \in \mathbb{R}$ *and* $x_j \in \mathbb{R}$ *satisfy:*

$$p_i \le x_i \le q_i \quad \textit{and} \quad p_j \le x_j \le q_j \tag{4.24}$$

if and only if there exists $x_{ij} \in \mathbb{R}$ *satisfying:*

$$x_{ij} \ \ge\ \max\left\{p_j x_i + p_i x_j - p_i p_j,\ q_j x_i + q_i x_j - q_i q_j\right\} \tag{4.25}$$

$$x_{ij} \ \le\ \min\left\{p_j x_i + q_i x_j - q_i p_j,\ q_j x_i + p_i x_j - p_i q_j\right\}\ . \tag{4.26}$$

By imposing the constraints (4.25) and (4.26) $(i, j = 1, \cdots, N;\ j \ge i)$ to the problem (4.11), a tighter lower bound can be obtained than the case where only the constraints, $p_i \le x_i \le$

q_i $(i = 1, \cdots, N)$, are imposed.

Notice that this approach introduces additional $4 \times \frac{1}{2}N(N+1)$ scalar inequality constraints, which may significantly slows down the algorithm when N is large. On the other hand, the constraints, $p_i \leq x_i \leq q_i$ $(i = 1, \cdots, N)$, only introduce $2 \times N$ additional constraints. The choice between these two approaches must be made by considering the trade-off between the computational efficiency and the estimation accuracy of the lower bound.

Bounding: Upper Bound Computation

A feasible solution that gives an upper bound for the original problem (4.10) must be also computed at each region. The simplest, cheapest approach is to use the solution, x, obtained in the preceding lower bound computation (Fujioka and Hoshijima [31]). As can be observed in the results of numerical experiments presented in Section 4.4, however, this approach often gives an upper bound much higher than the true optimum.

The rank minimization approach (Algorithm 4) can be applied to compute the upper bound at each given region. The result of the preceding lower bound estimation can be used as an initial point, $x^{(0)}$. In practice, the first couple of iterations of Step 2 in Algorithm 4 often gives a significant reduction in the estimated upper bound. Even only one step of solving the problem (4.7) often gives a significant improvement in the upper bound computation from the solution of the preceding lower bound estimation. Furthermore, the random search presented in Section 4.3.3 can be additionally applied to further improve the upper bound.

4.6 Summary

The BMI framework offers an unified approach to formulate a general class of H_∞ optimization problems with arbitrary constraints or additional optimization objectives. In this chapter, the rank minimization approach to solve general BMI problems was presented. The proposed algorithm is based on the SDP relaxation approach to indefinite quadratic programming problems, which is analogous to the well-known relaxation method for a certain class of combinatorial problems. The linearization-based local search algorithm is employed to reduce the relaxation gap. A direct applicability of random searches is also a strong advantage of the proposed approach.

Considering that none of global search algorithms for BMI problems are polynomial-time algorithms due to the *NP*-hardness of BMI problems, the proposed algorithm is more practical than any existing global search approaches from the viewpoint of the computational efficiency. Four numerical experiments were presented to show the search performance of the proposed approach. Although its performance to find the global solution may not be satisfactory in some cases, it can be at least used to improve the control performance by applying the "path-following" approach presented in Sections 4.4.3 and 4.4.4.

The application of the proposed approach to global search was also discussed. When the local search fails to give a satisfactory result, one can alternatively apply the BB method, which utilizes the result of the local search. Similarly as any other variations of BB method, however, it generally requires heavy computations.

Chapter 5

H_∞ State Observers I: H_∞ Optimization of Luenberger State Observers and Its Application to Fault Detection Scheme

5.1 Introduction

5.1.1 H_∞ Optimization of Luenberger State Observers

Optimal state estimation (or filtering) problems have been studied for decades in parallel with optimal control problems. The celebrated Kalman filtering approach [2], which offers the optimal state estimation algorithm for linear systems when the power spectral density of the noise is known, is deeply entrenched in the control literature. Consider a linear

time-invariant (LTI) system of the following state-space representation:

$$\begin{aligned} \dot{x}(t) &= Ax(t) + Bu(t) + B_w w(t) \\ y(t) &= Cx(t) + D_w w(t) \end{aligned} \tag{5.1}$$

where $x(t) \in \mathbb{R}^n$ is the state vector, $u(t) \in \mathbb{R}^{m_1}$ is the control input, $y(t) \in \mathbb{R}^{p_1}$ is the measured output, and $w(t) \in \mathbb{R}^{m_2}$ denotes the noise or external disturbances.

The Luenberger state observer has the following structure:

$$\dot{\hat{x}}(t) = A\hat{x}(t) + Bu(t) + L(y - C\hat{x}(t)) \tag{5.2}$$

where $\hat{x}(t) \in \mathbb{R}^n$ is the estimated state vector and $L \in \mathbb{R}^{n \times p_1}$ is the observer gain matrix. Notice that the system matrices of the observer coincide with those of the plant model. The structure of the Kalman filter is the same as this observer. In case of Kalman filter, the estimator gain matrix, L, is optimized such that the H_2 norm of the transfer function from the noise, $w(t)$, to the state estimation error, $x(t) - \hat{x}(t)$, is minimized. It is well known that the Kalman filter gain can be computed by solving one algebraic Ricatti equation (ARE) [2].

The H_∞-optimal filtering problem was first addressed in the late-1980s by Elsayed and Grimble [24] based on polynomial techniques [52]. In 1991, Nagpal and Khargonekar [76] presented the ARE-based formulation of H_∞-optimal state observers. It was shown that the H_∞ optimization problem of Luenberger state observers for an LTI system could be, analogous to the H_2 optimization case, reparameterized as a problem to solve a set of AREs. Other pioneering works on this subject include [7], where Bernstein and Haddad consider H_2 optimal filtering problems with an H_∞ estimation error bound, and [93], where Shaked studies the H_∞ filtering problem in a frequency domain setting.

The H_∞-optimal state observers have the following favorable properties compared to H_2-optimal state observers. First, the H_∞ optimization is preferable when there is significant uncertainty in the power spectral density of the exogenous signals [124], which is assumed to be known in the Kalman filter approach. The H_∞-optimal state observer ensures that the energy gain from disturbances to the estimation error is less than a prescribed level, γ, while the Kalman filter makes $\gamma \to \infty$. The other advantage of H_∞ state observers is that γ can be used to tune the gain of the observer, which provides more flexibility to the observer design procedure. Practical application examples of classical H_∞ state observers include [26], where Feng et al. employ the H_∞ observer to estimate state variables of automated passenger vehicle dynamics for the assistance of manual vehicle steering. Compared to the popularity that the celebrated Kalman filter has enjoyed, however, there has not been as many practical applications of H_∞-optimal state observers reported in the literature.

As demonstrated in the design of controllers in Chapter 3, the H_∞ optimization offers an intuitive and efficient approach to explicitly design frequency responses of the closed-loop system. This chapter proposes the application of this approach to the design of Luenberger state observers. For this purpose, the augmentation of dynamics weightings to the optimization setup is crucial. The conventional formulation of H_∞ state observers does not, however, allow the augmentation of dynamic performance weightings, since it makes the problem a nonconvex optimization problem. This chapter presents an extension of the conventional H_∞ optimization algorithm of Luenberger state observers to more general frequency-domain H_∞ loop-shaping design problems.

5.1.2 Application to Fault Detection Filter Design

As an application example in which the frequency-domain estimation error performance of a Luenberger state observer is particularly important, the proposed approach is applied to the design of fault detection filters for lateral control of automated passenger vehicles.

The design of reliable, fault-tolerant control systems requires that system failures be detected and identified such that the system feedback is not excessively corrupted. Fault detection and isolation (FDI) problems in dynamic systems have been an active research area in recent years. See e.g. Patton et al. [84] and Isermann [56] for an overview of fault diagnosis and management methodologies. In particular, this chapter focuses on the state estimator design in model-based fault detection schemes. The model-based fault detection schemes (see e.g. Frank [27]) utilizes the principle of analytical redundancy. Assuming that the overall process model mostly agrees with the actual process dynamics, faults that change the process behavior will lead to a mismatch ("residuals") between estimated and measured signals. If this mismatch exceeds a prescribed threshold value, a fault is said to have occurred.

The application of frequency domain approaches to the fault detection filter design was initiated by Viswanadham et al. [111]. They proposed a simple form for constructing the residual generator and suggested the application of H_∞ optimization to FDI problems. Frank and Ding [28] formulated the FDI problem in a more systematic manner and presented the H_∞ optimization algorithm to solve it by using factorization techniques. In these approaches, the estimation error dynamics of state observers in the frequency domain is particularly important.

It should be noted that the robust design problems of state observers have attracted more

attention in recent years. In order to reduce false alarm rates and improve fault detection accuracy, residual generators must be robust against model uncertainties and external disturbances. For example, Song and Collins [98] presented the application of the robust H_2 optimization scheme to the design of fault detection filters, which guarantees favorable estimation performance under any parametric perturbations in the plant model within prescribed ranges. However, robust observer design schemes usually require heavy computations and/or often give conservative results from the viewpoint of estimation performance. Although the approach presented in this chapter does not explicitly address the robustness issue, it offers a simple and effective way to incorporate the designer's expertise and understanding of the physical system and design objectives into the observer design.

The remainder of this chapter is organized as follows. First, Section 5.2 reviews the H_∞ optimization algorithm of Luenberger state observers in the case where only static weightings are augmented. Section 5.3 proposes an algorithm to solve more general problems with dynamic weightings. Section 5.4 presents an application example of the proposed approach to the design of fault detection filters for lateral control of automated passenger vehicles. A brief summary is given in Section 5.5.

5.2 H_∞ Optimization of Luenberger State Observers with Static Weightings

This section reviews the H_∞ optimization algorithm of Luenberger state observers in the case where only static weightings are augmented in the optimization objective. In such a case, the problem can be reparameterized as an LMI problem, and thus the global optimum

can be always found by convex optimization. The materials presented in this section are crucial to understanding the motivation of the nonconvex optimization approach proposed in the next section; when dynamic weightings are augmented instead of static weightings, the problem cannot be parameterized as a convex optimization problem.

The problem is formulated as follows. Suppose the plant dynamics is given in the state-space representation (5.1). Consider the Luenberger state observer of the structure (5.2). The objective is to optimize the observer matrix, L, such that the H_∞ norm of the transfer function matrix from the external disturbance, $w(t)$, to the weighted state estimation error, $z(t)$, is minimized. $z(t)$ is defined by:

$$z(t) := W_s(x(t) - \hat{x}(t)) \tag{5.3}$$

where $W_s \in \mathbb{R}^{p_2 \times n}$ is a constant weighting matrix. Denote this transfer function matrix by $T_{w \to z}(s)$.

Lemma 11 (H_∞ Optimization of Luenberger State Observers with Static Weightings) *The continuous-time H_∞-optimal observer gain matrix, L^*, that minimizes $\|T_{w\to z}(s)\|_\infty$ can be obtained by $L^* = X^{-1}F$, where $(F,\, X)$ is the optimal solution set of the following SDP problem:*

$$\begin{aligned} &\text{minimize} \quad \gamma \\ &\text{over} \quad X \in \mathbb{R}^{n\times n},\ F \in \mathbb{R}^{n\times p_1} \quad \text{and} \quad \gamma \in \mathbb{R} \\ &\text{subject to} \quad \begin{bmatrix} A^TX + XA - C^TF^T - FC & XB_w & W_s^T \\ B_w^TX & -\gamma I & 0 \\ W_s & 0 & -\gamma I \end{bmatrix} \prec 0 \\ &\qquad\qquad\qquad\qquad\qquad\qquad\qquad\qquad\qquad\qquad X \succ 0\,. \end{aligned} \tag{5.4}$$

Proof: First, notice that this problem is analogous to the H_∞ optimization problem of a state feedback controller presented in Section 2.3.2.

Combining the plant dynamics (5.1) and the observer dynamics (5.2), the state estimation error dynamics, $T_{w\to z}(s)$, is given in the following state space representation:

$$\begin{aligned} \dot{e}(t) &= (A - LC)e(t) + B_w w(t) \\ z(t) &= W_s e(t) \end{aligned} \tag{5.5}$$

where $e(t) := x(t) - \hat{x}(t)$. By applying the Bounded Real Lemma (Lemma 1 in Section 2.3.2), it can be shown that $\|T_{w\to z}(s)\|_\infty < \gamma$ if and only if there exists $X \succ 0$ such that

$$\begin{bmatrix} (A-LC)^T X + X(A-LC) & XB_w & W_s^T \\ B_w^T X & -\gamma I & 0 \\ W_s & 0 & -\gamma I \end{bmatrix} \prec 0\,. \tag{5.6}$$

By defining a new variable $F := XL$, the above inequality can be rewritten in the LMI form (5.4). Notice that X is always invertible, since it is restricted to be strictly positive definite. □

Note that the present LMI formulation is essentially equivalent to the ARE formulation of this problem presented by Nagpal and Khargonekar [76].

5.3 H_∞ Optimization of Luenberger State Observers with Dynamic Weightings

This section considers the same problem with a dynamic weighting matrix, $W_p(s)$, augmented instead of the static weighting, W_s. That is, the objective is to optimize the ob-

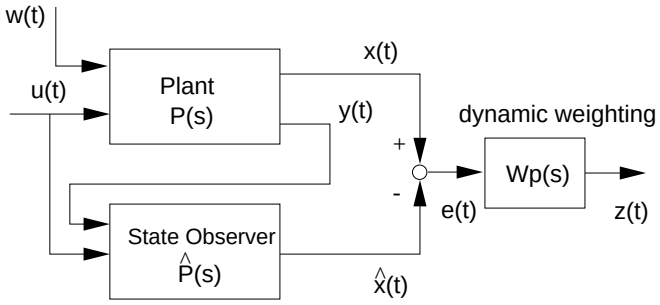

Figure 5.1: Block diagram of state estimation error dynamics

server matrix, L, such that $\|T_{w\to z}(s)\|_\infty$ is minimized, where the weighted state estimation error vector, $z(t)$, is defined in the s-domain as follows:

$$z(s) = W_p(s)(x(s) - \hat{x}(s)) \,. \tag{5.7}$$

The block diagram of $T_{w\to z}(s)$ is shown in Figure 5.1.

It can be easily seen that this problem cannot be rewritten as an LMI problem by using the variable transformation as shown in the proof of Lemma 11. When dynamic weights are augmented, the state observer $\hat{P}(s)$ is no longer a full state estimator, since the state variables of dynamic filters are not estimated (they do not exist in the physical system). The same observation applies to the H_∞ state feedback controller synthesis problem presented in Section 2.3.2.

The fixed-structure H_∞ controller optimization algorithm presented in Section 3.3 can be applied to solve this problem in a straightforward manner. To show this, first consider the transfer function from the external disturbance, $w(t)$, to the state estimation error vector, $e(t)$, without a dynamic weighting matrix, $W_p(s)$. From the state estimation error

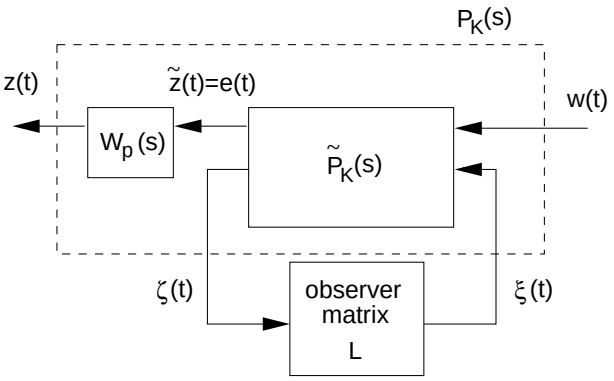

Figure 5.2: Extraction of the observer matrix, L

dynamics (5.5), reconstruct the extended plant model $\tilde{P}_K(s)$ as follows:

$$\begin{aligned} \dot{e}(t) &= Ae(t) + B_w w(t) - \xi(t) \\ \tilde{z}(t) &= e(t) \\ \zeta(t) &= Ce(t)\,. \end{aligned} \tag{5.8}$$

It is easy to see that $F_L(\tilde{P}_K(s), L)$ is equal to the the state estimation error dynamics, $T_{w\to e}(s)$ (see Figure 5.2).

When a dynamic weighting matrix $W_p(s)$ is augmented, let $P_K(s)$ be the serial combination of $\tilde{P}_K(s)$ and $W_P(s)$ as shown in Figure 5.2. Then, $F_L(P_K(s), L)$ becomes equal to the transfer function from $w(t)$ to $z(t)$.

Notice that the observer matrix, L, is a constant $n \times p_1$ full block matrix whose entries are all independently tunable. Therefore, the H_∞ optimization algorithm of a static output feedback controller presented in Section 3.3.2 can be applied to locally solve this problem in the same manner.

5.4 Application Example: Fault Detection Filter Design for Lateral Control of Automated Passenger Vehicles

5.4.1 Introduction

It is widely recognized that building commercial automated highways necessitates the development of a safe, reliable and efficient fault management system for the complete Automated Highway Systems (AHS). See Isermann [57] for a comprehensive review of fault management schemes for automated vehicles in the context of AHS.

Vehicle lateral control forms an integral part of AHS. The sensitive nature of the lateral dynamics of vehicles has motivated research towards the development of fault management systems to ensure safe operation of vehicles even in the event of faults. This section focuses on the fault detection scheme for lateral control of automated passenger vehicles, which is a part of a larger scheme to develop a reliable and efficient fault management system for AHS. As an application example in which the frequency-domain estimation error performance of Luenberger state observer is particularly important, the H_∞ optimization approach proposed in the previous section is applied to the design of fault detection filters.

5.4.2 Model Description

The design of fault detection filters is based on the simplified lateral motion model of a passenger vehicle presented by Hingwe [49, Chapter 3]. Figure 5.3 shows a front-wheel steered vehicle model on a curve of radius R_{ref}. As in the HDV control case presented in Section 3.7, magnets buried along the highway center lane are utilized as a reference for the

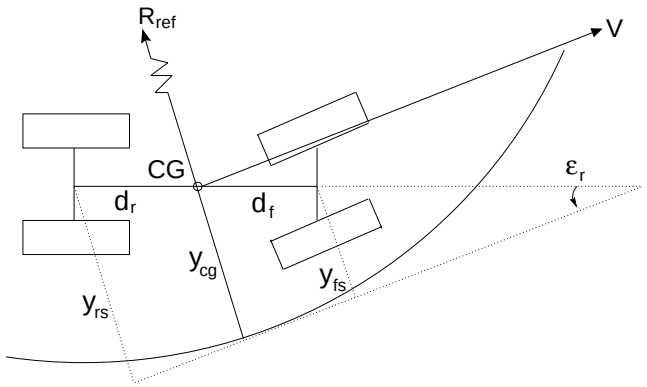

Figure 5.3: Four-wheel vehicle following a reference path

lane following operation. Magnetometers mounted on the front and rear bumpers of the vehicle are used to measure the lateral deviation of the vehicle from the road center line. The "bicycle model" presented in [49] neglects the roll and pitch motion in the vehicle and assumes that the relative yaw angle is maintained small. Under these assumptions, the lateral motion of the vehicle can be represented by the following linearized model:

$$\dot{x} = Ax + B_1\delta + B_2\dot{\epsilon}_d \tag{5.9}$$

where $x = [\ y_{cg} \quad \dot{y}_{cg} \quad \epsilon_r \quad \dot{\epsilon}_r\ ]^T$ is the state variable vector: y_r is the lateral displacement of the vehicle's center of gravity (CG) relative to the road centerline, and ϵ_r is the yaw angle of the vehicle relative to the road centerline (See Figure 5.3). δ is the steering angle and it is the control input. $\dot{\epsilon}_d$ is the yaw rate of the road frame and is regarded as a disturbance. See [49, 26] for detailed descriptions of the system matrices, $A \in \mathbb{R}^{4\times 4}$ and $B_1,\ B_2 \in \mathbb{R}^{4\times 1}$. The lateral errors measured at the front bumper (y_{fs}) and the rear bumper (y_{rs}) are given as follows.

$$\begin{bmatrix} y_{fs} \\ y_{rs} \end{bmatrix} = \begin{bmatrix} 1 & 0 & d_1 & 0 \\ 1 & 0 & -d_2 & 0 \end{bmatrix} x =: Cx \tag{5.10}$$

where d_1 and d_2 are the distances from the vehicle's CG to the locations of front and rear magnetometers, respectively.

A SISO linear controller was implemented for lateral control of the vehicle in lane-following maneuvers. The input to the controller is defined by using the geometric look-ahead distance scheme [85] as follows:

$$y_s = \frac{d_2 + d_s}{d_1 + d_2} y_{fs} + \frac{d_1 - d_s}{d_1 + d_2} y_{rs} \tag{5.11}$$

where d_s can be arbitrarily specified. Notice that y_s represents the lateral error at the location of the virtual sensor which is at a distance d_s ahead of the vehicle's CG. When d_s is greater than d_f, the virtual sensor is placed "outside" the physical limit of the vehicle. The controller, $C(s)$, is essentially given as the combination of a second-order linear lead-lag filter and a notch filter to account for roll-yaw coupling. It was successfully implemented on a test vehicle and its control performance was verified in simulation and experimentation. The closed-loop configuration is depicted in Figure 5.4.

5.4.3 Fault Detection Scheme

Rajamani et al. [89] developed a complete fault diagnostic system for automated passenger vehicles, which detects and identifies all possible faults in twelve sensors and three actuators (e.g. wheel speed sensor, radar range sensor, longitudinal accerometer, throttle angle sensor, magnetometers; brake actuator, steering actuator, and throttle actuator) used in lateral and longitudinal control systems of the vehicle. The fault diagnostic system monitors all sensor outputs and actuators. A bank of state observers, each of which is based on different combination of sensor measurements, generates residuals to detect and isolate each possible fault. This section focuses only on a fault detection scheme for two sets of magnetometers

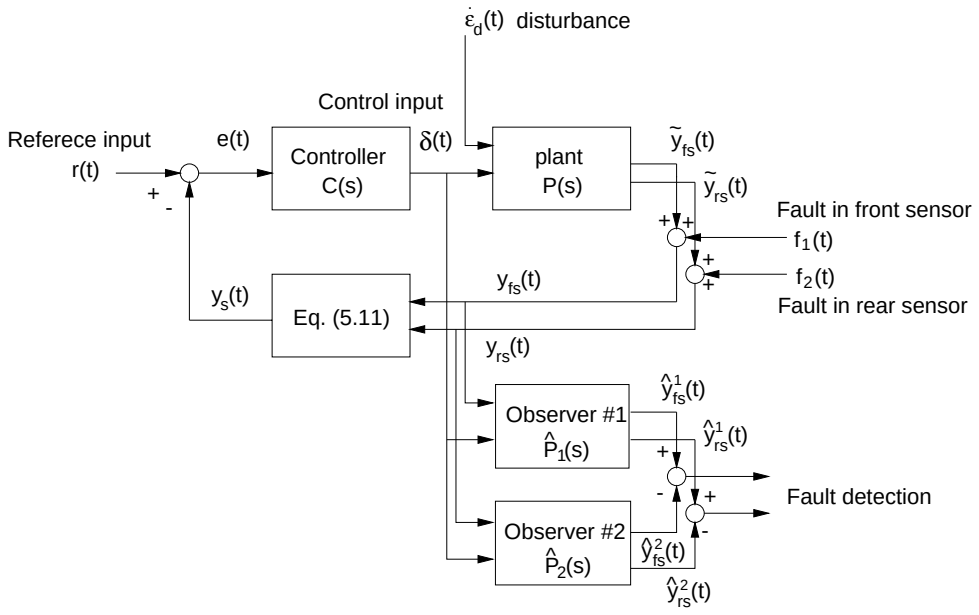

Figure 5.4: Block diagram of fault detection scheme based on dedicated observers

to measure lateral displacements of the vehicle. It can be seen as a subsystem of a complete fault diagnostic system. The same approach can be applied to the tuning of any fault detection filters.

Figure 5.4 depicts a block diagram of the fault detection architecture for magnetometers. The dedicated state observer #1, $\hat{P}_1(s)$, estimates the lateral displacements of the vehicle at the front and rear bumpers based on the measured lateral error at the front bumper, y_{fs}, and the steering angle, δ. Denote its estimates by $\hat{y}^1_{fs}$ and $\hat{y}^1_{rs}$. The dedicated state observer #2, $\hat{P}_2(s)$, estimates the same two variables based on the measured lateral error at the location of the rear sensor, y_{rs}, and the steering angle, δ. Denote its estimates by $\hat{y}^2_{fs}$ and $\hat{y}^2_{rs}$.

The magnetometer fault considered here appears as an offset on sensor measurements, y_{fs}

and y_{rs}. Furthermore, faults are assumed not to occur in both magnetometers simultaneously. Two dedicated state observers, $\hat{P}_1(s)$ and $\hat{P}_2(s)$, are designed such that the differences of their estimates, $\hat{y}_{fs}^1 - \hat{y}_{fs}^2$ and $\hat{y}_{rs}^1 - \hat{y}_{rs}^2$, are kept smaller than the prescribed constant levels during non-faulty operations. Suppose that, for example, a fault occurred in the front sensor. Then, the dedicated observer #1 can no longer estimate the correct lateral errors, since it is based on faulty sensor measurement, while the observer #2 is not affected by this fault. Therefore, by monitoring the difference of each observer's estimates, one can detect the fault. This is a basic idea of the dedicated observer based fault detection scheme.

A critical issue in the design of such dedicated observers is the robustness against external disturbances and model uncertainties. In particular, the most significant disturbance to the lateral dynamics of the vehicle is the centering force at curved roads, which acts mostly as a static disturbance. Since a magnetometer fault also appears as a static offset, steady-state estimation errors of dedicated observers must be small to distinguish faults from static disturbances.

Suryanarayanan and Tomizuka [100] proposed a fault tolerant controller for lateral control of automated passenger vehicles, which guarantees the stability of the closed-loop system even when one of magnetometers is lost. It consists of two dedicated state observers and the state feedback based on their estimates. The state feedback gain is optimized such that the stability of the closed-loop system is preserved even under the occurrence of a fault in either of the two magnetometers. The architecture of dedicated observers is exactly the same as the one shown in Figure 5.4. Therefore, the fault detection scheme presented in this section can be implemented without adding any redundancy on this fault tolerant control architecture.

5.4.4 Design Procedure of Dedicated Observers

Design Objectives

The dedicated state observers, $\hat{P}_1(s)$ and $\hat{P}_2(s)$, have the following Luenberger-type state observer structures:

$$\begin{aligned}
\hat{P}_1(s): \qquad \dot{\hat{x}}_1 &= A\hat{x}_1 + B_1\delta + L_1(y_{fs} - \hat{y}^1_{fs}) \\
\begin{bmatrix} \hat{y}^1_{fs} \\ \hat{y}^1_{rs} \end{bmatrix} &= C\hat{x}_1\,, \\
\hat{P}_2(s): \qquad \dot{\hat{x}}_2 &= A\hat{x}_2 + B_1\delta + L_2(y_{rs} - \hat{y}^2_{rs}) \\
\begin{bmatrix} \hat{y}^2_{fs} \\ \hat{y}^2_{rs} \end{bmatrix} &= C\hat{x}_2\,,
\end{aligned} \tag{5.12}$$

where y_{fs} and y_{rs} are measured lateral errors of the vehicle at the locations of the front and rear magnetometers, respectively. $\hat{x}_1 \in \mathbb{R}^4$ and $\hat{x}_2 \in \mathbb{R}^4$ are state variables of $\hat{P}_1(s)$ and $\hat{P}_2(s)$. The observer system matrices, (A, B_1, C), coincide with those of the plan model given in Eq. (5.9).

First, the observer matrices, L_1 and L_2, were obtained by using the Kalman filter design [2] (the variances of external disturbances and measurement noise were assumed to be 5×10^{-6}). Denote these Kalman filters as $\hat{P}_1^{old}(s)$ and $\hat{P}_2^{old}(s)$.

The frequency responses of estimation error dynamics of $\hat{P}_1^{old}(s)$ and $\hat{P}_2^{old}(s)$ from the external disturbance, $\dot{\epsilon}_d$, to the estimation error, $e_{fs} := y_{fs} - \hat{y}_{fs}$ and $e_{rs} := y_{rs} - \hat{y}_{rs}$, are shown in Figure 5.7 (dashed lines). Denote these transfer functions by $T_{\dot{\epsilon}_d \to e_{fs}}(s)$ and $T_{\dot{\epsilon}_d \to e_{rs}}(s)$, respectively.

The figure implies that $\hat{P}_1^{old}(s)$ and $\hat{P}_2^{old}(s)$ are not effective for the fault detection purpose by the following reasons:

1. The steady state gains of error dynamics are not sufficiently small, especially that of $\hat{P}_2^{old}(s)$ in the $T_{\dot{\epsilon}_d \to e_{fs}}(s)$ dynamics (the upper-left figure).

2. The differences of steady state gains of $\hat{P}_1^{old}(s)$ and $\hat{P}_2^{old}(s)$ are not sufficiently small, especially that in the $T_{\dot{\epsilon}_d \to e_{fs}}(s)$ dynamics (the upper-left figure). Since the fault detection scheme is based on the differences of two observers' estimates, they must be small during non-faulty operation.

Time domain simulations, which will be presented in Section 5.4.5, also show that $\hat{P}_1^{old}(s)$ and $\hat{P}_2^{old}(s)$ are not effective for the fault detection purpose.

The objective of this section is to re-tune the observer matrices, L_1 and L_2, such that both observers show desirable estimation error dynamics for more accurate fault detection.

Design of $\hat{P}_2(s)$

It is easy to see that the problem to optimize L_1 and L_2 at the same time cannot be transformed into a static output feedback synthesis problem as shown in Section 5.3. Therefore, L_1 and L_2 are optimized in an alternating manner to obtain a locally optimal solution, similarly as presented in Section 3.6.

First, consider the tuning problem of L_2, with L_1 fixed to the Kalman filter gain obtained above. The tuning objective is to reduce the gain of $T_{\dot{\epsilon}_d \to e_{fs}}(s)$ and $T_{\dot{\epsilon}_d \to e_{rs}}(s)$, especially at lower frequencies, without sacrificing the estimation stability. It can be interpreted as an H_∞ optimization problem as follows:

$$\min_{L_2} \left\| \begin{array}{c} W_{p1}(s) T_{\dot{\epsilon}_d \to e_{fs}}(s) \\ W_{p2}(s) T_{\dot{\epsilon}_d \to e_{rs}}(s) \end{array} \right\|_\infty \tag{5.13}$$

where $W_{p1}(s)$ and $W_{p2}(s)$ are dynamic performance weightings, which specify the desired shapes of $|T_{\dot{\epsilon}_d \to e_{fs}}(j\omega)|$ and $|T_{\dot{\epsilon}_d \to e_{rs}}(j\omega)|$, respectively. As was presented in Sections 3.5 and 3.6, $W_{p1}(s)$ and $W_{p2}(s)$ are designed based on actual frequency responses of $T_{\dot{\epsilon}_d \to e_{fs}}(s)$ and $T_{\dot{\epsilon}_d \to e_{rs}}(s)$ when the Kalman filter, $P_2^{old}(s)$, is used.

The problem (5.13) can be transformed into an H_∞ optimization problem of a static output feedback gain matrix as shown in Section 5.3. It can be locally solved by applying the algorithm presented in Section 3.3.2. All computations have been carried out on *MATLAB* by using *LMI Control Toolbox* [34] (see Section 2.2.3). The overall plant model in the problem (5.13) is eighth order (the estimation error dynamics model is fourth order and the performance weightings add totally four state variables). The (sub-)optimal solution, denoted by $\hat{P}_2^{new}(s)$, achieves the H_∞ norm (5.13) of 1.425, while $\hat{P}_2^{old}(s)$ gives 15.91.

Figure 5.5 compares the frequency responses of estimation error dynamics of $\hat{P}_2^{old}(s)$ and $\hat{P}_2^{new}(s)$. "Wp1" and "Wp2" represent the inverse frequency responses of performance weightings, $W_{p1}(s)$ and $W_{p2}(s)$, respectively. The gain reduction at lower frequencies can be clearly observed in both error dynamics.

Design of $\hat{P}_1(s)$

Then, consider the tuning problem of L_1, with L_2 fixed to the value obtained above. Since the fault detection scheme is based on estimation gaps of two observers, they must be small during non-faulty operations. Considering this requirement, the optimization objective for L_1 is given as follows:

$$\min_{L_1} \left\| \begin{array}{l} W_{p1}(s)(T^1_{\dot{\epsilon}_d \to e_{fs}}(s) - T^2_{\dot{\epsilon}_d \to e_{fs}}(s)) \\ W_{p2}(s)(T^1_{\dot{\epsilon}_d \to e_{rs}}(s) - T^2_{\dot{\epsilon}_d \to e_{rs}}(s)) \end{array} \right\|_\infty \tag{5.14}$$

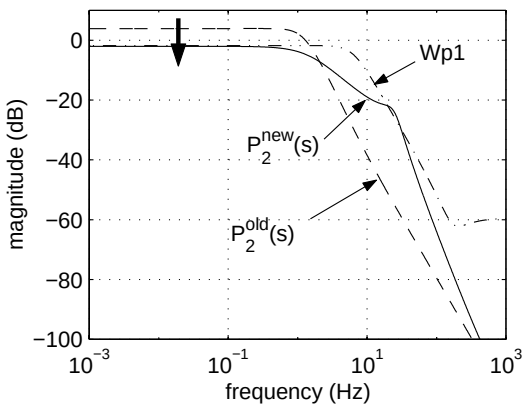

(a) Estimation error dynamics of y_{fs}, $|T_{\dot{\epsilon}_d \to e_{fs}}(j\omega)|$

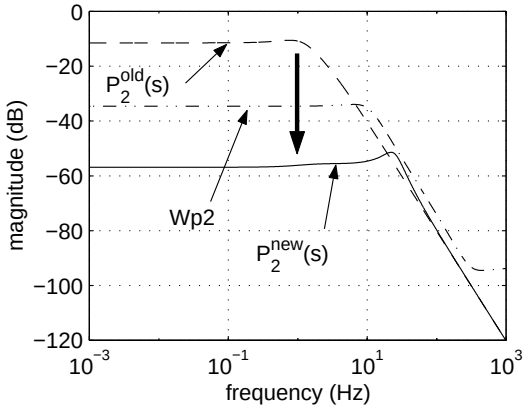

(b) Estimation error dynamics of y_{rs}, $|T_{\dot{\epsilon}_d \to e_{rs}}(j\omega)|$

Figure 5.5: Comparison of estimation error dynamics of the Kalman filter, $P_2^{old}(s)$, and the re-tuned setting, $P_2^{new}(s)$

where $T^1_{\dot{\epsilon}_d \to e_{fs}}(s)$ and $T^1_{\dot{\epsilon}_d \to e_{rs}}(s)$ denote the estimation error dynamics of the dedicated observer #1, $\hat{P}_1(s)$, and $T^2_{\dot{\epsilon}_d \to e_{fs}}(s)$ and $T^2_{\dot{\epsilon}_d \to e_{rs}}(s)$ denote the estimation error dynamics of the dedicated observer #2, $\hat{P}_2(s)$. In this problem, the performance weightings, $W_{p1}(s)$ and $W_{p2}(s)$, are set to $W_{p1}(s) = W_{p2}(s) = 1$.

Note that the above problem assumes that L_2 is fixed, and therefore, $T^2_{\dot{\epsilon}_d \to e_{fs}}(s)$ and $T^2_{\dot{\epsilon}_d \to e_{rs}}(s)$ are fixed. Therefore, the problem (5.14) can be transformed to an H_∞ optimization problem of a static output feedback gain matrix (See Figure 5.6). Notice that $P^1_K(s)$ and $P^2_K(s)$ are respectively constructed such that:

$$F_L(P^1_K(s), L_1) = \begin{bmatrix} T^1_{\dot{\epsilon}_d \to e_{fs}}(s) \\ T^1_{\dot{\epsilon}_d \to e_{rs}}(s) \end{bmatrix}, \quad F_U(P^2_K(s), L_2) = \begin{bmatrix} T^2_{\dot{\epsilon}_d \to e_{fs}}(s) \\ T^2_{\dot{\epsilon}_d \to e_{rs}}(s) \end{bmatrix}. \tag{5.15}$$

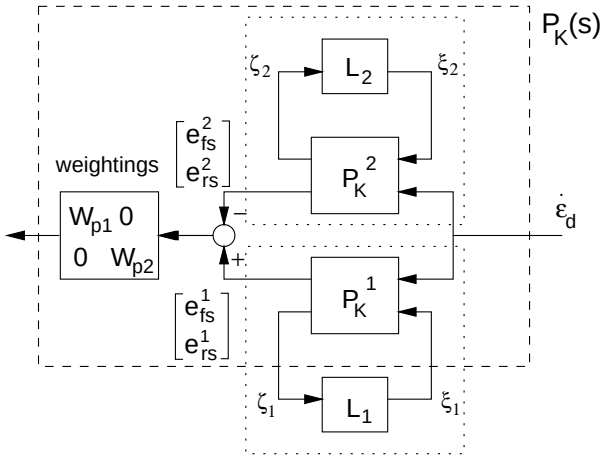

Figure 5.6: Block diagram of optimization setting for L_1

The overall plant model in the problem (5.14) ($P_K(s)$ in Figure 5.6) is eighth order. The (sub-)optimal solution, denoted by $\hat{P}_1^{new}(s)$, achieves the H_∞ norm (5.14) of 0.400, while $\hat{P}_1^{old}(s)$ gives 0.626. Figure 5.7 shows each estimation error dynamics of the Kalman filters, $\hat{P}_1^{old}(s)$ and $\hat{P}_2^{old}(s)$ (dashed lines), and the re-tuned observers, $\hat{P}_1^{new}(s)$ and $\hat{P}_2^{new}(s)$ (solid lines). In Figure 5.7 (a), it can be observed that the steady state error of $\hat{P}_2(s)$ was reduced by the tuning, while that of $\hat{P}_1(s)$ was slightly increased to reduce the gap between two observers. Figure 5.7 (b) shows that the steady state errors of two observers were both significantly reduced and, therefore, the difference of steady state errors was also reduced. Since no significant improvement was achieved by further iterations, the design procedure was terminated at this point.

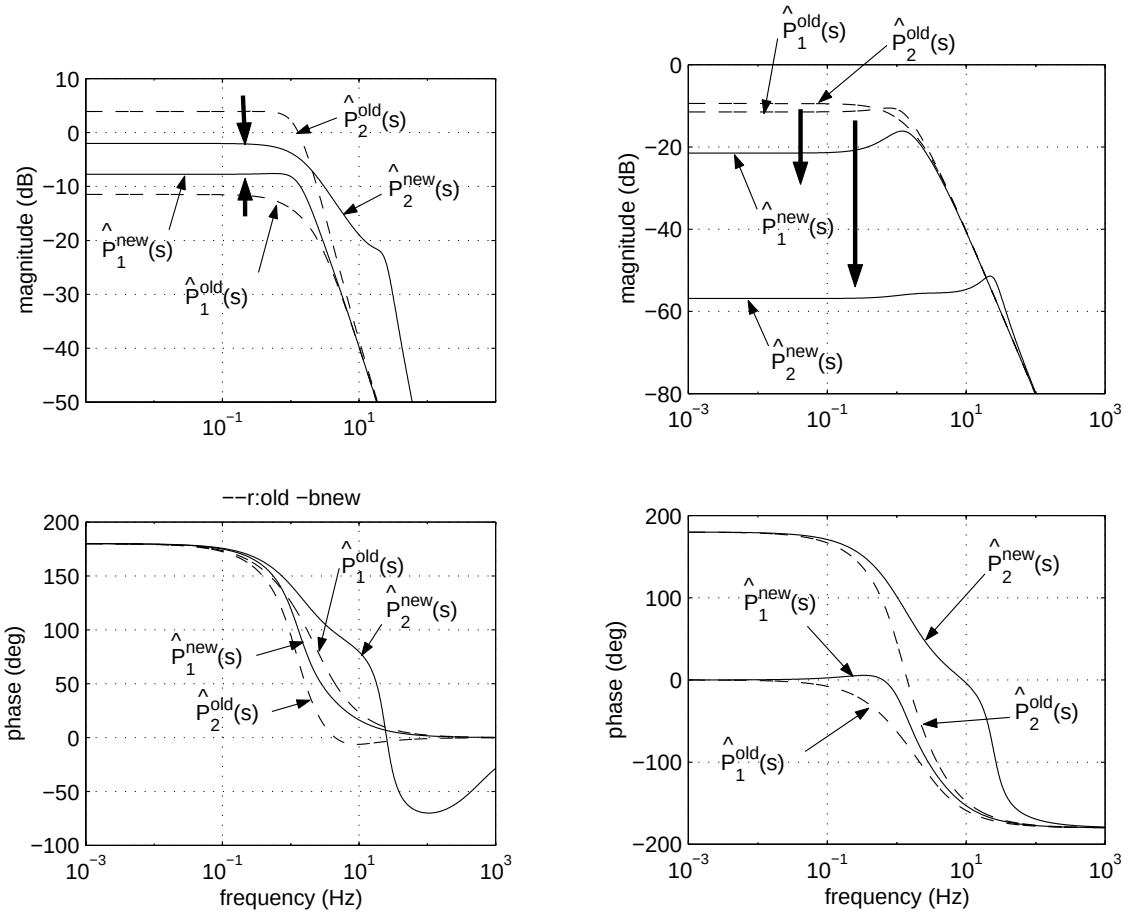

(a) Estimation error dynamics of y_{fs}, $|T_{\dot{e}_d \to e_{fs}}(j\omega)|$

(b) Estimation error dynamics of y_{rs}, $|T_{\dot{e}_d \to e_{rs}}(j\omega)|$

Figure 5.7: Comparison of estimation error dynamics of the Kalman filters, $P_1^{old}(s)$ and $P_2^{old}(s)$, and the re-tuned settings, $P_1^{new}(s)$ and $P_2^{new}(s)$

5.4.5 Simulation Results

Time domain simulations were conducted to show the effectiveness of the proposed tuning method of dedicated state observes.

Figure 5.8 shows the simulated estimation responses of the Kalman filters, $\hat{P}_1^{old}(s)$ and $\hat{P}_2^{old}(s)$. A fault occurs in the front magnetometer at the distance 220 m, when the vehicle is on a curved road of radius 800 m. The fault results in an offset of 0.05 m in the y_{fs} measurement. The plant model is assumed to be in the nominal condition: M (sprung mass of the vehicle) = 1740 kg, μ (road adhesion coefficient) = 0.85, and v (longitudinal velocity of the vehicle) = 15 m/s (=54 km/hr).

The estimation gap of two observers, $\hat{y}_{fs}^1 - \hat{y}_{fs}^2$ and $\hat{y}_{rs}^1 - \hat{y}_{rs}^2$, are shown in Figure 5.9. It can be observed that the steady-state amplitude of $\hat{y}_{fs}^1 - \hat{y}_{fs}^2$ does not differ much before and after the fault occured. Therefore, the fault cannot be detected from the response of $\hat{y}_{fs}^1 - \hat{y}_{fs}^2$. This is because the steady state estimation error of each observer is large due to static disturbances even under non-faulty operations.

Then, the fault detection performance of the re-tuned dedicated observers, $\hat{P}_1^{new}(s)$ and $\hat{P}_2^{new}(s)$, was evaluated by using the same simulation scenario. Figure 5.10 shows the estimation gap profiles, $\hat{y}_{fs}^1 - \hat{y}_{fs}^2$ and $\hat{y}_{rs}^1 - \hat{y}_{rs}^2$, when $\hat{P}_1^{new}(s)$ and $\hat{P}_2^{new}(s)$ are used. The steady state errors between two observers became smaller during non-faulty operations, and thus the fault can be easily detected by setting the threshold values at $0.02 \sim 0.04\, m$ for both of $|\hat{y}_{fs}^1 - \hat{y}_{fs}^2|$ and $|\hat{y}_{rs}^1 - \hat{y}_{rs}^2|$. Figure 5.11 shows the simulation results in the same condition when the measurement noise of the mean 0.02 m (experienced in practice) is added to the output of both the sensors.

Finally, it should be noted that the present fault detection scheme is by nature robust against

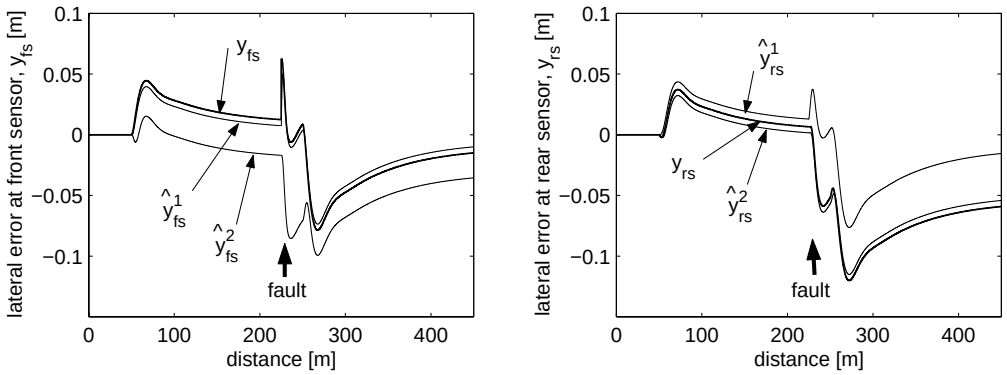

Figure 5.8: Measured and estimated lateral errors at the locations of the front sensor, y_{fs} (left), and the rear sensor, y_{rs} (right), when the Kalman filters, $\hat{P}_1^{old}(s)$ and $\hat{P}_2^{old}(s)$, are used (y_{fs} and y_{rs}: measured lateral errors, $\hat{y}^1_{fs}$ and $\hat{y}^1_{rs}$: estimation by $\hat{P}_1^{old}(s)$, $\hat{y}^2_{fs}$ and $\hat{y}^2_{rs}$: estimation by $\hat{P}_2^{old}(s)$)

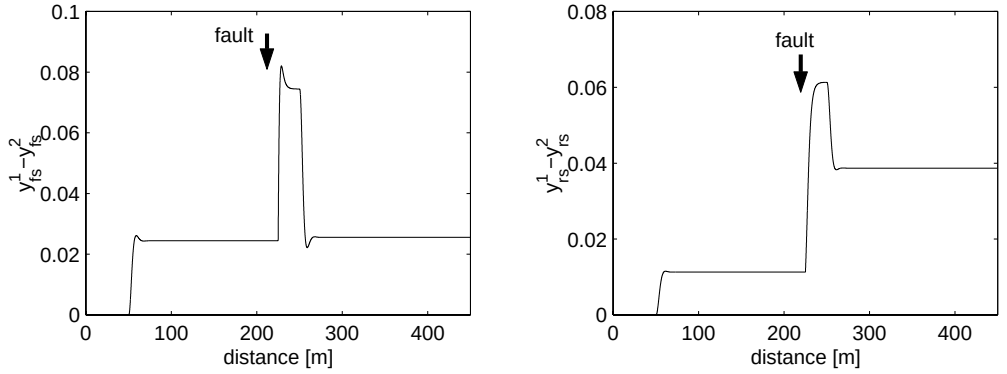

Figure 5.9: The estimation gap profiles, $\hat{y}^1_{fs} - \hat{y}^2_{fs}$ (left) and $\hat{y}^1_{rs} - \hat{y}^2_{rs}$ (right), corresponding to Figure 5.8

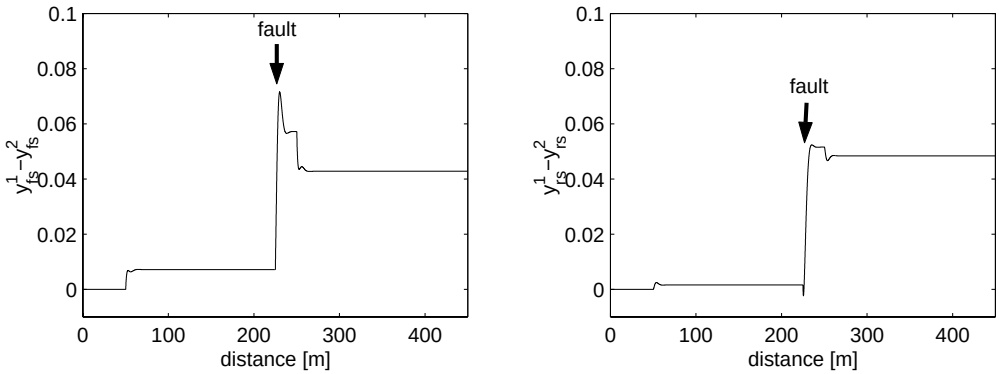

Figure 5.10: The estimation gap profiles, $\hat{y}^1_{fs} - \hat{y}^2_{fs}$ (left) and $\hat{y}^1_{rs} - \hat{y}^2_{rs}$ (right), of the re-tuned observers, $\hat{P}^{new}_1(s)$ and $\hat{P}^{new}_2(s)$, in the nominal condition ($M = 1,740\,kg$, $\mu = 0.85$, $v = 15\,m/s$)

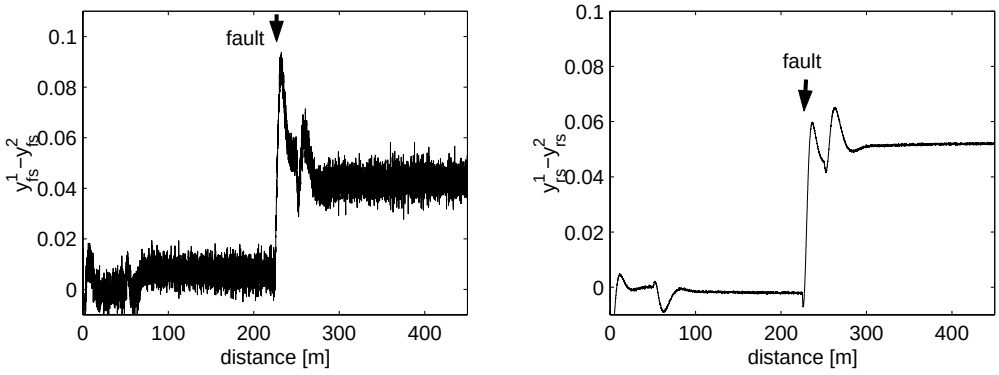

Figure 5.11: The estimation gap profiles, $\hat{y}^1_{fs} - \hat{y}^2_{fs}$ (left) and $\hat{y}^1_{rs} - \hat{y}^2_{rs}$ (right), of the re-tuned observers $\hat{P}^{new}_1(s)$ and $\hat{P}^{new}_2(s)$, with measurement noise

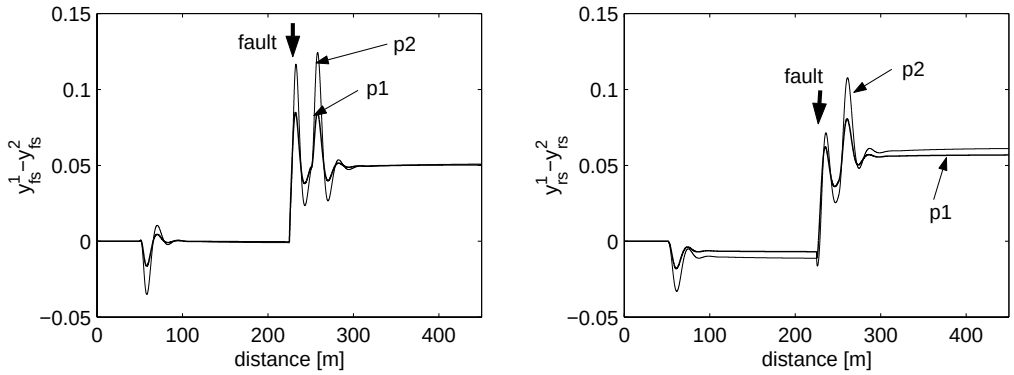

Figure 5.12: The estimation gap profiles, $\hat{y}^1_{fs} - \hat{y}^2_{fs}$ (left) and $\hat{y}^1_{rs} - \hat{y}^2_{rs}$ (right), of the re-tuned observers, $\hat{P}_1^{new}(s)$ and $\hat{P}_2^{new}(s)$, in two perturbed conditions ("p1": $M = 2,610\,kg$, $\mu = 1.0$, $v = 20\,m/s$) ("p2": $M = 870\,kg$, $\mu = 0.5$, $v = 10\,m/s$)

model uncertainties to some extent, although the robustness issue was not explicitly considered in the design of dedicated observers. Figure 5.12 shows the simulation results in two perturbed conditions, ("p1": $M = 2,610\,kg$, $\mu = 1.0$, $v = 20\,m/s$) and ("p2": $M = 870\,kg$, $\mu = 0.5$, $v = 10\,m/s$). $\hat{P}_1^{new}(s)$ and $\hat{P}_2^{new}(s)$ can produce similar residuals at steady state even in perturbed conditions.

5.5 Summary

In this chapter, the H_∞ optimization algorithm of Luenberger state observers was proposed. The conventional formulation of H_∞-optimal state observers does not allow the augmentation of dynamic performance weightings in the optimization setup, since it makes the problem a nonconvex optimization problem. The H_∞ optimization algorithm of fixed-structure controllers presented in Chapter 3 can be straightforwardly applied to such cases. The proposed approach offers an intuitive way to explicitly design the estimation error dy-

namics of the observer in the frequency domain. As an application example, the proposed approach was applied to the design of fault detection filters for lateral control of automated passenger vehicles. For accurate fault detection in vehicle control systems, the robustness of the dedicated observers against external disturbances of low frequencies is particularly important. The proposed approach was applied to re-tune the observer gain matrices of two dedicated observes. Simulation results showed the effectiveness of the proposed re-tuning method.

Chapter 6

H_∞ State Observers II: Taming Internal Dynamics by Mismatched and H_∞-Optimized State Observer

6.1 Introduction

6.1.1 Matched and Mismatched State Observers

The previous chapter has considered the H_∞ optimization problem of Luenberger-type state observers (5.2). The system matrices of Luenberger state observers coincide with those of the plant model, and only the observer matrix, L, can be tuned to obtain desirable estimation error dynamics. In the previous chapter, it was shown that the H_∞ optimization problem of the observer matrix can be solved by convex optimization if no dynamic weighting is

augmented in the optimization objective. If a dynamic weighting is augmented, then the problem can be locally solved by equivalently transforming into a static output feedback synthesis problem.

This chapter considers the state observer of the following structure:

$$\begin{aligned} \dot{x}_o(t) &= A_o x_o(t) + B_{o1} u(t) + B_{o2} y(t) \\ \hat{x}(t) &= C_o x_o(t) + D_{o1} u(t) + D_{o2} y(t) \,. \end{aligned} \tag{6.1}$$

The state estimate vector, $\hat{x}$, is given as the output vector of the observer, not as the state vector. The observer system matrices, $(A_o, B_{o1}, B_{o2}, C_o, D_{o1}, D_{o2})$, are not restricted to coincide with the system matrices of the plant (i.e. the system matrices of the observer and those of the plant are "mismatched"). Even their sizes do not have to coincide with those of the plant system matrices. Therefore, the choice of observer system matrices is completely open. By properly choosing the system matrices, the mismatched state observers can show better estimation performance than Luenberger state observers.

It should be noted that the mismatched state observer is not a new idea. The mismatched state observers is merely the generalization of Luenberger state observers. There has not been, however, many control applications of mismatched observers reported in the literature, mainly because Luenberger state observers are simpler to design, especially when they are used in state feedback control. More applications of optimal mismatched observers can be found in the field of signal processing. The H_∞ optimization of mismatched observers has particularly attracted more attention in recent years, mainly due to its capability to explicitly deal with the robustness issue. The objective of robust filtering problems is to design an observer such that it guarantees the certain estimation performance even under the existence of model uncertainties or parametric perturbations. Robust filtering problems

are generally hard to solve. Considerable research efforts have been devoted from the view point of robust optimization, including the robust H_∞ optimization (Xie et al. [118] and Wang et al. [115]) and robust H_2 optimization (Xie et al. [119], Tuan et al. [108], and Song and Collins [98]).

This chapter focuses more on the application of mismatched state observers. The application of mismatched observers to the state estimation under the feedback linearization control scheme is proposed. The feedback linearization control scheme is a nonlinear state feedback control that offers a simple and effective gain-scheduled control for linear parameter-varying (LPV) plants. This chapter demonstrates a novel application of mismatched observers to the problems where Luenberger state observers should not be applied in order to achieve desirable closed-loop performance.

6.1.2 Application of Mismatched State Observers to Feedback Linearization Control Scheme

Linear parameter-varying (LPV) systems are linear time-varying plants whose state-space matrices are fixed functions of a vector of known time-varying parameters, $\theta(t)$. They can be generally described by state-space equations of the following form:

$$\begin{aligned} \dot{x}(t) &= A(\theta(t))x(t) + B(\theta(t))u(t) \\ y(t) &= C(\theta(t))x(t) + D(\theta(t))u(t)\,. \end{aligned} \tag{6.2}$$

The simplest gain-scheduled controller design methodology for this class of plants is linear interpolation of locally designed linear controllers. First, the parameter space is divided into areas of small variation where the plant can be regarded as a linear time-invariant (LTI)

system. A local LTI controller is then designed for each frozen value of the parameter $\theta(t)$, and the overall control law is given as linear interpolation of these local controllers. This approach is effective only under the assumption that the scheduling parameter, $\theta(t)$, changes slowly (Shamma and Athans [95]). Researchers in H_∞ robust control field have developed several gain-scheduled linear control schemes that guarantee the stability and H_∞ norm performances of the closed-loop system for varying parameter $\theta(t)$ (e.g. Apkarian et al. [3] and Wu et al. [117]), although they either introduce conservativeness to controller design or require heavy computations.

Those linear interpolation methods essentially "approximate" a nonlinear plant by linear combination of a multiple of local linear models. On the other hand, the feedback linearization control (e.g. Slotine and Li [97]) cancels all parameter-dependent terms in the closed-loop input-output dynamics without using any linear approximation. It can be seen as a gain-scheduled state feedback controller in the sense that its state feedback gain matrix is dependent on the scheduling parameters.

When the relative degree of the plant is less than its order, the internal dynamics arises in the closed-loop system under the feedback linearization control, which may or may not be stable. This chapter considers the stabilization of systems with unstable internal dynamics. Conventional methods to avoid the undesirable internal dynamics include employment of the "outer-loop" linear feedback controller (e.g. Hingwe [49] presented the application of such a method to lateral control of passenger vehicles). Employment of the "outer-loop" controller makes the entire controller structure much more complicated. Furthermore, the closed-loop performances are likely dominated by the outer-loop controller, not by the inner-loop feedback linearization controller, which sometimes obscures the role of the feedback linearization controller.

If the feedback linearization control law includes the state feedback terms and the state vector is not directly available, it is necessary to design a state observer. When the Luenberger-type state observer is used, the internal dynamics is completely preserved (the separation theorem for the closed-loop eigenvalues for observer state feedback control [70]). While it may be argued that the feedback linearization scheme should not be used if the zero dynamics is unstable, the use of mismatched observer avoids to make it internal dynamics. An illustrative example will be given later in this chapter to clarify this point. By making the choice of state matrices of the observer completely open, the observer can be tuned such that it not only provides the controller with good estimation of state variables of the plant, but also stabilizes the overall closed-loop system. The LMI-based H_∞ controller synthesis algorithm can be straightforwardly applied to such design. By cooperating with the H_∞ loop-shaping technique, the set of system matrices of the observer can be optimized such that it gives the estimates of the plant state variables with the desired estimation error dynamics.

The remainder of this chapter is organized as follows. In the next section, the feedback linearization control scheme is outlined. The proposed design methodology of the state observer is presented in Section 6.3. Sections 6.4 and 6.5 present two application examples. In the first example, the feedback linearization controller and the proposed mismatched observer were applied to a second order system to illustrate how the proposed mismatched observer stabilizes the entire closed-loop system. The second example is the lateral control problem of heavy-duty vehicles (HDVs). Numerical simulations are conducted to show time-domain closed-loop performances of the designed controller and observer. Much of what is presented in this chapter can be found in Ibaraki and Tomizuka [55].

6.2 Feedback Linearization Control Scheme

The feedback linearization control scheme determines the control input such that it cancels all nonlinear terms in the closed-loop input-output dynamics. See e.g. [97] for its general formulation. Here, as an example, consider a SISO second-order dynamic system of the following form:

$$\begin{aligned} \ddot{q}(t) + A_{22}(\theta)\dot{q}(t) + A_{21}(\theta)q(t) &= B(\theta)u(t) \\ y(t) &= C(\theta)q(t) \end{aligned} \tag{6.3}$$

where $q(t)$ is a vector of n state variables, $u(t)$ is a scalar control input, $y(t)$ is a scalar output and, θ is a vector of scheduling parameters. Suppose $C(\theta)B(\theta) \neq 0$ for any θ. Define the control law by

$$\begin{aligned} u(t) = \frac{1}{C(\theta)B(\theta)}\{&C(\theta)A_{21}(\theta)q(t) + C(\theta)A_{22}(\theta)\dot{q}(t) \\ &-k_1\dot{y}(t) - k_2 y(t) - k_3\int_0^t y(\tau)d\tau + v(t)\} \end{aligned} \tag{6.4}$$

where k_1, k_2, and k_3 are constant. The closed-loop input-output dynamics becomes

$$\ddot{y}(t) + k_1\dot{y}(t) + k_2 y(t) + k_3\int_0^t y(\tau)d\tau = v(t)\,. \tag{6.5}$$

The integral term in the control law (6.4) is added to reject static disturbances. Notice that Eq. (6.5) is completely independent of θ.

Equation (6.3) can be rewritten in the standard state space representation by defining the state vector, $x = [\ q(t)^T \quad \dot{q}(t)^T\ ]^T$. This can be combined with the control law (6.4) to describe the closed-loop dynamics. Notice that there are only three tunable controller parameters, while the closed-loop system is $(2n+1)$th order. Therefore, it is impossible to assign all closed-loop poles by the choice of the controller gains. The internal modes that

cannot be controlled by the feedback linearization controller are called internal dynamics, which may or may not be stable.

6.3 Mismatched and H_∞-Optimized State Observer

One way to deal with unstable internal dynamics is to employ an "outer-loop" linear controller (e.g. Hingwe [49]). The entire closed-loop configuration is shown in Figure 6.1. A linear time-invariant (LTI) H_∞ controller is used as an outer-loop controller in order to stabilize the entire closed-loop system and enhance its robustness.

This chapter proposes to design the state observer such that it not only provides good estimates of the plant state variables, but also stabilizes the entire closed-loop system. The closed-loop configuration is shown in Figure 6.2. Advantages of the proposed approach are clear; first, the overall controller structure is much simpler. Furthermore, the desired closed-loop input-output dynamics is easier to obtain since, in the outer-loop controller approach, the overall input-output dynamics is often determined by the outer-loop controller, not by the inner-loop feedback linearization controller.

When the classical Luenberger state observer (5.2) is used for estimating the state vector in the feedback linearization control law, the internal dynamics is completely preserved in the overall closed-loop system. To see this, consider the plant model (5.1), the Luenberger state observer (5.2), and the observer state feedback law: $u(t) = F\hat{x}(t) + v(t)$. The separation theorem for the closed-loop eigenvalues for observer state feedback control [70] states that every eigenvalue of the overall closed-loop system is given by either that of $A + BF$ or $A - LC$. That is, the eigenvalues of the combined system of the plant and controller are

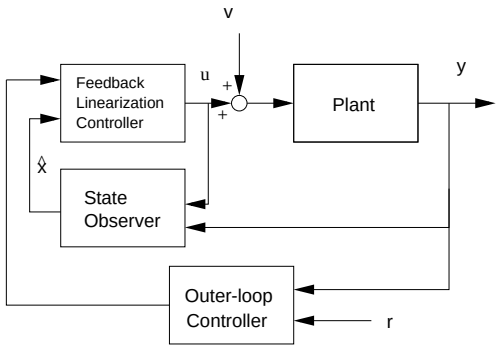

Figure 6.1: Closed-loop configuration with the outer-loop controller

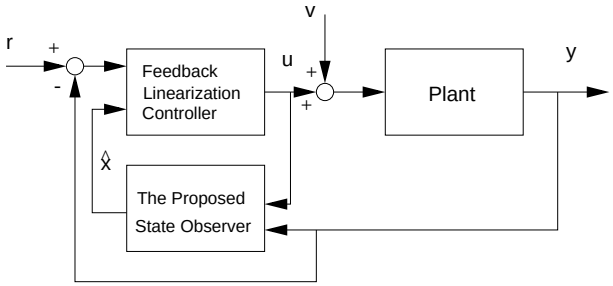

Figure 6.2: Closed-loop configuration with the proposed mismatched observer

completely preserved in the overall closed-loop system. Notice that $A + BF$ includes the modes in the internal dynamics. In other words, the Luenberger observer does not affect the internal dynamics.

Consider the application of the mismatched state observer of the form (6.1). Recall that the observer system matrices $(A_o, B_{o1}, B_{o2}, C_o, D_{o1}, D_{o2})$ are not restricted to coincide with the system matrices of the plant. The set of those system matrices is required to satisfy the following design objectives: 1) the observer outputs the estimated state variables of the plant with desired estimation error dynamics, and 2) the overall closed-loop system is

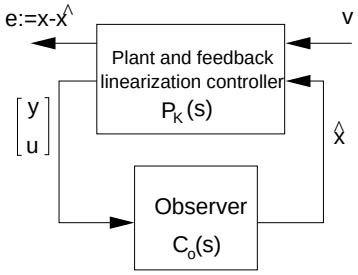

Figure 6.3: H_∞ synthesis of the state observer

stabilized. These requirements can be written in the form of the H_∞ norm performance objective as follows:

$$\|W_o(s)F_L(P_K(s), C_o(s))\|_\infty < 1 \tag{6.6}$$

where $W_o(s)$ is a performance filter transfer function matrix, $P_K(s)$ denotes the combined system of the plant (6.3) and the feedback linearization controller (6.4), and $C_o(s)$ is the transfer function of the mismatched state observer (6.1). $F_L(P_K(s), C_o(s))$ denotes the closed-loop dynamics from v to $e := x - \hat{x}$, as shown in Figure 6.3.

For the simplicity, suppose the scheduling parameter vector, θ, is fixed to some nominal value in the plant dynamics (6.3) and the control law (6.4), and thus $P_K(s)$ can be regarded as an LTI system. Then, the standard full-order H_∞ controller synthesis algorithm (see Section 2.3.3) can be applied to search for such a state observer structure, since the choice of the observer system matrices is completely open. Notice that the observer, $C_o(s)$, is designed such that the overall closed-loop system under the observer-based state feedback control is stabilized. Also note that the full-order H_∞ controller synthesis algorithm gives the state observer $C_o(s)$ of the same order as the combination of $P_K(s)$ and $W_o(s)$. The reduced-order H_∞ controller synthesis algorithm (Section 3.3.2) can be also applied to reduce the order of $C_o(s)$.

In the Luenberger observer, only the observer gain matrix, L, can be tuned to obtain the desired estimation error dynamics. By making every system matrix open for tuning, the observer structure that stabilizes the entire closed-loop system could be found. Notice that this observer is inherently mismatched (i.e. the system matrices of the observer do not match those of the plant) and thus the separation theorem for the closed-loop eigenvalues does not apply. In other words, the closed-loop input-output dynamics is affected by the observer dynamics. By appropriately choosing the performance filter $W_o(s)$ in Eq. (6.6) and designing the estimation error dynamics of the observer properly, however, the effect of the observer dynamics on the closed-loop input-output dynamics can be minimized.

Remarks:

1. When the scheduling parameters are varying, although the closed-loop input-output dynamics is still time-invariant due to the cancellation of parameter-dependent terms by feedback linearization, the internal dynamics becomes time-varying. In such cases, the above state observer, $C_o(s)$, does not even guarantee the stability of the closed-loop system, since it was designed under the assumption that $P_K(s)$ was an LTI system. If variations of scheduling parameters cause serious performance deterioration, more advanced robust optimization methods (e.g. μ-synthesis) or gain-scheduled controller design methods (e.g. Apkarian et al. [3] and Wu et al. [117]) should be applied, although they generally require a heavier computational load and/or result in more complex controllers.

2. When the Luenberger observer is used for state estimation, the closed-loop input-output dynamics is given by Eq. (6.5) for any θ. Therefore, the desired closed-loop

dynamics can be easily obtained by properly tuning three controller parameters, (k_1, k_2, k_3). This is a strong advantage of the feedback linearization control scheme. The Luenberger observer, however, should not be used when the internal dynamics is unstable. The proposed approach guarantees the stability of the overall closed-loop system even in such a case, by slightly "sacrificing" the estimation performance.

3. The feedback linearization control scheme can be applied not only to LPV systems, but also to general nonlinear systems. The proposed observer design method focuses, however, only on LPV systems, which can be regarded as LTI systems when scheduling parameters are fixed.

6.4 Application Example I: An Illustrative Second-order Plant Example

Consider a second-order system of the following form:

$$\begin{aligned} \dot{x}_1(t) &= x_2(t) \\ \dot{x}_2(t) &= a_1 x_1(t) + a_2 x_2(t) + u(t) \\ y(t) &= x_1(t) - x_2(t) \end{aligned} \tag{6.7}$$

where $u(t)$ is a scalar control input and $y(t)$ is a scalar system output. For simplicity, let a_1 and a_2 be constant ($a_1 = a_2 = 1$). The feedback linearization control law is given by

$$u(t) = -a_1 x_1(t) - (1 + a_2) x_2(t) - k y(t) + v(t) \tag{6.8}$$

where k is constant and $v(t)$ is a new input. Then, the closed-loop input-output dynamics becomes

$$\dot{y}(t) + ky(t) = v(t) \tag{6.9}$$

The overall closed-loop dynamics is given by combination of Eqs. (6.7) and (6.8):

$$\frac{d}{dt}\begin{bmatrix} x_1(t) \\ x_2(t) \end{bmatrix} = \begin{bmatrix} 0 & 1 \\ k & 1-k \end{bmatrix}\begin{bmatrix} x_1(t) \\ x_2(t) \end{bmatrix} + \begin{bmatrix} 0 \\ 1 \end{bmatrix} v(t) \tag{6.10}$$

The closed-loop poles are at $s = 1, -k$. The pole at $s = -k$ dominates the closed-loop input-output dynamics. The unstable pole at $s = 1$ is unobservable from the output and defines the internal dynamics. Note that it cannot be altered by the controller gain. Here, k is set to 0.1.

Notice that the control law (6.8) assumes that both state variables are available. The Luenberger observer is formulated by

$$\frac{d}{dt}\begin{bmatrix} \hat{x}_1(t) \\ \hat{x}_2(t) \end{bmatrix} = \begin{bmatrix} 0 & 1 \\ a_1 & a_2 \end{bmatrix}\begin{bmatrix} \hat{x}_1(t) \\ \hat{x}_2(t) \end{bmatrix} + \begin{bmatrix} 0 \\ 1 \end{bmatrix} u(t) + \begin{bmatrix} l_1 \\ l_2 \end{bmatrix} e(t) \tag{6.11}$$

where $e(t) := y(t) - (\hat{x}_1(t) - \hat{x}_2(t))$. The closed-loop pole locations with the above Luenberger state observer ($l_1 = 10$ and $l_2 = 5$) are shown in Figure 6.4 (left) ("$\circ$"). Compared with the closed-loop poles of Eq. (6.10) shown in the same figure ("+"), it can be seen that the Luenberger observer simply adds two new poles. The pole at $s = 1$ is not affected at all by the Luenberger observer and the closed-loop system is unstable.

Next, the proposed mismatched observer is designed for this plant. The design objective is given by

$$\left\| W_o(s) T^{cl}_{v \to x - \hat{x}}(s) \right\|_\infty \leq 1 \tag{6.12}$$

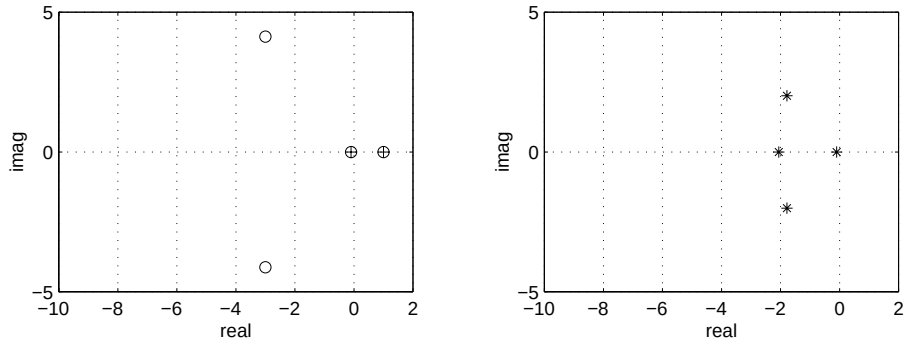

Figure 6.4: Closed-loop pole locations with direct state feedback (+), the Luenberger observer (∘) (left) and the proposed mismatched observer (∗) (right)

where $W_o(s) = \frac{5\times10^{-4}(s+10)}{s+5\times10^{-4}}$ is the performance filter. $T^{cl}_{v\to x-\hat{x}}(s)$ denotes the closed-loop transfer function matrix from $v(t)$ to $x(t) - \hat{x}(t)$. Figure 6.4 (right) shows the closed-loop poles with the designed mismatched observer. Notice that the unstable internal dynamics has been replaced by a dynamic mode governed by the new stable pole near $s = -2$. The input-output dynamics pole at $s = -k = -0.1$ is still preserved. Two extra poles, which may be interpreted as observer poles*, are introduced near the input-output dynamics pole. These two modes associated with the observer and the mode governed by the stable pole near $s = -2$ are significantly faster than the original input-output dynamics due to the pole at $s = -k = -0.1$. It makes sense to replace the zero dynamics, which does not show up in the input-output response, by dynamics much faster than the input-output dynamics.

Figure 6.5 (a) and (b) show the output response (y) and internal mode responses (x_1 and x_2) to a unit step input for the designed mismatched observer. The dashed line in (a) shows the ideal response (Eq. (6.9)). Notice that this plant is a reverse reaction plant. Yet, the optimized observer feedback system approximates the ideal response well, although it

*Since the separation principle does not apply, it is not strictly correct to call them observer poles.

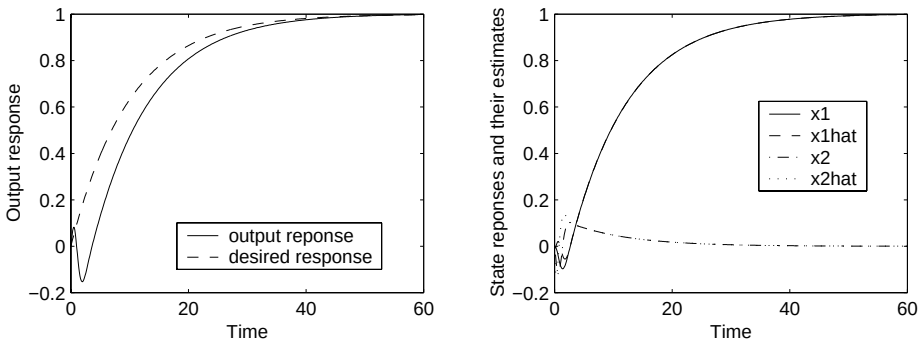

Figure 6.5: (a) Step responses of the output, y (left), and (b) step responses of internal modes, x_1 ("x1") and x_2 ("x2"), and their estimates, $\hat{x}_1$ ("x1hat") and $\hat{x}_2$ ("x2hat") (right), when the designed observer is applied.

cannot remove the reverse reaction completely.

6.5 Application Example II: Application to Lateral Control of HDVs

6.5.1 Model Description

This section considers the application of the feedback linearization control scheme to the lateral motion of a single-unit HDV. See Section 3.7.1 for an overview of lateral control of HDVs. The controller design is based on the linearized model of lateral motion of a single-unit HDV (tractor-semitrailer type) presented in Section 3.7.2. The linearized lateral motion model of an HDV is given in Eq. (3.55). Recall that the system matrix, D, in a function of v (longitudinal velocity of the vehicle). The longitudinal velocity of the vehicle is measurable or easy to estimate. Since it is well known that the variation of the vehicle velocity has a

significant effect on the vehicle dynamics (Patwardhan et al. [85]), several "gain-scheduled" controllers to cancel the velocity-dependent terms in the lateral dynamics of the vehicle have been proposed in the literature (see Section 3.7.1). This is a strong motivation to apply the feedback linearization control scheme to the lateral control problem of HDVs. Note that the input signal to the feedback linearization controller is defined as follows:

$$y_s = y_r + d_s \epsilon_r =: C_1 q \tag{6.13}$$

where $C_1 = [\ 1 \quad d_s \quad 0\ ]$ and d_s is a constant called the "look-ahead" distance (see Section 5.4.2). Here, d_s is set to $8\,m$. The lateral displacement of the tractor's center of gravity, y_r, and the yaw angle of the tractor relative to the road, ϵ_r, are measured.

6.5.2 Controller Design

The control objective is to keep the lateral tracking error at the tractor center of gravity and the off-tracking error at the rear of the trailer to be small in lane-following maneuvers. The objective of applying the feedback linearization controller to lateral control of the HDV model is to cancel all terms that are dependent on the longitudinal velocity, v, such that the desired disturbance-displacements dynamics can be obtained for any velocity.

First note that only A_{22} is dependent on v in Eq. (3.55). The feedback linearization controller (6.4) was first designed. If all states variables of the plant are assumed available, then the closed-loop input-output dynamics is given by Eq. (6.5). The controller gains, (k_1, k_2, k_3), were designed such that Eq. (6.5) gave the desired input-output dynamics. One of the simplest algorithms for the tuning of controller parameters is pole assignment. For vehicle control, the robustness against modeling uncertainties or parametric perturbations

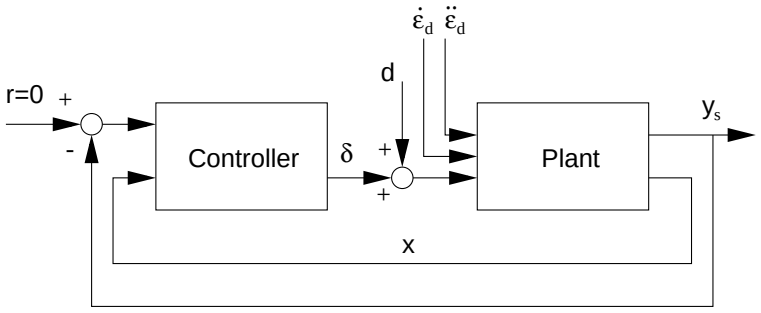

Figure 6.6: Closed-loop configuration under the assumption that all states are available

is generally a more important issue rather than transient response performance. Note that the robustness of the entire closed-loop system is more likely determined by the choice of the controller gains of the feedback linearization controller, not the choice of the state observer. The tuning objective of the controller gains, $(k_1,\ k_2,\ k_3)$, is given as follows:

$$\text{Find } K = (k_1, k_2, k_3) \quad \text{such that} \quad \left\| \begin{array}{c} W_p(s) T^{cl}_{d \to y_s}(s) \\ W_u(s) T^{cl}_{d \to \delta}(s) \end{array} \right\|_\infty \leq 1 \tag{6.14}$$

where $T^{cl}_{d \to y_s}$ denotes the closed-loop transfer function from the disturbance d to y_s, and $T^{cl}_{d \to \delta}$ denotes the closed-loop transfer function from d to the control input δ (see Figure 6.6). $W_p(s)$ is the performance filter, which specifies the desired dynamics of $T^{cl}_{d \to y_s}(s)$. $W_u(s)$ is the uncertainty filter that is designed based on the "acceptable" range of model uncertainties. This problem formulation is essentially the same as the one presented in Section 3.7. The performance filters, $W_p(s)$ and $W_u(s)$, are designed in the similar way as presented in Section 3.7, and thus the details of their design procedure are not repeated. They are given

as follows:

$$\begin{aligned} W_u(s) &= \frac{9.8s^2 + 19.002s + 13.248}{s^2 + 24.090s + 13.380} \\ W_p(s) &= \frac{s+1}{200s + 0.002}\,. \end{aligned} \tag{6.15}$$

The problem (6.14) can be solved by using the H_∞ optimization algorithm of fixed-structure controllers presented in Section 3.3. The optimal set of controller gains, $(k_1,\ k_2,\ k_3) = (4.3294,\ 3.2391,\ 1.7443)$, achieved the closed-loop H_∞ gain of 1.00098.

6.5.3 Observer Design

For this problem, the internal dynamics that arises when the Luenberger state observer is applied is stable. It has, however, two poorly damped internal modes, which deteriorate the closed-loop output responses especially in perturbed conditions. The mismatched state observer is designed such that the closed-loop system does not have the undesirable internal dynamics.

The mismatched observer is designed to meet the internal stability requirement and the H_∞ performance requirement (6.6) with the following performance filter:

$$W_o(s) = \frac{s+2}{0.05(s+0.002)} \tag{6.16}$$

The designed observer, $C_o(s)$, is eighth order and achieves the closed-loop H_∞ gain (6.6) of 1.162. Note that the order of the plant is six. The standard full-order H_∞ control synthesis algorithm gives the controller of the same order as the combined system of the plant, the controller, and the performance filter. Figure 6.7 shows frequency responses of state estimation error dynamics, $T^{cl}_{\epsilon_d \to x-\hat{x}}$. The dashed line represents the frequency response of

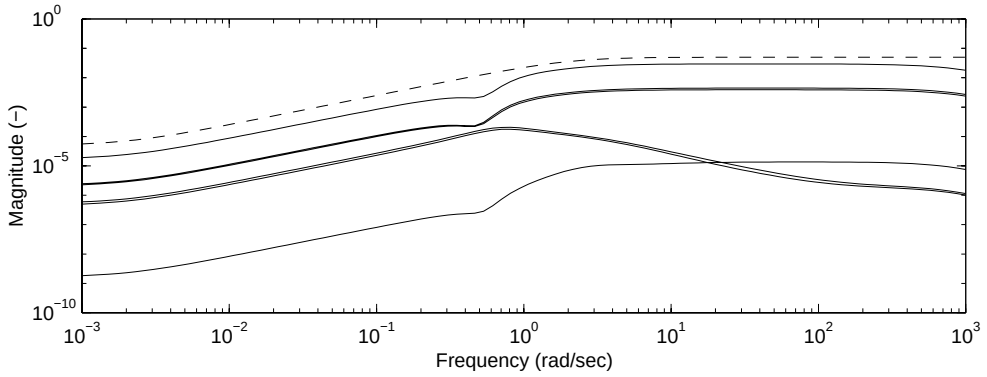

Figure 6.7: Frequency responses from disturbance input, $\dot{\epsilon_d}$, to estimation error vector, $e(t) := x(t) - \hat{x}(t)$ (solid lines). The dashed line represents the inverse frequency response of the performance filter, $W_o(s)$.

the inverse of $W_o(s)$.

Since the design of the controller parameters, (k_1, k_2, k_3), was based on the assumption of direct state feedback, the performance requirements given in Eq. (6.14) may not be satisfied when the designed observer, $C_o(s)$, is implemented. However, by properly designing the estimation error dynamics of the observer, $C_o(s)$, the control performance of the entire closed-loop system can be expected to become "close" to the direct state feedback case.

6.5.4 Simulation Results

Time-domain simulations were conducted to show the closed-loop performance of the designed feedback linearization controller and H_∞ observer. The same road curvature scenario as the one given in Section 3.7.5 was used. Figure 6.8 shows the simulation results for the nominal condition and two perturbed conditions. Figure 6.9 shows state estimation errors corresponding to Figure 6.8. The maneuver was accomplished with an overshoot from the

lane centerline less than 40 cm in all the cases. It can be observed that the designed feedback linearization controller gives more stable responses in a wider range of longitudinal velocities than the time-invariant MISO PI controller designed in Section 3.7, or the time-invariant H_∞ controllers presented by Wang and Tomizuka [113] and Mammar [72]. The designed controller and observer gave smooth responses even when parameter perturbations on m_2 and μ were introduced.

Figures 6.10 and 6.11 show the comparison between the direct state feedback case (i.e. all state variables of the plant are assumed available) and the case where the designed mismatched observer is used. Figure 6.10 shows the state responses in both cases under the perturbed condition ($v = 5\ m/s$, $\mu = 0.6$, $m_2 = 5000\ kg$). Figure 6.11 shows the closed-loop pole locations of each system. It can be seen that the closed-loop system with direct state feedback has the mode governed by the poles almost on the imaginary axis, which makes the output responses intolerably oscillating. On the other hand, the mismatched observer replaces those undamped modes by the modes governed by the poles near $(-0.1 \pm 0.5j)$, and thus it shows much more stable responses.

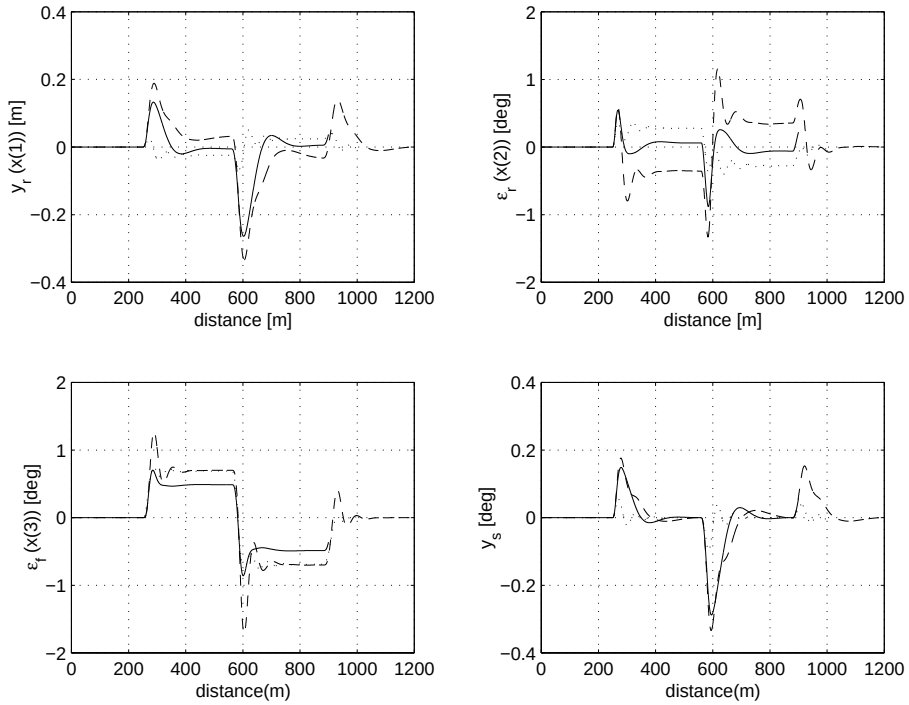

Figure 6.8: Closed-loop simulations under the nominal condition (solid: $v = 18\ m/s$, $\mu = 0.8$, $m_2 = 10670\ kg$) and two perturbed conditions (dashed: $v = 25\ m/s$, $\mu = 1.0$, $m_2 = 24000\ kg$) (dotted: $v = 5\ m/s$, $\mu = 0.6$, $m_2 = 5000\ kg$)

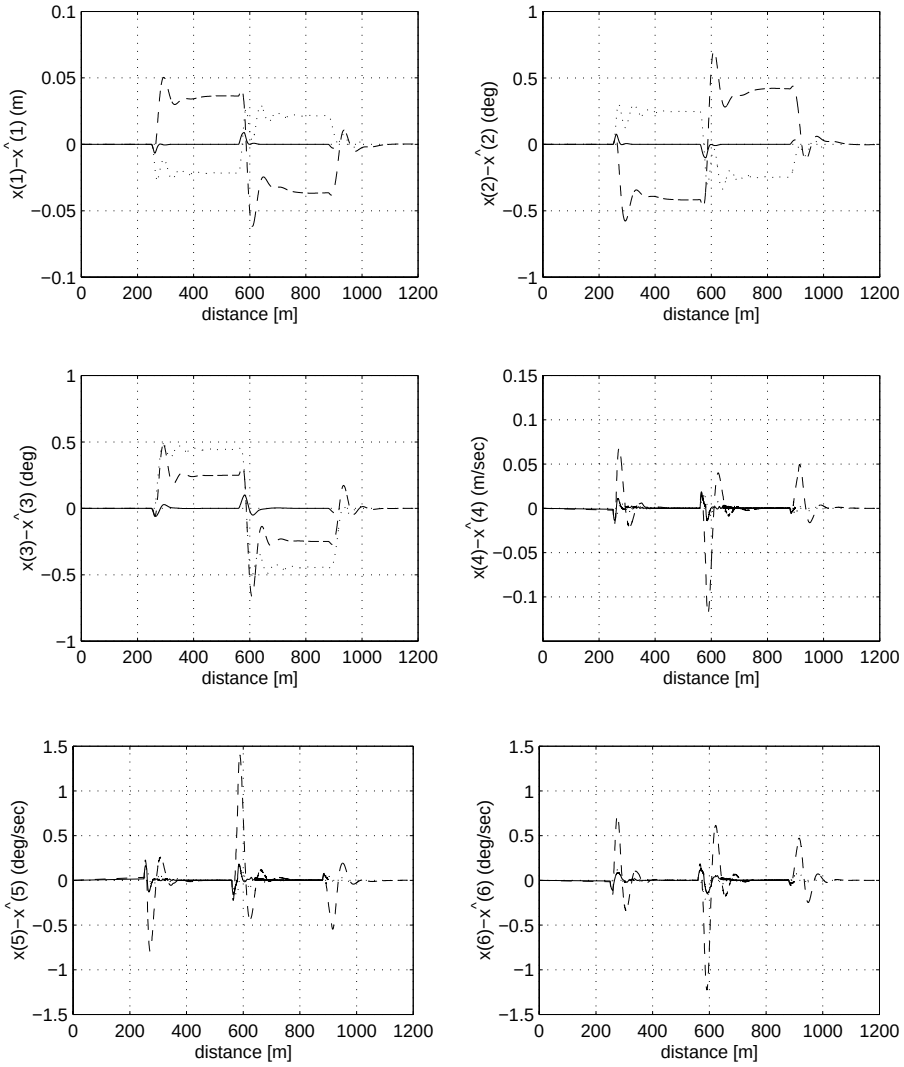

Figure 6.9: State estimation errors corresponding to Figure 6.8

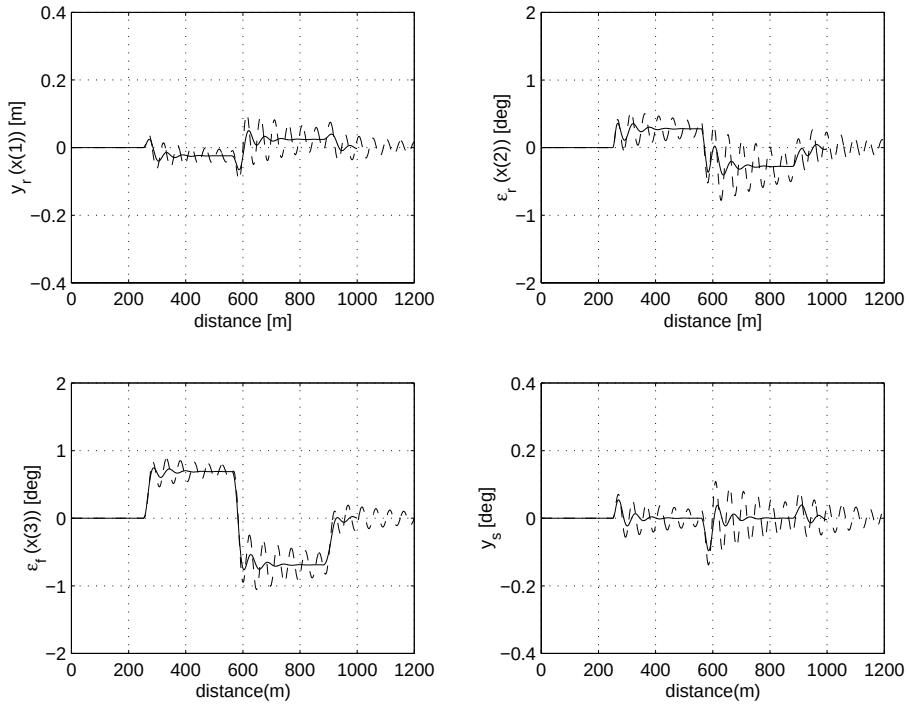

Figure 6.10: The closed-loop responses of $y_s(t)$ with direct state feedback (dashed) and the designed mismatched observer (solid) under the perturbed condition ($v = 5\ m/s$, $\mu = 0.6$, $m_2 = 5000\ kg$)

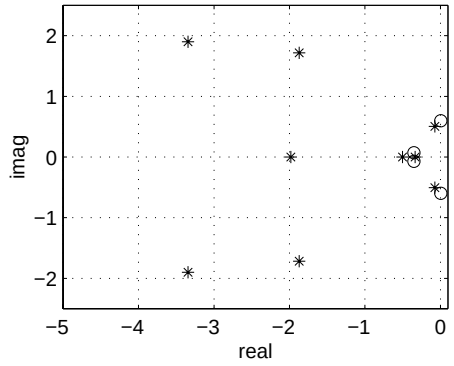

Figure 6.11: Closed-loop pole locations of the system with direct state feedback ($\circ$) and the designed mismatched observer ($*$) under the same conditions as in Figure 6.10

6.6 Summary

The major problem of the feedback linearization control scheme is the stability of the internal dynamics, which arises when the relative degree of the plant is less than its order. When the Luenberger state observer is applied for state estimation, the internal dynamics is completely preserved. This chapter presented the design methodology of a state observer that not only provides the controller with good estimation of the plant states, but also stabilizes the entire closed-loop system.

By applying the proposed mismatched observer, the internal dynamics becomes observable from the output and affects the input-output dynamics since the separation principle no longer applies. By replacing the unstable internal dynamics by significantly faster modes, however, the effect of the new poles on the closed-loop input-output dynamics can be minimized. Two application examples were presented. In the second example, the proposed approach was applied to the lateral control problem of HDVs. It was verified by numerical simulations that the proposed controller and observer structure showed favorable responses in a wide range of longitudinal velocities of the vehicle.

Chapter 7

Conclusions and Future Research

7.1 Conclusions

The LMI-based H_∞ controller synthesis theory guarantees that if the controller is allowed to have the same order as the plant, and every system matrix of the controller is freely tunable, then the H_∞ optimization problem can be solved by convex optimization, and the global optimum can be numerically found in quite an efficient and reliable manner. A critical limitation of the LMI-based H_∞ optimization algorithm is that it allows no additional constraint to be imposed on the problem; the closed-loop H_∞ norm constraint must be the only constraint imposed on the problem in order for it to be globally solvable by convex optimization. This dissertation have studied an extension of the LMI-based H_∞ optimization algorithm to the problems that cannot be parameterized as a convex optimization problem. Specific contributions of this dissertation are on: 1) H_∞ and scaled-H_∞ optimization of

fixed-structure controllers, 2) rank minimization approach for solving BMI problems with random search, 3) H_∞ optimization of Luenberger state observers, and 4) H_∞ optimization of mismatched observers. Each contribution is summarized below.

H_∞ and Scaled-H_∞ Optimization of Fixed-structure Controllers

This dissertation first proposed an algorithm to solve the H_∞ optimization problem of fixed-structure controllers via the reduced-order H_∞ controller synthesis. The proposed algorithm starts from the transformation of the fixed-structure H_∞ controller optimization problem into an H_∞ optimization problem of a static output feedback controller. Then, the cone complementarity linearization algorithm is used to locally solve the H_∞ optimization problem of a static output feedback controller. The proposed approach is a local search algorithm and, therefore, there is no guarantee that it finds the global optimum. It performs, however, excellent in many practical applications. An analogous approach can be also applied to scaled-H_∞ optimization problems, which are often used as an approximation of μ-synthesis problems for mixed real/complex model uncertainties.

Based on the proposed H_∞ optimization algorithm for fixed-structure controllers, this dissertation demonstrated a tuning method of controller parameters to explicitly design frequency responses of the closed-loop system. The proposed approach offers an intuitive and efficient way to re-tune controller parameters, which were finely tuned by an expert engineer, and improve the control performance. The following three practical application examples were presented: 1) the tuning of a SISO PID controller for head positioning of a magnetic hard disk drive (HDD), 2) the tuning of a discrete-time observer feedback controller for head positioning of an HDD, and 3) the tuning of a MISO PI controller for the lateral control of an automated heavy-duty vehicle (HDV). The effectiveness of the proposed re-tuning

method was demonstrated by simulation and experimentation.

Rank Minimization Approach for Solving BMI Problems with Random Search

Secondly, this dissertation proposed a novel local search approach for solving general BMI problems. The BMI framework offers an unified approach to formulate a general class of H_∞ optimization problems with arbitrary constraints or additional optimization objectives. The proposed algorithm is based on the SDP relaxation approach to BMI problems and the linearization-based local search algorithm, which is analogous to the algorithm employed to solve reduced-order H_∞ controller synthesis problems. The direct applicability of a random search is also a strong advantage of the proposed approach.

Four numerical experiments were conducted to show the search performance of the proposed approach. Although its performance to find the global solution was not satisfactory in some cases, it can be at least used to improve the controller performance by applying the "path-following" approach. Considering that none of global search algorithms for BMI problems are polynomial-time algorithms due to the *NP*-hardness of BMI problems, the proposed algorithm is more practical than any existing global search approaches from the viewpoint of the computational efficiency. It is more reliable than conventional, simpler local search algorithms from the viewpoint of the likelihood of finding the global solution.

H_∞ Optimization of Luenberger State Observers

The design method of Luenberger state observers based on H_∞ optimization was presented. The conventional formulation of H_∞-optimal state observers does not allow the augmentation of dynamic weightings in the optimization objective, since it makes the problem a nonconvex optimization problem. It was shown that the proposed fixed-structure H_∞ con-

troller optimization algorithm could be applied to such cases in a straightforward manner. The proposed approach was applied to the design of fault detection filters for lateral control of automated passenger vehicles. The simulation results showed the effectiveness of the proposed tuning method to obtain desirable estimation error dynamics of dedicated observers.

H_∞ Optimization of Mismatched State Observers

The H_∞ optimization of Luenberger state observers was extended to the design of more general mismatched state observers, and a novel application of H_∞-optimal mismatched state observers to the observer-based feedback control was presented. The feedback linearization control scheme is simple but quite effective for the control of an LPV plant. When the Luenberger-type state observer is used, the feedback linearization control scheme may generate undesirable internal dynamics. This dissertation proposed to tune the mismatched state observer by using H_∞ optimization such that it not only provides good estimation of state variables of the plant, but also stabilizes the overall closed-loop system. As an application example, the proposed approach was applied to lateral control of HDVs. It was verified by numerical simulations that the proposed controller and observer structure showed favorable responses in a wide range of longitudinal velocities of the vehicle.

7.2 Future Research

Numerical optimization in controller design has been an active research area in control engineering. The ultimate goal on this subject is to develop a "black box" architecture that computes the optimal solution from any design constraints and objectives provided by

the designer. There still remain unsolved problems in optimal control in spite of intense research for decades. For example, the classical LMI-based H_∞ controller optimization theory can be applied only to special cases where the controller is allowed to have the same order as the plant, and every system matrix of the controller is freely tunable. As discussed in this dissertation, any additional constraints make the problem a nonconvex optimization problem, and thus it cannot be solved by the conventional LMI-based approach.

The BMI formulation presented in Chapter 4 has been studies as a tool that has a potential to extend the conventional optimal control theory to more general problems. Although numerous algorithms have been proposed to solve general BMI problems in the literature, none of the global search algorithms are sufficiently efficient to solve problems of practical size. Due to the *NP*-hardness of BMI problems, it is highly likely that there exists no algorithm that can globally solve general BMI problems in a practical efficiency. The importance of solving BMI problems is, however, clear for the extension of optimal control theories. The following are suggestions for future research directions:

1. *Local search approaches.* This dissertation proposed a novel algorithm to locally solve BMI problems in Chapter 4. Due to the *NP*-hardness of BMI problems, local search approaches seem more promising for practical applications. The algorithm proposed in this dissertation may become slow when the problem size is large. More efficient and reliable algorithms must be developed to apply BMI-based approaches to practical control problems.

2. *Specific nature of BMI problems.* This dissertation proposed an algorithm to solve the H_∞ optimization problem of fixed-structure controllers via the reduced-order H_∞ controller synthesis. Although the proposed approach is restricted to this specific problem

and cannot be applied to general BMI problems, it often shows better search performance than other general-purpose algorithms. Future research must focus more on the nature of each specific problem to develop more efficient and reliable global/local search algorithms.

3. *Random search.* In recent years, random searches have attracted more attention as a tool that has a potential to substantially enhance the computational efficiency. As shown in this dissertation, the combination of deterministic and nondeterministic approaches seems promising to improve the efficiency and reliability of search algorithms.

4. *Application to large-scale problems.* Numerical optimization approaches offers more advantages when applied to large-scale engineering problems. However, the algorithms discussed in this dissertation are not sufficiently efficient for large-scale problems. In particular, further research effort must be devoted to the development of efficient algorithms for large SDP problems. Efficient algorithms to solve sparse SDP problems are also of importance.

Bibliography

[1] F. Alizadeh, *Optimization over the positive-definite cone: interior point methods and combinatorial applications*, in Advances in Optimization and Parallel Computing, P. Pardalos, ed., North-Holland, 1992.

[2] B. D. O. Anderson and J. B. Moore, *Optimal filtering*, Prentice Hall, Englewood Cliffs, N.J., 1979.

[3] P. Apkarian, P. Gahinet, and G. Becker, *Self-scheduled H_∞ control of linear parameter-varying systems: a design example*, Automatica, 31 (1995), pp. 1251–1261.

[4] P. Apkarian and H. D. Tuan, *LMI-constrained concave programs in robust control*, in Proc. of the American Control Conf., San Diego, CA, June 1999, pp. 1395–1399.

[5] K. J. Aström and T. Hägglund, *PID Controllers: Theory, Design, and Tuning*, Instrument Society of America, Research Triangle Park, NC, 1988.

[6] E. Beran, L. Vandenberghe, and S. Boyd, *A global BMI algorithm based on the generalized Benders decomposition*, in Proc. of the European Control Conference, July 1997.

[7] D. S. Bernstein and W. M. Haddad, *Steady-state Kalman filtering with an H_∞ error bound*, Systems and Control Letters, 12 (1989), pp. 9–16.

[8] D. S. Bernstein, W. M. Haddad, and C. N. Nett, *Minimal complexity control law synthesis, part 2: Problem solution via H_2/H_∞ optimal static output feedback*, in Proc. of American Control Conf., Pittsburgh, PS, June 1989, pp. 2506–2511.

[9] S. Boyd, V. Balakrishnan, and P. Kabamba, *A bisection method for computing the H_∞ norm of a transfer matrix and related problems*, Mathematics of Control Signals and Systems, 2 (1989), pp. 207–219.

[10] S. Boyd, L. El Ghaoui, E. Feron, and V. Balakrishnan, *Linear Matrix Inequalities in System and Control Theory*, vol. 15 of Studies in Applied Mathematics, SIAM, Philadelphia, PA, 1994.

[11] S. Boyd and L. Vandenberghe, *Convex optimization*. Lecture Notes for EE290N: Convex Optimization and Applications, offered at University of California at Berkeley, Fall 1999.

[12] N. A. Bruinsma and M. Steinbuch, *A fast algorithm to compute the H_∞ norm of a transfer function matrix*, Systems and Control Letters, 14 (1990), pp. 287–293.

[13] C. Chen and M. Tomizuka, *Dynamic modeling of articulated vehicles for automated highway systems*, in Proc. of American Control Conference, Seattle, WA, 1995, pp. 653–657.

[14] ——, *Steering and independent braking control for tractor-semitrailer vehicles in automated highway systems*, in Proc. of the 34th IEEE Conf. on Decision and Control, New Orleans, 1995, pp. 1561–1566.

[15] K. K. Chew, *Control system challenges to high track density magnetic disk storage*, IEEE Trans. on Magnetics, 32 (1995), pp. 1799–1804.

[16] J. Ding, M. Tomizuka, and H. Numasato, *Design and robustness analysis of dual stage servo system*, in Proc. of the American Control Conf., Chicago, IL, June 2000, pp. 2605–2609.

[17] J. C. Doyle, *Synthesis of robust controllers and filters with structured plant uncertainty*, in Proc. of IEEE Conf. on Decision and Cont., San Antonio, TX, Dec. 1983, pp. 109–114.

[18] J. C. Doyle, K. Glover, P. Khargonekar, and B. Francis, *State-space solutions to standard H_2 and H_∞ control problems*, IEEE Trans. on Automatic Control, AC-34 (1989), pp. 831–847.

[19] E. G. Collins, Jr., D. Sadhukhan, and L. T. Watson, *Robust controller synthesis via nonlinear matrix inequalities*, Int. J. of Control, 72 (1999), pp. 971–980.

[20] L. El Ghaoui, V. Balakrishnan, E. Feron, and S. Boyd, *On maximizing a robustness measure for structured nonlinear perturbations*, in Proc. of the American Control Conf., Chicago, IL, June 1992, pp. 2923–2924.

[21] L. El Ghaoui and P. Gahinet, *Rank minimization under LMI constraints: a framework for output feedback problems*, in Proc. of the European Control Conf., July 1993.

[22] L. El Ghaoui and S.-I. Niculescu, *Robust decision problems in engineering: An LMI approach*, in Advances in Linear Matrix Inequality Methods in Control, L. El Ghaoui and S. I. Niculescu, eds., SIAM, Philadelphia, PA, 2000.

[23] L. El Ghaoui, F. Oustry, and M. AitRami, *A cone complementarity linearization*

algorithm for static output-feedback and related problem, IEEE Trans. on Automatic Control, 42 (1997), pp. 1171–1176.

[24] A. Elsayed and M. J. Grimble, *A new approach to the H_∞ design of optimal digital linear filters*, IMA J. of Mathematical Control and Information, 6 (1989), pp. 233–251.

[25] R. S. Erwin, A. G. Sparks, and D. S. Bernstein, *Fixed-structure robust controller synthesis via decentralized static output feedback*, Int. J. of Robust and Nonlinear Control, 8 (1998), pp. 499–522.

[26] K.-T. Feng, H.-S. Tan, M. Tomizuka, and W.-B. Zhang, *Look-ahead human-machine interface for assistance of manual vehicle steering*, in Proc. of the American Control Conference, San Diego, CA, 1999, pp. 1228–1232.

[27] P. M. Frank, *Fault diagnosis in dynamic systems using analytical and knowledge-based redundancy — A survey and some new results*, Automatica, 26 (1990), pp. 459–474.

[28] P. M. Frank and X. Ding, *Frequency domain approach to optimally robust residual generation and evaluation for model-based fault diagnosis*, Automatica, 30 (1994), pp. 789–804.

[29] G. Franklin, J. D. Powell, and M. L. Workman, *Digital Control of Dynamic Systems*, Addison-Wesley Publishing Company, 1990.

[30] E. Frazzoli, Z.-H. Mao, J.-H. Oh, and E. Feron, *Aircraft conflict resolution via semidefinite programming*, To appear in AIAA Journal of Guidance, Control and Dynamics, (2000).

[31] H. Fujioka and K. Hoshijima, *Bounds for the BMI eigenvalues problems — A good lower bound and a cheap upper bound*, Trans. of SICE, 33 (1997), pp. 616–621.

[32] P. Gahinet, *Explicit controller formulas for LMI-based H_∞ synthesis*, in Proc. of the American Control Conf., Baltimore, Maryland, June 1994, pp. 2396–2400.

[33] P. Gahinet and P. Apkarian, *A linear matrix inequality approach to H_∞ control*, Int. J. of Robust Nonlinear Control, 4 (1994), pp. 421–448.

[34] P. Gahinet, A. Nemirovskii, A. J. Laub, and M. Chilali, *The LMI control toolbox*, in Proc. of the 33rd Conf. on Decision and Control, Lake Buena Vista, FL, 1994, pp. 2038–2041.

[35] J. C. Geromel, C. C. de Souza, and R. E. Skelton, *LMI numerical solution for output feedback stabilization*, in Proc. of the American Control Conf., Baltimore, MD, June 1994, pp. 40–44.

[36] L. E. Ghaoui, R. Nikoukhah, and F. Delebecque, *LMITOOL: A package for LMI optimization*, in Proc. of the 34th Conf. on Decision and Control, New Orleans, LA, December 1995, pp. 3096–3101.

[37] K. Glover and J. C. Doyle, *State-space formulae for all stabilizing controllers that satisfy an H_∞-norm bound and relations to risk sensitivity*, Systems and Control Letters, 11 (1988), pp. 167–172.

[38] M. X. Goemans and D. P. Williamson, *Improved approximation algorithms for maximum cut and satisfiability problems using semidefinite programming*, J. of the Assoc. for Computing Machinery, 42 (1995), pp. 1115–1145.

[39] K.-C. Goh, M. G. Safonov, and G. P. Papavassilopoulos, *A global optimization approach for the BMI problem*, in Proc. of the 33rd Conf. on Decision and Control, Lake Buena Vista, FL, Dec. 1994, pp. 2009–2014.

[40] E. Grassi and K. Tsakalis, *PID controller tuning by frequency loop-shaping*, in Proc. of the 35th IEEE Conf. on Decision and Control, Kobe, Japan, Dec. 1996, pp. 4776–4781.

[41] M. Green and D. J. N. Limebeer, *Linear Robust Control*, Prentice Hall, Eaglewood Cliffs, NJ, 1995.

[42] K. M. Grigoriadis and R. E. Skelton, *Low order control design for LMI problems using alternating projection methods*, Automatica, 32 (1995), pp. 1117–1125.

[43] E. G. Grochowski and R. F. Hoyt, *Future trends in hard disk drives*, IEEE Trans. on Magnetics, 32 (1996), pp. 1850–1854.

[44] A. Hassibi, J. How, and S. Boyd, *Low-authority controller design via convex optimization*, in Proc. of IEEE Conf. on Decision and Control, Tampa, FL, Dec. 1998, pp. 140–145.

[45] ——, *A path-following method for solving BMI problems in control*, in Proc. of the American Control Conf., San Diego, CA, 1999, pp. 1385–1389.

[46] D. Hernandez, S.-S. Park, R. Horowitz, and A. K. Packard, *Dual-stage track following servo design for hard disk drives*, in Proc. of the American Control Conf., San Diego, CA, 1999, pp. 4116–4121.

[47] P. Hingwe, A. K. Packard, and M. Tomizuka, *Linear parameter varying con-*

troller for automated lane guidance — Experimental study on tractor semi-trailers, in Proc. of the 2000 American Control Conference, Chicago, IL, 2000, pp. 2038–2042.

[48] P. Hingwe and M. Tomizuka, *Two alternative approaches to the design of lateral controllers based on sliding mode control*, in ASME Int. Mechanical Engineering Congress and Exposition, vol. DSC.-56/ DE.-86, San Francisco, CA, 1995, pp. 99–104.

[49] P. S. Hingwe, *Robustness and Performance Issues in the Lateral Control of Vehicles in Automated Highway Systems*, PhD thesis, University of California at Berkeley, 1997.

[50] M. Hirata, K. Z. Lieu, and T. Mita, *Head positioning control of a hard disk drive using H_∞ theory*, in Proc. of the 31st Conf. on Decision and Control, Tucson, Arizona, 1992, pp. 2460–2461.

[51] R. Horst and H. Tuy, *Global optimization: Deterministic approaches*, Springer-Verlag, Berlin, second ed., 1993.

[52] K. J. Hunt, ed., *Polynomial methods in optimal control and filtering*, P. Peregrinus on behalf of the Institution of Electrical Engineers, London, 1993.

[53] S. Ibaraki and M. Tomizuka, *Rank minimization approach for solving BMI problems with random search.* Submitted to *the American Control Conf.*, Arlington, VA, 2001.

[54] S. Ibaraki and M. Tomizuka, *H_∞ optimization of fixed structure controllers*, in Proc. of the 2000 International Mechanical Engineering Congress and Exposition, Orlando, FL, Nov. 2000.

[55] S. Ibaraki and M. Tomizuka, *Taming internal dynamics by mismatched and H_∞-optimized state observers*, in Proc. of the 2000 American Control Conf., Chicago, IL, June 2000, pp. 715–719.

[56] R. Isermann, *Supervision, fault-detection and fault-diagnosis methods — An introduction*, Control Engineering Practice, 5 (1997), pp. 639–652.

[57] ——, *Diagnosis methods for electronic controlled vehicles.* Plenary lecture in 5th International Symposium on Advanced Vehicle Control, Ann Arbor, MI, 1999.

[58] T. Iwasaki and M. A. Rotea, *Rank-one scaled H_∞ control synthesis with flight control application*, in Proc. of the American Control Conf., Seattle, WA, June 1995, pp. 422–426.

[59] ——, *Fixed-order scaled H_∞ synthesis*, Optimal Control Applications and Methods, 18 (1997), pp. 381–398.

[60] T. Iwasaki and R. E. Skelton, *All controllers for the general H_∞ control problem: LMI existence conditions and state space formulas*, Automatica, 30 (1994), pp. 1307–1317.

[61] A. Kamath and N. Karmarkar, *A continuous approach to compute upper bounds in quadratic maximization problems with integer constraints*, in Recent Advances in Global Optimization, C. Floudas and P. Pardalos, eds., Princeton University Press, Oxford, 1992, pp. 125–140.

[62] I. Kanellakopoulos and M. Tomizuka, *Commercial trucks and buses in automated highway systems*, in Automated Highway Systems, P. Ioannou, ed., Plenum Publishing Corporation, 1996, pp. 213–245.

[63] D. Karger, R. Motwani, and M. Sudan, *Approximate graph coloring by semidefinite programming*, in Proc. of the 35th Annual Sympo. on Foundations of Computer Science, 1994, pp. 2–13.

[64] N. Karmarkar, *A new polynomial-time algorithm for linear programming*, Combinatorica, 4 (1984), pp. 373–395.

[65] T. Kawabe and T. Tagami, *A real coded genetic algorithm for matrix inequality design approach of robust PID controller with two degrees of freedom*, in Proc. of the 12th IEEE International Symposium on Intelligent Control, Istanbul, Turkey, July 1997, pp. 119–124.

[66] M. Kawanishi, T. Yada, and T. Sugie, *Controller design of 2 mass-spring system based on BMI optimization*, in Proc. of IEEE Conf. on Decision and Control, Kobe, Japan, Dec. 1996, pp. 2363–2364.

[67] P. P. Khargonekar and M. A. Rotea, *Mixed H_2/H_∞ control: A convex optimization approach*, IEEE Trans. on Automatic Control, 36 (1991), pp. 824–837.

[68] K. Konishi and S. Shin, *Matrix-based SDP relaxation for QMI problems*, Submitted to Trans. of SICE.

[69] S. M. Liu and G. P. Papavassilopoulos, *Numerical experience with parallel algorithms for solving the BMI problem*, in Proc. of the 13th World Congress of IFAC, vol. D, San Francisco, CA, 1996, pp. 387–392.

[70] D. G. Luenberger, *Observing the state of a linear system*, IEEE Trans. on Military Electronics, MIL–8 (1964), pp. 74–80.

[71] S. A. Malan, M. Milanese, and M. Taragna, *Robust tuning for PID controllers with multiple performance specifications*, in Proc. of the 33th IEEE Conf. on Decision and Cont., Lake Buena Vista, FL, Dec. 1994, pp. 2684–2689.

[72] S. Mammar, *Robust reduced order two-degrees-of-freedom tractor-semitrailer lateral control*, in Proc. of the American Control Conference, San Diego, CA, June 1999, pp. 3158–3162.

[73] M. Mesbahi, *On the semi-definite programming solution of the least order dynamic output feedback synthesis*, in Proc. of the American Control Conference, San Diego, CA, 1999, pp. 2355–2359.

[74] M. Mesbahi, M. G. Safonov, and G. P. Papavassilopoulos, *Bilinearity and complementarity in robust control*, in Advances in Linear Matrix Inequality Methods in Control, L. E. Ghaoui and S.-I. Niculescu, eds., SIAM, Philadelphia, 2000.

[75] R. Motwani and P. Raghavan, *Randomized Algorithms*, Cambridge University Press, Cambridge, 1995.

[76] K. M. Nagpal and P. P. Khargonekar, *Filtering and smoothing in an H_∞ setting*, IEEE Trans. on Automatic Control, 36 (1991), pp. 152–166.

[77] A. Nemirovski and P. Gahinet, *The projective method for solving linear matrix inequalities*, Mathematical Programming, 77 (1997), pp. 163–190.

[78] A. Nemirovskii, *Several NP-hard problems arising in robust stability analysis*, Mathematics of Control, Signals, and Systems, 6 (1994), pp. 99–105.

[79] Y. Nesterov and A. Nemirovski, *A general approach to polynomial-time algo-*

rithms design for convex programming, tech. rep., Centr. Econ. and Math. Inst., USSR Acad. Sci., Moscow, USSR, 1988.

[80] Y. E. Nesterov and M. J. Todd, *Self-scaled cones and interior-point methods in nonlinear programming*, Tech. Rep. 1091, Cornell Univ., April 1994.

[81] C. N. Nett, D. S. Bernstein, and W. M. Haddad, *Minimal complexity control law synthesis, part 1: Problem formulation and reduction to optimal static output feedback*, in Proc. of American Control Conf., Pittsburgh, PS, June 1989, pp. 2056–2064.

[82] W. Niu, S. Ibaraki, M. Tomizuka, and T. Nguyen, *Tuning of a digital disk drive servo controller using fixed-structure H_∞ controller optimization.* Submitted to *European Control Conf.*, Porto, Portugal, 2001.

[83] A. Packard, K. Zhou, P. Pandey, J. Leonhardson, and G. Balas, *Optimal, constant I/O similarity scaling for full-information and state-feedback control problems*, Systems and Control Letters, 19 (1992), pp. 271–280.

[84] R. J. Patton, P. M. Frank, and R. N. Clark, eds., *Fault diagnosis in dynamic systems : theory and applications*, Prentice-Hall international series in systems and control engineering, Prentice Hall, Englewood Cliffs, NJ, 1989.

[85] S. Patwardhan, H.-S. Tan, and J. Guldner, *A general framework for automatic steering control: system analysis*, in Proc. of the 1997 American Control Conference, Albuquerque, New Mexico, 1997, pp. 1598–1602.

[86] A. L. Peressini, F. E. Sullivan, and J. J. Uhl, Jr., *The Mathematics of Nonlinear Programming*, Springer-Verlag, New York, 1988.

[87] I. R. Peterson, *Disturbance attenuation and H_∞ optimization: A design method based on the algebraic Ricatti equation*, IEEE Trans. on Automatic Control, AC-32 (1987), pp. 427–429.

[88] S. Poljak and Z. Tuza, *Maximum cuts and largest bipartite networks*, in DIMACS series in Discrete Mathematics and Theoretical Computer Science, W. Cook, L. Lovász, and P. Seymour, eds., AMS, 1995.

[89] R. Rajamani, A. Howell, C. Chen, J. K. Hedrick, and M. Tomizuka, *A complete fault diagnostic system for automated vehicles*, in Proc. of the 14th IFAC World Congress, vol. B, Beijing, P. R. China, July 1999, pp. 439–444.

[90] M. A. Rotea and T. Iwasaki, *An alternative to the D-K iteration?*, in Proc. of the American Control Conf., Baltimore, MD, June 1994, pp. 53–57.

[91] M. G. Safonov, *Optimal diagonal scaling for infinity-norm optimization*, Systems and Control Letters, 7 (1986), pp. 257–260.

[92] M. G. Safonov, K. C. Goh, and J. H. Ly, *Control system synthesis via bilinear matrix inequalities*, in Proc. of the American Control Conf., Baltimore, MD, June 1994, pp. 45–49.

[93] U. Shaked, *H_∞ minimum error state estimation of linear stationary processes*, IEEE Trans. on Automatic Control, 35 (1990), pp. 554–558.

[94] J. S. Shamma, *Robust stability with time-varying structured uncertainty*, IEEE Trans. on Automatic Control, 39 (1994), pp. 714–724.

[95] J. S. Shamma and M. Athans, *Gain scheduling: Potential hazards and possible remedies*, IEEE Control Systems, 12 (1992), pp. 101–107.

[96] N. Z. Shor, *Cut-off methods with space extension in convex programming problems*, Cybernetics, 13 (1977), pp. 94–96.

[97] J. E. Slotine and W. Li, *Applied Nonlinear Control*, Prentice Hall, Englewood Cliffs, NJ, 1991.

[98] T. Song and E. G. Collins, Jr., *Robust H_2 estimation with application to robust fault detection*, in Proc. of the American Control Conference, Chicago, IL, June 2000, pp. 1200–1204.

[99] M. Steinbuch and M. L. Norg, *Advanced motion control: an industrial perspective*, European Journal of Control, 4 (1998), pp. 278–293.

[100] S. Suryanarayanan and M. Tomizuka, *Observer based 'look-ahead' scheme for fault tolerant lateral control of automated vehicles*, in Proc. of the 5th Int. Symposium on Advanced Vehicle Control, Ann Arbor, Michigan, August 2000, pp. 269–274.

[101] M. Tai and M. Tomizuka, *Dynamic modeling of multi-unit heavy vehicles*, in Proc. of the 1998 Int. Mechanical Engineering Congress and Exposition, Anaheim, CA, 1998, pp. 673–680.

[102] ——, *Robust lateral control of heavy duty vehicles for automated highway systems*, in Proc. of the 14th IFAC World Congress, vol. Q, Beijing, P. R. China, July 1999, pp. 37–42.

[103] R. H. C. Takahashi, P. L. D. Peres, and P. A. V. Ferreira, *Multiobjective H_2/H_∞ guaranteed cost PID design*, IEEE Control Systems, 17 (1997), pp. 37–47.

[104] O. Toker and H. Özbay, *On the NP-hardness of solving bilinear matrix inequalities and simultaneous stabilization with static output feedback*, in Proc. of the American Control Conference, Seattle, WA, 1995, pp. 2525–2526.

[105] ——, *On the complexity of purely complex μ computation and related problems in multidimensional systems*, IEEE Trans. on Automatic Control, 43 (1998), pp. 409–414.

[106] M. Tomizuka, M. Tai, J.-Y. Wang, and P. Hingwe, *Automated lane guidance of commercial vehicles*, in Proc. of the 1999 IEEE Int. Conf. on Control Applications, Kohala Coast, Hawaii, 1999, pp. 1359–1364.

[107] H. D. Tuan, P. Apkarian, S. Hosoe, and H. Tuy, *D. C. optimization approach to robust control: feasibility problems*, Int. J. of Control, 73 (2000), pp. 89–104.

[108] H. D. Tuan, P. Apkarian, and T. Q. Nguyen, *Robust and reduced-order filtering: new characterizations and methods*, in Proc. of the American Control Conference, Chicago, IL, June 2000, pp. 1327–1331.

[109] L. Vandenberghe and S. Boyd, *SP: Software for semidefinite programming.* Available at http://www.stanford.edu/~boyd/.

[110] ——, *Semidefinite programming*, SIAM Review, 38 (1996), pp. 49–95.

[111] N. Viswanadham, J. H. Taylor, and E. C. Luce, *A frequency domain approach*

to failure detection and isolation with application, Control – Theory and Advanced Technology, 3 (1987), pp. 45–72.

[112] Y. Wakasa, *Global optimization algorithms for BMI problems*, Trans. of the Inst. of Systems, Control and Information Engineers, 43 (1999), pp. 258–265. (in Japanese).

[113] J.-Y. Wang and M. Tomizuka, *Dynamic analyses and robust steering controller design for automated lane guidance of heavy-duty vehicles*, Asian Journal of Control, 2 (2000), pp. 140–154.

[114] ——, *Gain-scheduled H_∞ loop-shaping controller for automated guidance of tractor semi-trailers combination vehicles*, in Proc. of the 2000 American Control Conference, Chicago, IL, 2000, pp. 2033–2037.

[115] Z. Wang, B. Huang, and H. Unbehauen, *Robust H_∞ observer design of linear state delayed systems with parametric uncertainty: the discrete-time case*, Automatica, 35 (1999), pp. 1161–1167.

[116] C. J. Wenk and C. H. Knapp, *Parameter optimization in linear systems with arbitrarily constrained controller structure*, Trans. on Automatic Control, AC-25 (1980), pp. 496–500.

[117] F. Wu, X. H. Yang, A. Packard, and G. Becker, *Induced $\mathcal{L}_2$ norm control for LPV systems with bounded parameter rate*, Int. J. of Nonlinear and Robust Control, 6 (1996), pp. 983–998.

[118] L. Xie, C. E. de Souza, and M. Fu, *H_∞ estimation for discrete-time linear uncertain systems*, Int. J. of Robust Nonlinear Control, 42 (1991), pp. 111–123.

[119] L. Xie, Y. C. Soh, and C. E. de Souza, *Robust Kalman filtering for uncertain discrete-time systems*, IEEE Trans. on Automatic Control, 39 (1994), pp. 1310–1314.

[120] Y. Yamada and S. Hara, *An LMI approach to local optimization for constantly scaled H_∞ control problems*, Int. Journal of Control, 67 (1997), pp. 233–250.

[121] ——, *The matrix product eigenvalue problem*, in Proc. of the 36th Conf. on Decision and Control, San Diego, CA, Dec. 1997, pp. 4926–4931.

[122] S. D. Yen and W. S. Levine, *Mixed H_2/H_∞ optimization: a BMI solution*, in Proc. of IEEE Conf. on Decision and Control, San Diego, CA, Dec. 1997, pp. 460–465.

[123] D. B. Yudin and A. S. Nemirovski, *Informational complexity and efficient methods for solving complex extremal problems*, Matekon, 13 (1977), pp. 25–45.

[124] G. Zames, *Feedback and optimal sensitivity: Model reference transformations, multiplicative seminorms, and appropriate inverses*, IEEE Trans. on Automatic Control, AC-26 (1981), pp. 301–320.

[125] K. Zhou, J. C. Doyle, and K. Glover, *Robust and Optimal Control*, Prentice Hall, Upper Saddle River, NJ, 1996.

[126] K. Zhou and P. P. Khargonekar, *An algebraic Ricatti equation approach to H_∞ optimization*, Systems and Control Letters, 11 (1988), pp. 85–91.